ABSTRACT

Title of Document:	THE NOVEL USE OF NITROXIDE ANTIOXIDANTS AS FREE RADICAL SCAVENGERS IN ULTRA-HIGH MOLECULAR WEIGHT POLYETHYLENE (UHMWPE) FOR TOTAL JOINT REPLACEMENTS
	Marina Konstantinovna Chumakov, Doctor of Philosophy, 2010
Directed By:	Professor Mohamad Al-Sheikhly, Department of Materials Science and Engineering

Ultra-high molecular weight polyethylene (UHMWPE) has been the standard load-bearing material used in total joint replacements since the 1960s. However, oxidative degradation can lead to premature aging and wear of UHMWPE, requiring implant revision. The novel use of nitroxide antioxidants to prevent oxidation in UHMWPE was proposed and the resulting structure and property changes were evaluated in this work. Standard sterilization and crosslinking methods of ^{60}Co gamma or high energy electron beam radiation produce alkyl free radicals on the polymer chain. Alkyl radicals react to form bimolecular crosslinks and long-lived allyl radicals at high dose rates; at low dose rates they tend to react with oxygen to form peroxyl radicals. The peroxyl radicals further interact with the polymer chain producing hydroperoxides and more free radicals, leading to oxidative degradation.

As an alternative to post-irradiation remelting, which allows radical recombination but reduces fatigue strength, antioxidants can be introduced into UHMWPE to scavenge residual radicals. Nitroxides are stable organic compounds that have a strong paramagnetic signal and are very efficient in preventing lipid peroxidation and in providing radioprotection in biological tissues. The nitroxides used are 2,2,6,6–tetramethylpiperidine–1–oxyl (TEMPO) and 4-hydroxy–TEMPO (Tempol). Through radical-radical interactions, radiolytically-produced alkyl radicals in UHMWPE are scavenged by the nitroxide radical. This is demonstrated through Electron Paramagnetic Resonance (EPR) spectroscopy where the paramagnetic nitroxide signal decays as it interacts with carbon-centered radicals in UHMWPE. Pulse radiolysis kinetics studies also show that alkyl radicals in UHMWPE preferentially react with nitroxides in the absence of oxygen. Controlled infiltration of UHMWPE with nitroxides is also observed using EPR.

The resulting crosslink densities were investigated using Thermomechanical Analysis. It was observed that the addition of nitroxides after irradiation does not alter the crosslink density. Tensile testing of crosslinked and nitroxide-doped UHMWPE demonstrates increased ultimate tensile strength and toughness and the material exhibits an increase in crystallinity. Additionally, accelerated aging of specimens containing trace levels of nitroxide show very low oxidation levels when placed in an aggressive oxygen environment. Consequently, low concentrations of nitroxides diffused into UHMWPE after crosslinking produce an oxidation-resistant and highly crosslinked material for improved implant performance.

THE NOVEL USE OF NITROXIDE ANTIOXIDANTS AS FREE RADICAL SCAVENGERS IN ULTRA-HIGH MOLECULAR WEIGHT POLYETHYLENE (UHMWPE) FOR TOTAL JOINT REPLACEMENTS

By

Marina Konstantinovna Chumakov

Dissertation submitted to the Faculty of the Graduate School of the
University of Maryland, College Park, in partial fulfillment
of the requirements for the degree of
Doctor of Philosophy,
2010

Advisory Committee:
Professor Mohamad Al-Sheikhly, Chair
Professor Peter Kofinas
Professor Kyu Yong Choi
Associate Professor John Fisher
Assistant Professor Adam Hsieh
Professor Emeritus Joseph Silverman
Dr. Dianne Poster

Acknowledgements

Many people have contributed to the completion of this dissertation. I would like to sincerely thank everyone who has offered advice, an attentive ear or their precious time to me during my Ph.D.

First of all, I would like to profoundly thank my advisor, Dr. Al-Sheikhly, for providing me with the opportunity to work in his group, for constant inspiration to do my best and for pushing me to go outside my comfort zone in order to achieve. I would like to thank Dr. Silverman for the many involved conversations that motivated me to reach higher and to tackle the tough questions. Dr. McDermott served as an essential collaborator and mentor at the FDA. I would like to thank him for campaigning on my behalf, for the opportunities in participating at the regulatory level, and for the great discussions we had. Mr. Vince Adams deserves immense thanks for the countless hours he helped me design my experiments and solve technical problems, as well as lending an ear when things got tough. Also, I would like to thank Amanda Forster for her support, helpful discussion and donation of crucial instruments without which this dissertation would be incomplete. Dr. David Schroeder deserves thanks for the invaluable donation of UHMWPE barstock.

Chiefly, this dissertation was possible due to the unwavering and unreserved support and love from my parents. I could not have completed this work without their constant persuasion to achieve and the immense sacrifices that they made. I would like to also thank my close friends for encouraging me and providing an outlet for my frustrations. To Laura – for the memories and countless times she helped edit. To Steve – for his love, support and waiting up those long nights.

Table of Contents

List of Tables

List of Figures

Chapter 1: Background

The aim of this work is to develop a solution to the early failure of total joint replacements by investigating the nitroxide as an antioxidant additive for ultra-high molecular weight polyethylene (UHMWPE). Specifically, to effectively utilize nitroxide antioxidants to increase the oxidation and wear resistance of UHMWPE liners while maintaining a high degree of crosslinking achieved through high doses of ionizing radiation. Additionally, this work aims to investigate the competing mechanisms of bimolecular crosslinking, oxidation and nitroxide-polymer radical interaction. This introductory chapter will illustrate the motivations for this work. The role of free radical reactions in UHMWPE will also be discussed.

1.1 Introduction

Ultra-high molecular weight polyethylene (UHMWPE) has been used for total joint arthroplasty (replacement) since the early 1960s. UHMWPE is biocompatible and easy to process into compression molded liner cups or tibial inserts from resin or extruded into bar stock and machined. It exhibits a low coefficient of friction and has a high resistance to fatigue and wear due to its ultra–high weight–average molecular weight $\left(\overline{M_w}\right)$ (two – six million grams per mole) forming a semi–crystalline structure by the entanglement of its long chains. It is widely used in hip and knee endoprostheses in over 1.4 million operations annually around the world.[1] This procedure is not considered a permanent solution for many patients as adhesive and abrasive wear that occurs between the UHMWPE liner and the metal femoral head in

hip replacements, and fatigue and back-side wear that occurs in knee replacements. Wear produces small particles of UHMWPE debris, which cause an inflammatory response and bone resorption called peri-prosthetic osteolysis. This condition can be very painful and causes implants to loosen, which can require the patient to undergo revision surgery. Younger patients with active life-styles can quickly wear out their joint replacements resulting in successive revision surgeries. At 20 years after surgery, survivorship of implants in patients aged ≤ 40 years old at surgery is 67% versus 92% for patients 70-80 years old.[3]

Wear occurs in non-crosslinked and embrittled UHMWPE liners that have become oxidized upon exposure to air during ionizing irradiation. While irradiation of the polymer in an inert environment enhances crosslinking and wear resistance,[4] it leaves residual free radicals that then can react with oxygen to form the corresponding peroxyl radicals. Peroxyl radicals react further to form hydroperoxides, ketones, esters and more free radicals as well as causing chain scission.[5] Although thermal treatments may reduce residual free radical content, it has been found that annealing, performed below the melting temperature, can later cause oxidation *in vivo* and remelting of the polymer causes significant losses to the mechanical properties and fatigue strength.[6, 7] Hence, a recent popular approach to infiltrate UHMWPE with antioxidants is aimed to prevent oxidation and wear, while maintaining fatigue strength.[8] This work explores the use of a novel antioxidant and the ways in which this antioxidant can enhance polymer properties and implant lifetime.

1.2 History of UHMWPE in Total Joint Replacements

While the first joint replacement was performed in the 19th century, the expansion of this procedure is credited to Sir John Charnley. Following his studies of animal and human joints in the 1950s, he drew the conclusion that natural joints functioned so well because of their low coefficient of friction and lubrication. In 1962, Sir Charnley was the first to design a metal femoral head articulating against an ultra-high molecular weight polyethylene (UHMWPE) acetabular cup[1] and this design has been used since. Over the years, many other bearing models were introduced, including carbon-reinforced Poly II material, silane-crosslinked high density polyethylene (HDPE), highly crystalline Hylamer and PTFE bearing surfaces. Sir Charnley's PTFE design pre-dated UHMWPE and utilized a double-cup model that mimicked the natural joint. Despite PTFE's low friction and chemical inertness, the material was found to wear very rapidly, as shown in Figure 1.1. There were many PTFE designs, all of which showed very rapid wear. It was the natural wear-resistance of UHMWPE that propelled its use over other options at the time. Despite many failing alternative systems, there are many that are successfully in use today, including alumina ceramic bearing surfaces and metal-on-metal (MOM) bearings. Most importantly, in the 1970s, researchers began crosslinking UHMWPE with very high absorbed doses (over 1000 kGy)* of gamma radiation in air.[1] This led to the current use of lower doses of ionizing radiation to crosslink UHMWPE in an inert environment.

* Gray (Gy) = 1 J absorbed radiation energy per kg of mass; kGy = 1000 Gy

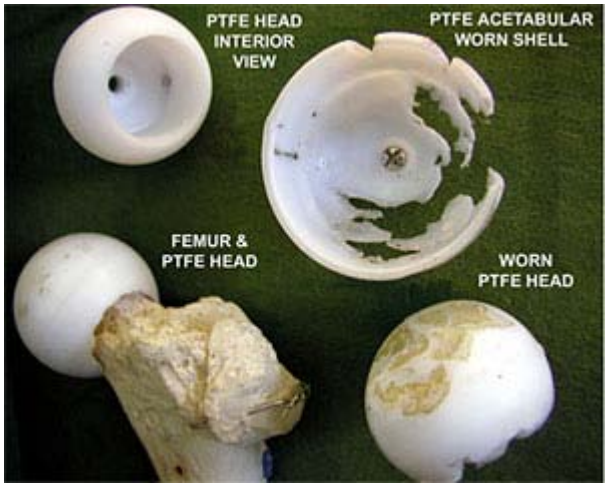

Figure 1.1: Sir John Charnley's early hip replacement designs made from PTFE showing very severe wear.[1]

Currently, UHMWPE is used in both total hip (THA) and knee (TKA) arthroplasties, as well as in lumbar disk replacements. It is one of three options for bearings utilized in the hip (ceramic on ceramic and MOM) and the only option, currently, for TKA. These designs are shown in Figure 1.2, where the UHMWPE is used to articulate a metal component. While the material and processing methodologies are often similar, current research has identified different failure modalities in the hip and knee, as discussed later.

.

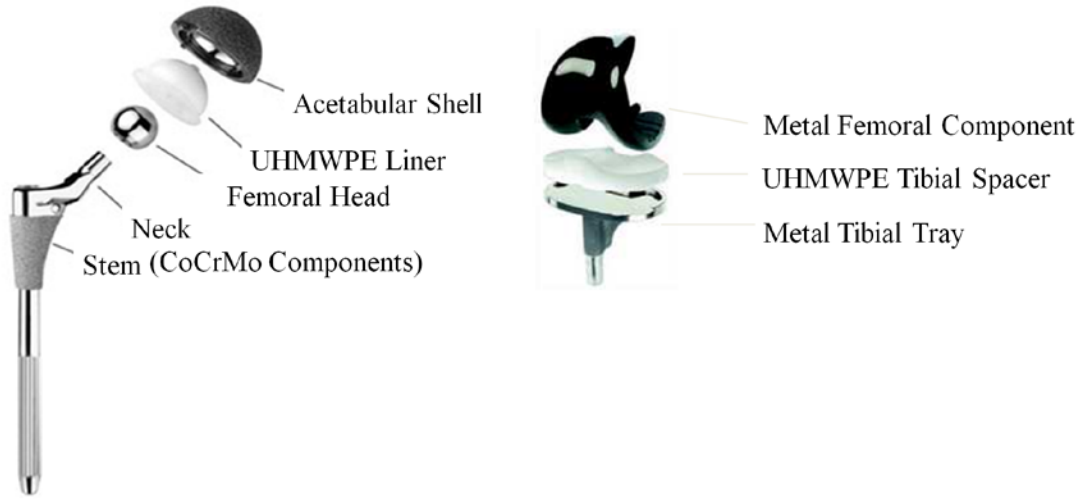

(a) (b)

Figure 1.2: Designs of total hip (a) and knee (b) replacements utilizing UHMWPE as a bearing surface. UHMWPE is one of three bearing surfaces in total hip replacements and the only bearing used in knee replacements.

Initially, most commercial designs used ethylene oxide for sterilization. In the 1970s and 1980s, ionizing radiation doses of 25 to 40 kGy were used as a cost-effective sterilization strategy with the advantage of reducing wear because of crosslinking of polymer chains. Since 1998, the approach to further reduce wear is achieved by generating a higher crosslink density in the amorphous region with higher doses of irradiation, around 100 kGy. Some commercial examples include X3® (Stryker Orthopedics, Mahwah, NJ) and ArComXL (Biomet Inc., Warsaw, IN).[1] Data from joint simulators on 32 mm acetabular cups have shown a 97% reduction in wear rates of a highly crosslinked UHMWPE bearing versus conventional material.[9] While crosslinking has shown reduction in wear rates, other issues have been identified recently. The irradiation of UHMWPE components in air causes oxidation due to free radical reaction with oxygen.[5] In fact, oxidation has been found to be associated with damage to UHMWPE components,[10, 11] like

delamination, rim fractures and impingement. Oxidative degradation causes the production of products such as hydroperoxides, ketones and ultimately chain scission, embrittling the material and producing wear particles. The prevention of oxidation in UHMWPE by adding antioxidants has been studied by several research groups and is the subject of this dissertation.

1.2.1 What is UHMWPE?

UHMWPE is a linear saturated homopolymer that has an ultra–high weight-average molecular weight $\left(\overline{M_w}\right)$ of two to six million g·mol^{-1}. The polymer has very long chains that are entangled with one another. It is semi-crystalline and a single chain has several small crystalline segments that are tied together through the amorphous regions, with a tie molecule. This structure is shown in Figure 1.3. UHMWPE is formed from ethylene (CH_2CH_2) containing up to 200,000 repeat units,[1] by Ziegler-Natta catalysis.[12] Types of polyethylene with shorter chains include low density and linear low density polyethylene (LDPE and LLDPE) as well as high density polyethylene (HDPE). The typical crystallinity of UHMWPE is 50 – 80 %. The crystalline lamellae are very small, around 10 – 50 nm in thickness and 10 – 50 μm in length.[13] The spacing between these lamellae are typically 50 nm.[14] This morphology and long linear entangled chains have the ability to blunt fatigue crack tip propagation and produce wear-resistance in UHMWPE. Its additional biocompatibility and low friction coefficient are other factors making it a successful bearing for total hip and knee arthroplasties.

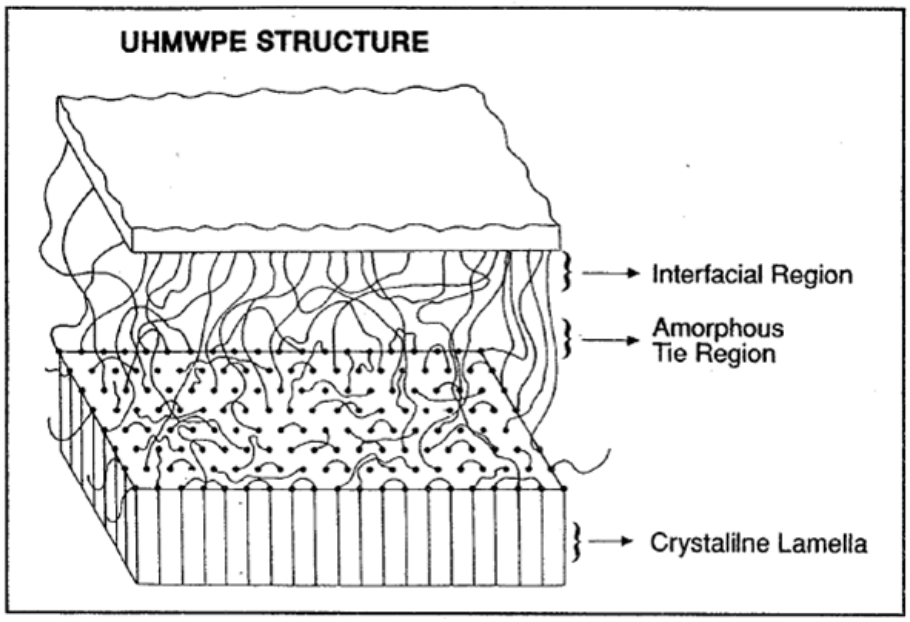

Figure 1.3: Diagram showing the semi-crystalline structure of UHMWPE where one chain can lie in the small crystalline lamellae and transverse the amorphous region via a tie molecule into another crystallite.[2]

1.2.2 Radiolysis of UHMWPE

Gamma radiation (^{60}Co) and high energy electron beam (EB) are the conventional sterilization methods for UHMWPE. Upon radiolysis, polyethylene forms cations, $R^{+\bullet}$, excited cations, $R^{+}*^{\bullet}$, electronically excited polyethylene, R*, and superexcited polyethylene, R**,[15] as shown in equation 1.1, where R = $(C_2H_4)_n$:

$$R \rightsquigarrow R^{+\bullet} + R^{+}*^{\bullet} + e^{-} + R* + R** \qquad (1.1)$$

Subsequently, two neutral alkyl radicals, $R^{\bullet}$, are formed from the neutralization after a hydrogen abstraction from the C–H backbone, in equation 1.2:[15]

$$R^{+\bullet} + RH \rightarrow RH_2^{+} + R^{\bullet} \rightarrow R^{\bullet} + R^{\bullet} + H_2 + e^{-} \qquad (1.2)$$

These alkyl radicals can then bimolecularly crosslink, as per equation 1.3:[16]

$$R^{\bullet} + R^{\bullet} \rightarrow R\text{-}R \qquad (1.3)$$

At high dose rates, bimolecular crosslinking reactions of alkyl radicals are enhanced. Mobility of the polymer chains in the amorphous region allows these free radicals to combine to form crosslinks and increase wear resistance of the polymer. Because the large lamellar spacing in the crystalline region does not allow free radical recombination, alkyl radicals must migrate to the crystalline-amorphous interface through hydrogen and electron hopping. The interfaces of the crystalline and amorphous regions are crucial because they contain high concentrations of diffused oxygen. Vinyl unsaturations are formed from radical cations in equation 1.4 and through disproportionation in equation 1.5, where R = $(CH_2\text{-}CH_2)_n$:[17, 18]

$$\begin{array}{l} RCH_2C^{+\bullet}H_2R \rightarrow RCH{=}C^{+\bullet}HR + H_2 \\ \qquad\qquad\qquad\quad \downarrow + e^- \\ \qquad\qquad\qquad\quad RCH{=}CHR \end{array} \qquad (1.4)$$

$$\begin{array}{l} RCH_2C^{\bullet}HCH_2R \\ \qquad + \\ RCH_2C^{\bullet}HCH_2R \end{array} \quad \rightarrow \quad \begin{array}{l} CH_2CH_2CH_2CH_2 \\ \qquad + \\ RCH_2CH{=}CHR \end{array} \qquad (1.5)$$

The alkyl radicals will hydrogen-hop until encountering these vinyl unsaturations to form relatively long-lived allyl radicals as shown in equation 1.6:

$$R^{\bullet} + RCH{=}CHR \rightarrow RCH{=}CHC^{\bullet}HR + RH \qquad (1.6)$$

At low dose rates, alkyl radicals predominantly react with diffused molecular oxygen to rapidly form the corresponding peroxyl free radicals. These peroxyl

radicals can abstract yet another hydrogen atom from the polymer chain producing hydroperoxides and more carbon-centered free radicals. Hydroperoxides will form the alkoxyl radical, which can produce more free radicals, as well. Two peroxyl radicals will form tetroxide, which quickly forms more hydroperoxides, ketones, acid groups and esters,[5] as well as chain scission. Although there are many more free radical reactions involved, the major reactions of interest are outlined in the schematic in Figure 1.4. These reactions are further discussed in section 6.1.

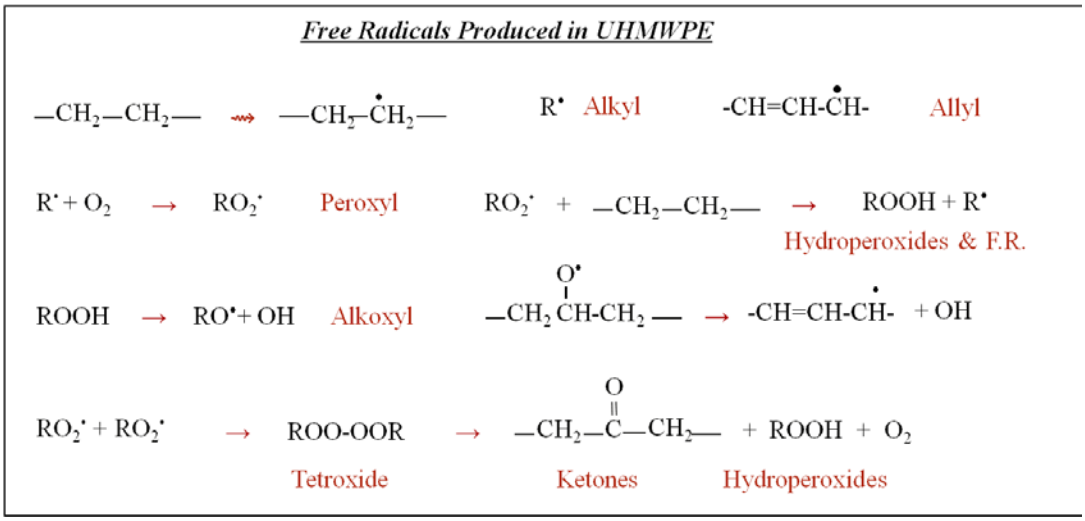

Figure 1.4: Free radical scheme of radiolytically-produced free radicals in UHMWPE. Hydrogen abstraction from the polymer chain produces alkyl radicals. Those radicals can form long-lived allyl free radicals when encountering a vinyl unsaturation. Peroxyl radicals are formed when molecular oxygen reacts with alkyl radicals. These peroxyl radicals will react with the polymer chain to form hydroperoxides and more free radicals. The alkoxyl radical is formed from hydroperoxides and forms more free radicals, as well. Two peroxyl radicals will form the tetroxide, which then decomposes to ketones, more hydroperoxides and ultimately causes chain scission.

In order to estimate free radical concentrations in UHMWPE, it is pertinent to know how many radicals of each type are yielded from irradiation or from each subsequent reaction. Free radical estimates allow for the evaluation of reaction rate

constants and estimation of the antioxidant concentrations necessary in UHMWPE to prevent oxidation. The *G*-value, or the number of molecules per 100 eV of energy deposited can be defined for each radical type. A table of these known values is shown in Table 1.1.

Table 1.1: *G*-values for Radiolytically-Produced Free Radicals or Species

Species	*G*-value (molecules/100 eV)	Source
Alkyl Radical, $R^{\bullet}$	3.3 – 4.46	[18, 19]
Vinyl Unsaturations CH=CH	2.2	[20]
Allyl Radicals	0.235 – 0.25	[21, 22]
G(X) Crosslinking	3	[23]

1.2.3 Competing Reactions

As described in the previous section, the irradiation of UHMWPE produces alkyl radicals on the polymer backbone as a hydrogen is abstracted. These alkyl radicals can undergo one of five reactions. Two alkyl radicals can bimolecularly crosslink[16] (equation 1.3, repeated below) which increases the wear-resistance of UHMWPE. Two alkyl radicals can form a *trans*-vinylene by disproportionation, as shown in equation 1.5 below. An alkyl radical can migrate through electron or hydrogen hopping and form an allyl radical when encountering a vinyl unsaturation, as shown in equations 1.6 below. In the presence of diffused oxygen either in the amorphous region, at the crystalline-amorphous interface or on the surface of the polymer, the alkyl radical will form the peroxyl radicals (equation 1.7) that begin the oxidation cascade. Lastly, an alkyl radical can react with an antioxidant, such as vitamin E (α-TOH) or nitroxide (>$NO^{\bullet}$) (equation 1.8) described in section 1.3.

$$R^{\bullet} + R^{\bullet} \rightarrow R - R \quad \text{bimolecular crosslink} \qquad (1.3)$$

$$\begin{array}{l} RCH_2C^{\bullet}HCH_2R \\ + \\ RCH_2C^{\bullet}HCH_2R \end{array} \rightarrow \begin{array}{l} CH_2CH_2CH_2CH_2 \\ + \\ RCH_2CH=CHR \end{array} \qquad (1.5)$$

$$R^{\bullet} + RCH=CHR \rightarrow RCH=CHC^{\bullet}H + RH \quad \text{allyl radical} \qquad (1.6)$$

$$R^{\bullet} + O_2 \rightarrow RO_2^{\bullet} \quad \text{peroxyl radical} \qquad (1.7)$$

$$R^{\bullet} + \begin{array}{c} \alpha\text{-TOH} \\ \text{or} \\ >NO^{\bullet} \end{array} \rightarrow \text{stable product} \qquad (1.8)$$

These reactions are competing for a finite number of free radicals (defined by a *G*-value) formed proportionally to the absorbed radiation dose. Thus, the goal is to maximize the crosslinking reaction, while minimizing oxidation. This may be achieved by using a high radiation dose rate and by reacting any residual free radicals with antioxidants, as shown in equation 1.8.

1.2.4 Oxidation

From clinical data of crosslinked UHMWPE, it can be gathered that while wear debris production leading to implant loosening may be one of the ultimate failure mechanisms of total joint replacements, it is not the cause. Recently, studies have shown that UHMWPE components become oxidized *in vivo*.[24] The result is embrittlement of the polymer and adhesive/abrasive wear that generates submicron debris particles, which can cause an inflammatory response, osteolysis and aseptic loosening of the implant. In addition, there is often joint failure compounded due to material fatigue, delamination and fracture (as well as poor alignment of the arthroplasty). When the UHMWPE becomes embrittled due to oxidation, a white

band can be observed under the surface in a cross-section of the material.[10, 25] This location is subject to mechanical failure as forces become concentrated there in knee components. Mechanical degradation is a key factor in failure. Change in the crystalline content of the degraded material increases the elastic modulus, produces a loss in ductility and toughness, and leads to embrittlement and delamination failure in UHMWPE. Early hip components have shown significant wear in THR, while abrasion and delamination are the main problems exhibited in TKR.

Ultimately, induction of oxidation seriously jeopardizes the progress of wear control due to increased crosslinking. Oxidation under the surface can lead to mechanical failure of UHMWPE by fatigue crack propagation or delamination. In response to the oxidation problem, thermal treatments are designed to eliminate residual free radicals in the crystalline regions of UHMWPE. Remelting of the polymer is performed just above the melting point, usually at 150°C. However, when cooling the polymer, crystalline lamellae reformation is limited by crosslinks, which reduces the crystallinity and fatigue strength of the UHMWPE.[26] Annealing involves heating the polymer to just under its melting point, T_m, which is approximately 137°C. While mechanical properties are unaffected, these annealed components have shown *in vivo* oxidation,[24] as the temperature is not sufficient for some radicals in the crystal to migrate and recombine. As a result, mechanical strength becomes a trade-off for reduced oxidation when using thermal treatments. Although both annealing and remelting ensure wear resistance, both methods create changes to the microstructure, crystalline content and lamellar thickness.

These microstructure changes have a negative effect on fracture toughness and

fatigue resistance. Yield stress and fracture stress reduction occur after remelting but not annealing.[27] Fatigue strength and crack propagation resistance have been shown to be reduced with remelting[6]. Material fracture may occur in the acetabular cup rim areas with small thickness (~ 5 mm in hip liners). This causes concern for fatigue crack propagation after an initial defect. Overall, while remelting is the norm for processing after crosslinking, it clearly has substantial limitations.

1.3 Antioxidants

Because mechanical strength and oxidation-resistance become a trade-off when using thermal treatments, other viable options have been explored in the 1990s and 2000s. Namely, the use of antioxidants like vitamin E (α-tocopherol)[8, 28, 29] has gained great popularity and a vitamin E-containing UHMWPE hip liner is currently on the market ((E1^{TM} – E-Poly XLPE by Biomet Inc.).[30] Other stabilizers, like hindered amine light stabilizers[31] and Irganox phenols have been investigated by other groups and manufacturers. The goal of using antioxidants as an alternative to thermal treatments is to maintain the fatigue resistance and tensile properties of UHMWPE while simultaneously avoiding oxidative degradation and wear debris production. The use of nitroxides for this purpose is novel and was first proposed by the author in 2007.[32]

1.3.1 Vitamin E (α-tocopherol)

Vitamin E (α-tocopherol) is the first antioxidant investigated as an alternative to annealing or remelting. This biocompatible molecule easily diffuses into the amorphous portion of UHMWPE due to the lipophilicity of its phytyl tail.[33] Upon

introduction into UHMWPE, α-tocopherol acts as a stabilizer and plasticizer.[28, 29] α-tocopherol can be introduced into the polymer by either mixing with the UHMWPE resin prior to compression molding, or after molding and before machining through diffusion. Through the hydrogen transfer mechanism, a hydrogen from the hydroxyl group of the chroman head is abstracted by a peroxyl radical in UHMWPE (equation 1.9):[34]

$$\alpha\text{-TOH} + RO_2^{\bullet} \rightarrow \alpha\text{-TO}^{\bullet} + ROOH \qquad (1.9)$$

Results have shown greatly reduced wear rates with α-tocopherol in comparison to conventionally γ-irradiated UHMWPE,[28, 29, 33] as well as increased oxidation onset temperature[28] and oxidation–resistance.[33] It has been debated the degree to which vitamin E significantly reduces crosslinking.[33, 35] Oral *et al*. showed in 2008 that a 200 kGy irradiation dose was required to produce crosslinking in 0.3 wt% α-tocopherol containing UHMWPE equivalent to crosslinking achieved with 65 kGy without vitamin E. This issue is critical if the α-tocopherol is consolidated with the resin prior to irradiation. Conversely, microstructure changes may be induced during thermal treatments to diffuse α-tocopherol[36] after irradiation. While the nitroxide antioxidant is used in this work, since E1™ is entering the joint replacement market,[30] it would be prudent to compare the nitroxide to the vitamin E-doped material.

Overall, while vitamin E shows an improvement in oxidation-resistance and fatigue-resistance, there are some limitations. The effect of α-tocopherol on microstructure, the plausibility of plasticization increasing chain motion,[37] and the

possible elution of the molecule out of the polymer are not well understood. This work is necessary to understand how antioxidants affect the microstructure and properties of UHMWPE and which parameters are crucial to engineer a new product. Most importantly, the hydrogen transfer mechanism by which vitamin E reacts with UHMWPE radicals is rather slow, when compared to the electron transfer mechanism or radical-radical interactions. The nitroxide class of antioxidants will be compared to vitamin E as a suitable antioxidant additive to UHMWPE.

1.3.2 Nitroxides

Nitroxides are stable free radicals that have a unique ability to behave as antioxidants through interaction with other free radicals. These biologically and biochemically relevant molecules have the ability to degrade superoxide[38, 39] and peroxide and undergo radical-radical interactions. They also have a unique ability to convert between the nitroxide radical, oxoammonium cation, and hydroxylamine forms,[38, 40, 41] shown in Figure 1.5. Their stability, high reactivity, and inter-conversion can be exploited to prevent oxidative degradation in UHMWPE. One valuable characteristic for UHMWPE radical scavenging is the ability of nitroxides to react with and scavenge a wide range of reactive species and to be regenerated efficiently back to the active form.[40]

As a class of antioxidants, nitroxides are commonly used as MRI contrast agents,[38] spin labeling reagents[41, 42], and electron paramagnetic resonance (EPR) probes, as well as superoxide dismutase (SOD) mimics[38, 40] and radioprotectants *in vivo*.[43] In cells, nitroxides can provide radioprotection in

millimolar concentrations.[43] As MRI contrasting and spin-labeling reagents, nitroxides yield information about the motion of biomolecules, membranes, and nanostructures.[41, 42, 44-47] Nitroxides are also used in living polymerizations called Nitroxide Mediated Radical Polymerization (NMRP) because the nitroxyl (NO) moiety has the ability to react with hydrogen bond donors.[48-51]

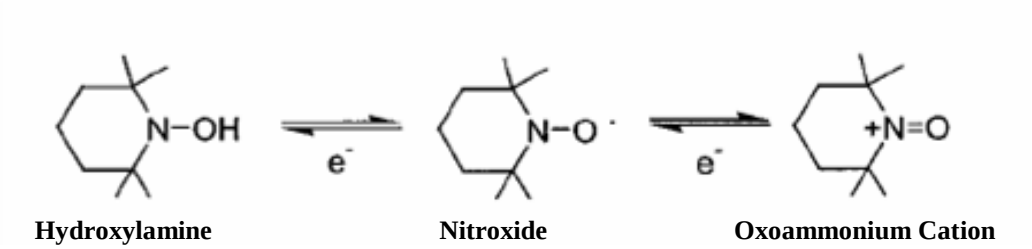

Figure 1.5: The reduction of the nitroxide radical to a hydroxylamine and oxidation to an oxoammonium cation. This reversibility may be exploited to scavenge many types of radicals, such as in UHMWPE.

Nitroxides have very long radical lifetimes, allowing efficient carbon–centered radical scavenging[52] and lipid peroxidation prevention.[38] The nitroxide radical can be very easily detected by EPR,[38] due to the unpaired electron interacting with the molecule's magnetically active nuclei.[42] Because the oxoammonium cation and hydroxylamine cannot be detected by EPR, it is easy to detect changes in concentrations of the nitroxide radical as well as its consumption and reaction with other species.

1.3.2.1 Free Radical Mechanisms

There are three mechanism by which the nitroxide (represented as >NO·) will be most efficient as an antioxidant in UHMWPE. The following reactions have been observed in lipid peroxidation prevention. Both lipid and polyethylene radicals are

carbon-centered, so a radiolytically-produced alkyl radicals in polyethylene should react with the nitroxide radical through the same radical-radical interactions to form a non-radical product, or >NOR[38, 40, 41, 53](equation 1.10). The peroxyl radical has been reported to react with the nitroxide radical through the electron-transfer mechanism to form non-radical products,[54] as shown in equation 1.11:

$$R\cdot + >NO\cdot \rightarrow >NOR \quad (1.10)$$

$$RO_2\cdot + >NO\cdot \leftrightarrow \text{intermediate} \rightarrow >N^+=O + RO_2^- \quad (1.11)$$

In addition, it is also proposed that a reduced hydroxylamine would be able to interact with the alkyl,[38, 54] alkoxyl[38], and peroxyl radicals, shown in equations 1.12-1.14, respectively, through the hydrogen transfer mechanism:

$$R\cdot + >NOH \rightarrow >NO\cdot + RH \quad (1.12)$$

$$RO\cdot + >NOH \rightarrow >NO\cdot + ROH \quad (1.13)$$

$$RO_2\cdot + >NOH \rightarrow >NO\cdot + ROOH \quad (1.14)$$

The nitroxides used in this research are 2,2,6,6-tetramethylpiperidine-1-oxyl (TEMPO) and 4-hydroxy-2,2,6,6-tetramethlypiperidine-1-oxyl (Tempol). Although the two molecules have very similar structures, TEMPO is more compatible with the hydrophobic environment of the UHMWPE chains, while Tempol is more hydrophilic, and thus less toxic. Toxicity will be discussed in the following section. Six-membered ring nitroxides are more reactive with radicals than five-membered rings.[55] Consequently, the TEMPO and Tempol molecules, shown in Figure 1.6, should exhibit rapid and efficient antioxidative behavior in UHMWPE.

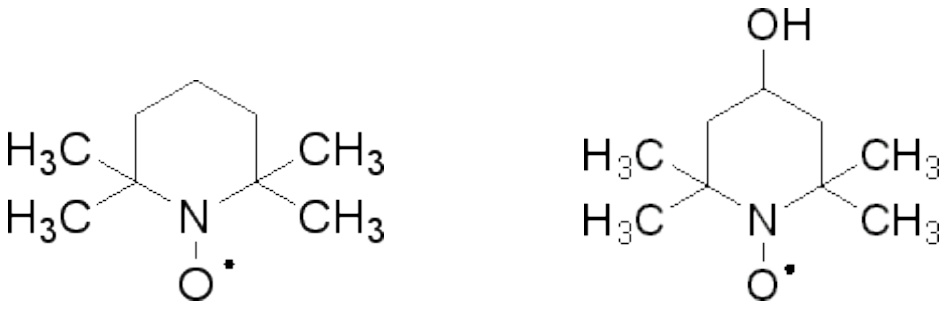

(a) (b)

Figure 1.6: Structures of a) 2,2,6,6-Tetramethylpiperidine-1-oxyl (TEMPO) and b) 4-Hydroxy-TEMPO (Tempol) to be used in this study.

1.3.2.2 Toxicity

The issue of nitroxide toxicity is complex. The toxicity of the nitroxide molecule depends on the structure of the molecule, its concentration in the tissue, and the cell type. Nitroxides are capable of permeating through cell membranes[56] and passing through the blood-brain-barrier.[57] These molecules have been found to act as radioprotectants in some cell types and to cause cell apoptosis in other cell types. For the most part, hypoxic cancer cells have shown to be responsive to the presence of nitroxides. The molecule TEMPO has been shown to cause apoptosis of breast cancer cells,[55] prostate carcinoma cells and to slow tumor growth in athymic mice.[58] At first glance, it seems that nitroxides provide radioprotection to healthy cells and cause cell death in cancer cells.

Some assessments of specific toxicity levels have been published. For example, Tempol (4-hydroxy-2,2,6,6-tetramethylpiperidine-N-oxyl) is found to have a maximum tolerated dose of 275 mg/kg in mice, despite its effective radioprotection *in vivo.*[59] There have not been any similar studies indicating a threshold in mice or other animals with TEMPO. Of course, toxicity and biocompatibility must be tested before a product containing a nitroxide would be available in a commercial product.

Researchers are developing the use of nitroxides for use in cancer treatments.[56, 58] Therefore, the cytotoxicity of these molecules will be determined as part of these studies. Furthermore, the TEMPO and Tempol molecules will be used in concentrations less than 10 mM and often in micromolar concentrations in this work, presumably enhancing the safety and effectiveness of these materials.

1.4 Alternative Methods

Some other alternatives to the post-irradiation thermal treatment or antioxidant infiltration presented here have been proposed in many different arenas. These alternatives involve such techniques as surface modification, creating a carbon nanotube-UHMWPE composite, sequential annealing, and grafting wear-resistant monomers to the UHMWPE surface.[60] Some surface modifications have involved ion implantation with nitrogen, helium, or creating a diamond-like coating (DLC) with carbon, hydrogen and argon. Another nanoscale modification uses photo-induced polymerization to graft 2-methacryloyloxyethyl phosphorylcholine (MPC) monomer to the UHMWPE surface.[61, 62] In addition, carbon nanotube composites have been investigated for improving mechanical properties[63] although biocompatibility of nanotubes for use in medical devices is still in question.[64] Other options to thermal treatments include sequential annealing.[9] This process involves irradiating the UHMWPE component to 30 kGy, then annealing at 130°C for 8 hours and repeating this procedure to a total absorbed dose of 90 kGy.[65] As a result, the sequential process allows free radical reduction at each cycle.

1.5 Global Objective

The global objective of this work is to investigate and develop the nitroxide as an antioxidant additive for ultra-high molecular weight polyethylene (UHMWPE) in order to increase the oxidation– and wear– resistance of UHMWPE liners for total joint replacements. The global hypothesis of this thesis is that the nitroxide will be a faster and more effective antioxidant for use in UHMWPE in total joint replacements, through the mechanism of carbon-centered radical scavenging by radical-radical interaction and the electron transfer mechanism. This thesis will explore whether nitroxides prevent oxidation in UHMWPE, experimentally show the mechanisms by which this occurs, and determine the final effect on the material microstructure and mechanical properties of the polymer.

1.5.1 Specific Hypotheses and Aims

1. Diffusion of the nitroxide molecule into UHMWPE can be performed at a controlled rate to produce a uniform distribution of the desired antioxidant concentration

- To quantify polyethylene doping and the resulting nitroxide concentrations using Fourier Transform Infrared (FTIR) spectroscopy and Electron Paramagnetic Resonance (EPR) spectroscopy
- Assess proper doping parameters to achieve a desired nitroxide concentration

2. Radiolytically-produced free radicals in UHMWPE will preferentially react with the nitroxide radical

- To investigate the reaction of the nitroxide with UHMWPE radicals by identifying and quantifying the type of free radicals observed by EPR, as a function of dose

3. Study of the reaction kinetics of free radicals in a solution of nitroxides in a liquid alkane pulsed with the electron beam will allow the understanding of the mechanism of the radical-radical interaction in UHMWPE

- To model polyethylene in a liquid hydrocarbon, octane will be used to measure the build up and decay of free radical transients by pulse radiolysis

4. Mechanical properties may change as a result of polymer modification and must be evaluated in order to propose the use of this antioxidant in total joint prostheses

- To evaluate the effect of nitroxides on the degree of crosslinking by Thermomechanical Analysis (TMA)
- To measure oxidation as a function of depth in bulk UHMWPE by three-dimensional FTIR mapping, after accelerated aging
- To determine the change in crystallinity of the polymer as a result of nitroxide modification by Differential Scanning Calorimetry (DSC).
- To test changes to tensile properties due to modification of the polymer

Chapter 2: Materials and Methods Used in the Investigation of Nitroxides for UHMWPE

The investigation of nitroxides as antioxidants for ultra-high molecular weight polyethylene (UHMWPE) involves the utilization of a number of analytical methods. Because these methods are used in several of the subsequent chapters, their descriptions are located here for easy reference. A description of the materials, irradiation facilities and instrumentation used to investigate the material property changes due to nitroxide infiltration into UHMWPE can be found below.

2.1 Materials

2.1.1 Ultra-High Molecular Weight Polyethylene (UHMWPE)

UHMWPE is provided by Biomet Inc. (Warsaw, IN) in the form of 1.75 inch diameter ram-extruded rods cut to 5 mm, 15 mm, and 24 mm thicknesses, forming a puck shape. The manufacturer specifies that this lot of UHMWPE possesses a density of 931 kg/m^3, a yield stress of 21.4 MPa, an ultimate tensile stress of 50.5 MPa, and an elongation at break of 362%. Samples are cut from the bulk material using a Leica RM2255 rotary microtome (Houston, TX) into 100 μm thin films or trimmed into 1 cm^3 cubes for accelerated aging. Pins for Electron Paramagnetic Resonance (EPR) are machined with a custom designed 1/8 inch diameter plug cutter. Samples for Thermomechanical Analysis (TMA) are machined into 1 mm thick strips. Pellets of 1 mm diameter are drilled from these strips, forming a cylindrical pellet with 1:1 height-to-width aspect ratio. Samples for Differential Scanning

Calorimetry (DSC) are cut with a 3.5 mm diameter die from bulk processed UHMWPE. Tensile dog bone specimens are cut with a custom die, proportionally most closely resembling ASTM Type III (ASTM Standard D638), from 3 mm thick machined UHMWPE strips.

2.1.2 Antioxidants

The nitroxides used in these studies were 2,2,6,6-tetramethylpiperidine-1-oxyl (TEMPO) and 4-hydroxy-2,2,6,6-tetramethylpiperidine-1-oxyl (Tempol) (Aldrich, Milwaukee, WI). These piperidine nitroxides have a six-member ring structure, as shown in Figure 1.5. The vitamin E used for comparison to the nitroxide molecules is DL-α-tocopherol (Sigma, Milwaukee, WI). UHMWPE samples are placed in a beaker containing vitamin E and heated to 100°C for either 30 minutes or 2 hours depending on the desired diffusion concentration, as described by Oral *et al*., and homogenized at 100°C.[66] Nitroxide diffusion/doping is addressed in section 3.4.

2.1.3 Solvents

The solvents used in conjunction with nitroxides were purged with with N_2 or argon. For nitroxide spin per gram calibration, *para*-xylene (Fluka Analytical Lot #1379138, Steinhein, Germany) is used to dilute TEMPO. For pulse radiolysis studies, electronic grade octane (Aldrich Chemical, Batch #16124AE, Milwaukee, WI) serves as a liquid hydrocarbon model. TMA analysis involves swelling specimens in decahydronaphthalene (Alfa Aesar, Lot #10115547, Heysham, Lancaster, UK).

2.2 Radiation Facilities

2.2.1 Cobalt-60 Gamma Source

Two ^{60}Co γ sources are used to irradiate, sterilize and crosslink UHMWPE. The original γ sources consisted of 26 kCi (September 1987) and 125 kCi (October 2007) ^{60}Co sources. The current activity is 1.33 kCi and 87.02 kCi (August 1, 2010), respectively. The ^{60}Co is doubly encapsulated in ten stainless steel pencils arranged in a planar or annular array for a diverse range of irradiation conditions. The 1.33 kCi source is arranged annularly, while the 87 kCi source is planar. Samples are placed in the vault at selected positions to produce the desired doses and dose rates. The older source, with a lower dose rate, is arranged in an annulus and the samples are placed in the center of the annulus for a uniform and maximized dose rate. A photo of the annular array at the bottom of the 14 foot pool is shown in Figure 2.1a and the top hat in the γ irradiation room in Figure 2.1b.

(a) (b)

Figure 2.1: The annular arrangement of the 1.39 kCi γ source at the bottom of the 14 foot pool of water (a) and the top hat of the pool (b). Specimens are placed in the center of the annulus and the ^{60}Co pencils are lifted to fit in the top hat, around the samples.

2.2.2 7 MeV Pulsed Linear Accelerator (LINAC) Electron Beam

The pulsed electron beam is a modified S-band clinical accelerator manufactured by Varian and modified by JM Company. This LINAC produces 3 μs pulses with peak currents up to 500 mA, with electron energies up to 9 MeV. For these experiments, the electron energy used was 7 MeV. It can be operated either in single pulse mode or to deliver a continuous train of pulses up to 330 Hz. The typical pulse repetition rate used for these experiments was 60 Hz. Photographs of the electron beam source and titanium target window are shown in Figure 2.2a and 2.2b, respectively. The electron beam exits the titanium window as a narrow pencil beam and spreads out away from the window. Consequently, the dose is high closer to the beam, with a small "spot" size. As distance is increased from the window, the dose begins to fall, yet the "spot" size increases as does the dose uniformity, both parallel and transverse to the beam. As a result, irradiations with the electron beam balance dose per pulse versus dose uniformity.

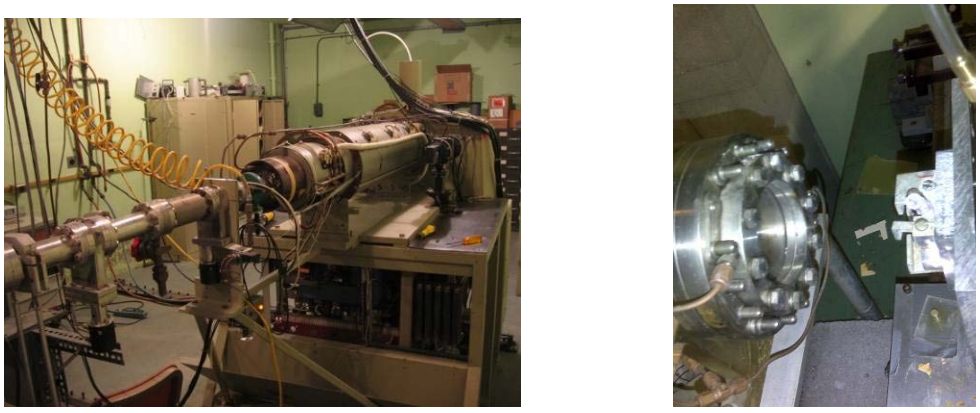

(a) (b)

Figure 2.2: The 7 MeV pulsed linear accelerator (LINAC). The electron beam source (a) and the titanium window (b) through which the pencil beam of electrons exit. Electrons are heated off of a tungsten filament and accelerated and steered down the beam to the titanium window. The pencil beam is narrow where it exits this thin window. While the dose falls with increasing distance, the dose uniformity as a function of depth increases.

2.2.3 6 MeV LINAC Electron Beam at the Notre Dame Radiation Laboratory

A second LINAC facility used is located at the Notre Dame Radiation Laboratory. This system utilizes a variable pulse width (from 2 ns to 1.5 μs) and 6 MeV electron energies. This facility is used for pulse radiolysis which will be detailed in section 2.6. The 6 MeV LINAC has a 20 MW, 2856 MHz klystron RF source. The pulsed frequency is 1 to 10 Hz or the LINAC can perform single pulses. The maximum beam current is 4 amps and the nominal beam diameter is 5 mm. The pulse-to-pulse dose stability is ±3%. The 6 MeV LINAC (2.3a) and monochromator and photomultiplier (2.3b) are shown in Figure 2.3. A series of lenses reflects the xenon light around a corner from the light source to the monochromator.

(a) (b)

Figure 2.3: Photographs of the 6 MeV LINAC at the Notre Dame Radiation Laboratory. The LINAC (a) and monochromator and photomultiplier (b) used in pulse radiolysis experiments detailed in sections 2.6 and 4.2.

2.3 Dosimetry Methods

2.3.1 Far West Films

The dosimetry method used to measure absorbed dose for electron beam irradiations is Far West Film dosimetry (FWT-60, Far West Technology, Inc., Goleta,

CA). These 42.5 μm thin colorless radiachromic films are derivatives of the family of aminotriphenyl-methane dyes that turn to a deeply colored state as a function of absorbed dose. Specifically, these dosimeters use a hexa(hydroxyethyl) aminotriphenylacetonitrile (HHEVC) dye. Their absorbed radiation dose range is 0.5 to 200 kGy and they are measured by observing the color change at 510 nm or 605 nm in a UV-visible spectrophotometer (section 2.5). The thickness of the Far West films is measured with a digital thickness gauge (Mitutoyo, Aurora IL). The absorbance is measured before and after irradiation, and then divided by thickness, as shown in Equation 2.1:

Far West Film response =

$$(A_{\text{irradiated, 605 or 510 nm}} - A_{\text{initial, 605 or 510 nm}})/\text{thickness (mm)} \qquad (2.1)$$

The wavelengths 605 nm and 510 nm are used for different absorbed dose ranges, 0.5 – 20 kGy and 20 kGy – 200 kGy, respectively. At 605 nm, the value calculated from equation 2.1 is compared to a calibration chart to find the absorbed dose. Dosimetry for irradiations above 20 kGy uses films measured at 510 nm and the calculated value is input into the formula in equation 2.2 derived from a calibration:

$$\Delta A/\text{mm} = 0.0973\ (\text{Absorbed dose, kGy}) + 1.6539 \qquad (2.2)$$

For electron beam irradiation, the calculated absorbed dose from either wavelength is divided by the number of pulses, used to obtain the absorbed dose in Gy/pulse.

2.3.2 Alanine Dosimetry

Alanine (Ala) is a crystalline α-amino acid that acts as a natural dosimeter in response to ionizing radiation. Upon irradiation, it forms an alkyl free radical whose paramagnetic concentration can be used to measure absorbed radiation dose. Alanine pellet dosimeters (FWT-50, Far West Technology, Inc., Goleta, CA) are compacted with binder and exhibit a very stable electron paramagnetic resonance (EPR) signal when irradiated to an absorbed dose of 2 Gy to 200 kGy and maintained in a controlled humidity and temperature environment. They exhibit a linear dose response to 3 kGy and higher doses are measured using a calibration curve, as specified in ISO/ASTM Standard 51607: Standard Practice for Use of an Alanine-EPR Dosimetry System. The structures of alanine and of the three possible alkyl radicals are shown in Figure 2.4. The primary radical type 2.4b comprises 55 – 60% of the total, and radical 2.4c and 2.4d are 30 – 35% and 5 – 10% of radicals, respectively.

The calibration curve is constructed according to standard specifications where the alanine dosimetry batch variability is determined and a calculated number of dosimeters are irradiated at each dose decade. The signal is then measured with the EPR (section 2.4), according to parameters described in the standard. The central peak-to-peak heights are calculated and a calibration curve is compiled (Figure 2.5), which is used to measure the absorbed dose of test samples.

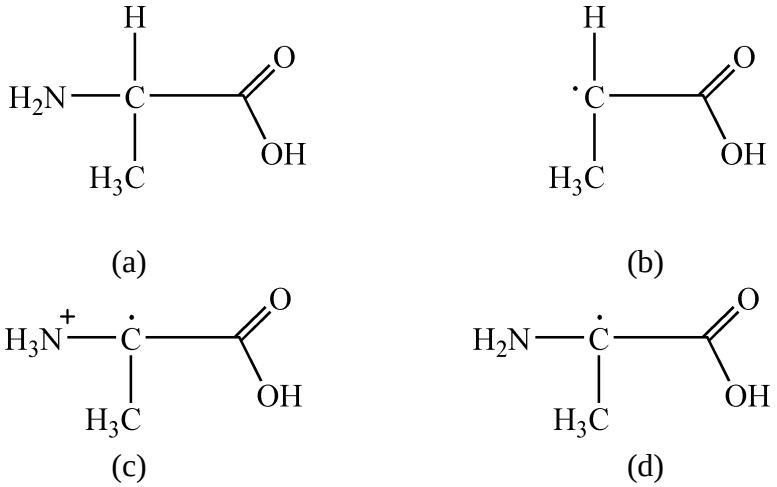

Figure 2.4: Structures of the amino acid alanine (a) and its alkyl free radicals that are formed proportional to absorbed dose. The radical type 1 (b) forms 55-60% of radicals, and there are 30-35 % of type 2 (c) and 5-10% of type 3 (d). Pellets of alanine (Far West Technology, Inc.) are irradiated in decades of absorbed dose and the free radical response, measured by EPR, is plotted to generate a calibration curve.

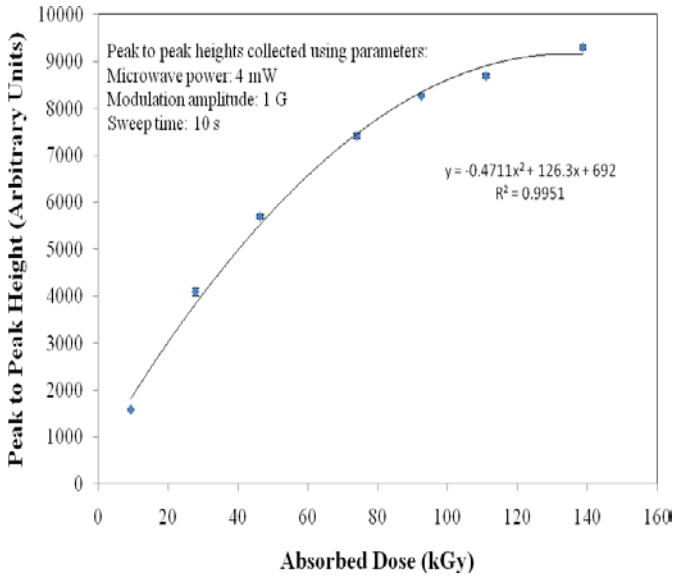

Figure 2.5: Calibration curve of Far West alanine pellet dosimeters (FWT-50-10 Lot T030901). After determining the variability of a batch of dosimeters, a specified number are used at each decade of radiation absorbed dose. The free radical spectra peak-to-peak heights (collected with parameters from ISO/ASTM 51607) are plotted for each absorbed dose. This curve is used to correlate experimental absorbed doses to a known response of the alanine dosimeters.

2.3.3 Potassium Thiocyanate

Potassium thiocyanate (KSCN) dosimetry is used to determine the absorbed dose per electron beam pulse with the pulse radiolysis system. In this system, an aqueous solution of KSCN pulsed with electrons produces a transient absorbance peak at 480 nm. The transient species is the formation of the $(CNS)_2^-$ ion from the $^{\bullet}OH$ radical, as shown in equations 2.3 and 2.4:[67]

$$^{\bullet}OH + CNS^- \rightarrow OH^- + CNS \quad (2.3)$$

$$CNS + CNS^- \rightarrow (CNS)_2^- \quad (2.4)$$

The $(CNS)_2^-$ species has a molar absorptivity of 710 $m^2 \cdot mol^{-1}$ which decays with a rate constant of 3×10^6 $m^3 \cdot mol^{-1}$. The dose is calculated from equations 2.5 and 2.6. In equation 2.5, $G(CNS)_2^- \cdot \varepsilon$ is the product of the *G*-value for $(CNS)_2^-$ and the molar absorptivity, l is the optical length (2 cm) of the solution cell, and ρ is the density of the solution.

$$\text{Absorbed dose} = A / (G(CNS)_2^- \cdot \varepsilon \cdot l \cdot \rho) \quad (2.5)$$

$$\text{Dose (Gy/pulse)} = \log (V_o/V) \cdot 21932.25 \quad (2.6)$$

A solution of 1 g KSCN per 500 mL of deionized H_2O is made. The sample cell, shown in Figure 2.6a, is filled with KSCN solution and placed in the intersection of the electron beam and Xe lamp. The photomultiplier is set at 480 nm and an initial absorbance and pulsed absorbance are measured. An example KSCN dosimetry trace is shown in Figure 2.6b.

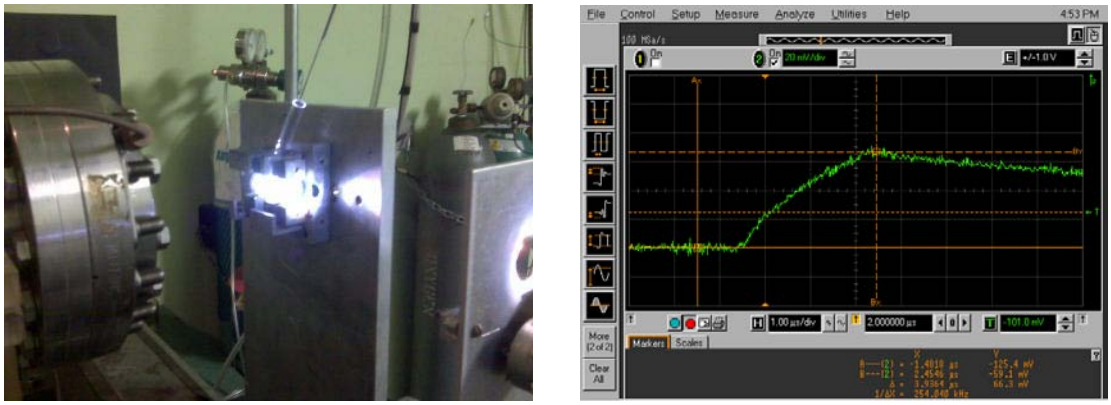

(a) (b)

Figure 2.6: KSCN dosimetry set-up with the solution cell sitting at intersection of Xe light and LINAC electron beam paths (a) and the oscilloscope trace showing the $(CNS)_2^-$ ion build-up and decay (b). The absorbance amplitude is recorded (measured in millivolts) and the ratio of the initial to final voltages is input into equation 2.6 to generate a measure of dose/pulse. This example trace shows a 71.5 Gy/pulse dose collected at 480 nm with 900 V amplification.

2.4 Electron Paramagnetic Resonance (EPR) Spectroscopy

2.4.1 Introduction and Theory

The EPR technique, also called Electron Spin Resonance (ESR) spectroscopy, is a tool used in many biochemical and biomedical applications. EPR can be used for dosimetry and identification and detection of paramagnetic species and for the detection of radical intermediates and kinetics. This makes EPR an excellent tool to detect the production of radiolytically-produced free radicals in UHMWPE. EPR can identify and quantify the concentration of diffused nitroxide, and measure the consumption or reaction of these radicals. Furthermore, the kinetics of nitroxide – UHMWPE radical-radical interactions can be determined. Most of the nitroxide concentration measurements are made with the EPR because it is a more sensitive method than UV-vis or FTIR.

EPR spectroscopy is based on the magnetic properties associated with an unpaired electron. The paramagnetic specimen is placed in a uniform magnetic field, which orients the unpaired electron with respect to the field. The orientation is parallel or antiparallel and all free radicals orient to one of these two possible states, with a slightly energy difference between them. At ambient temperatures, more electrons fill the lower energy state and that number increases as the temperature is lowered. The energy between the two states ΔE is given by equation 2.7:

$$\Delta E = h\nu = g\mu_B B_o \qquad (2.7)$$

where h is Plack's constant, υ is the frequency of radiation, B_o is the magnetic field, μ_B is the Bohr magneton, equal to 0.927×10^{-20} erg G^{-1}, and g is the spectroscopic splitting factor, a dimensionless number whose value depends upon the environment of the unpaired electron and equals 2.0023 for a free electron. The sample is subjected to electromagnetic radiation with a frequency υ causing the unpaired electrons to reverse their orientation with respect to the magnetic field according to the Zeeman effect. As there are more electrons in the lower-energy state, there is a net absorption of radiation energy, which can be observed as a spectroscopic absorption line which increases linearly with the magnetic field strength. In practice, the frequency is maintained at a constant value and the magnetic field strength is varied by means of small secondary coils so as to sweep across the value corresponding to maximum absorption. The size of the signal is defined as the integrated intensity or the area beneath the absorption curve, which is proportional of the concentration.

2.4.2 Instrument Set-up and Parameter Selection

The Bruker ESP 300 EPR spectrometer (Billerica, MA) operates in the X-band (9-10 GHz). The EPR parameters and their selection are discussed below. Peak to peak heights and double integrations of spectra are used to measure signal intensity. This intensity is then compared to a known calibration curve (presented in Chapter 3).

2.4.2.1 Power

Paramagnetic signal analysis requires the setting of instrument parameters according to the type of radical to be measured. Up to a saturation point, signal intensity increases linearly with the square root of the power. Increasing microwave power further will broaden the signal, distorting the lineshape (power saturation) leading to inaccurate quantitative measurements. The highest power at which the signal intensity still increases linearly with the square root of power gives the most accurate results. The highest power that results in a linear increase in signal height gives the most sensitive results.

This relationship is investigated for nitroxide radicals and for carbon-centered free radicals in UHMWPE. The increase in peak-to-peak height and the integrated signal intensity are evaluated, yielding the same relationship. This phenomenon is heavily dependent on the solvent or material matrix in which the radical is present. For example, Figure 2.7 demonstrates the signal intensity of TEMPO radical with power saturation in *para*-xylene (2.7a). Power saturation of TEMPO in UHMWPE (2.7b) and of carbon-centered (allyl) free radicals in UHMWPE (2.7c) is more

dramatic. These plots are collected through a measure of peak-to-peak signal intensity at each power setting.

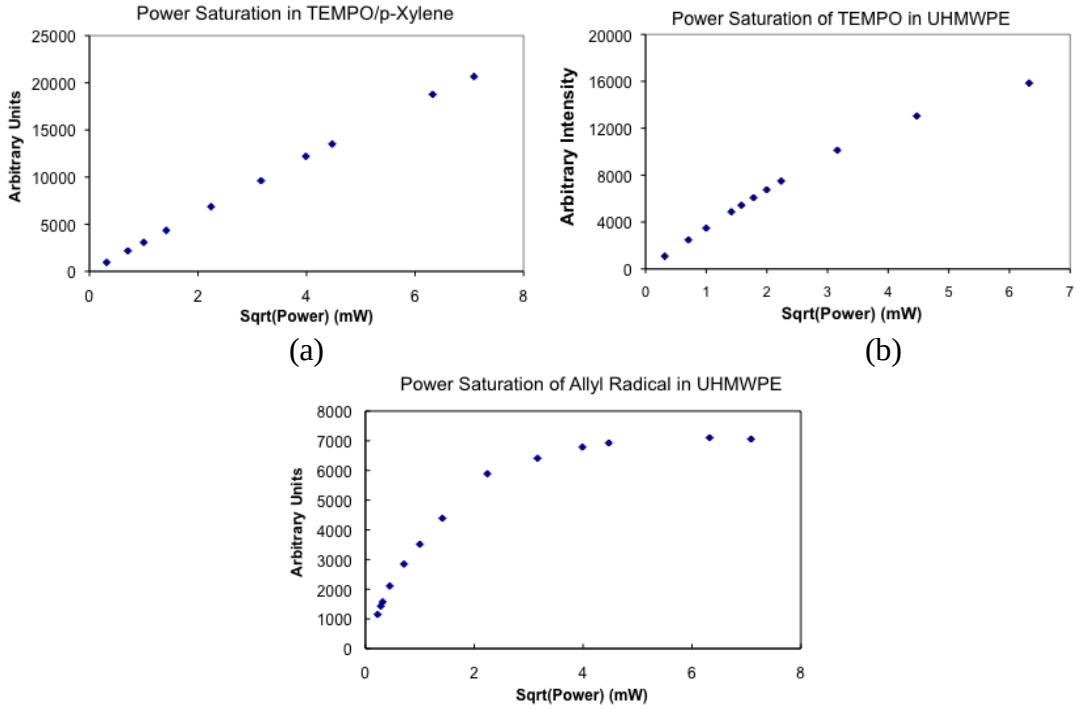

Figure 2.7: Power saturation of a) TEMPO radical in *para*-xylene, b) TEMPO radical in UHMWPE and c) allyl and other carbon-centered free radicals in UHMWPE. Power modulation is calculated as a measure of peak-to-peak height. The highest power at which a signal intensity increases linearly with the square root of the power gives the most accurate results.

Considering these radicals power saturate at different power levels, collection of spectra with a mixture of radicals is possible but accurate quantification is challenging. Although Figure 2.7a does not drastically respond to power, there is a deviation from linearity at around 10 mW. This occurs at 5 mW for the TEMPO radical in UHMWPE and as low as 0.2 mW with the carbon-centered free radicals in UHMWPE. With this wide range of power saturation levels, one of the two radicals will either be oversaturated or under-magnified at these two power levels. The best protocol is to collect spectra at 5 mW for accurate nitroxide radical quantification and

to repeat measurements at 0.2 mW when quantifying carbon centered free radicals. Most spectra in this study are collected at 5 mW for nitroxide spin per gram calculation.

2.4.2.2 Modulation Amplitude

Up to a saturation point, increasing modulation amplitude linearly increases the signal height and beyond the signal becomes overmodulated, and the lineshape is distorted. However, unlike power saturation, the area under the curve remains unchanged, even in overmodulated signals. The overmodulation of the free radical species encountered in this work is assessed with a measure of the peak-to-peak signal intensity measure.

Overmodulation is investigated in nitroxide radicals and in carbon-centered free radicals of UHMWPE. This phenomenon is heavily dependent on the type of radical present. For example, Figure 2.8 demonstrates the signal intensity of TEMPO radical with overmodulation in *para*-xylene (2.8a), UHMWPE (2.8b) and of carbon-centered free radicals in UHMWPE (2.8c).

Both the TEMPO radicals in *p*-xylene and UHMWPE exhibit rapid overmodulation at low modulation amplitudes. The allyl or carbon-centered free radicals present in UHMWPE also overmodulate, but at much higher amplitudes.

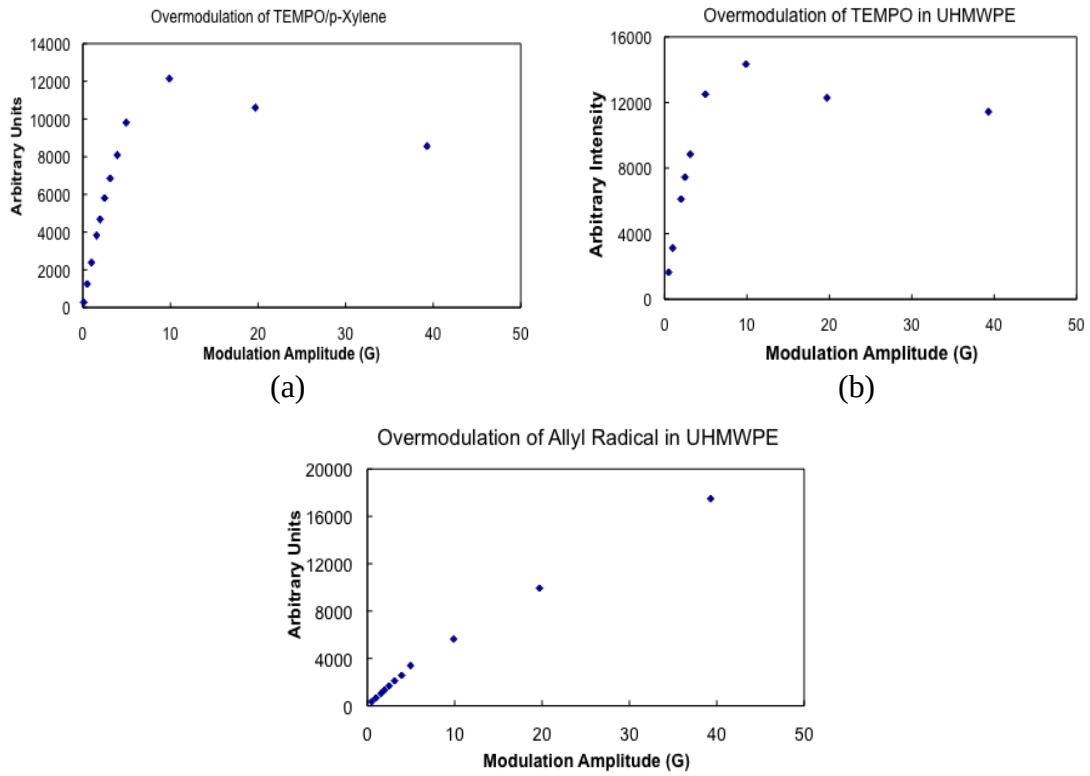

Figure 2.8: Overmodulation of a) TEMPO radical in *para*-xylene, b) TEMPO radical in UHMWPE and c) allyl and other carbon-centered free radicals in UHMWPE. Modulation amplitude overmodulation is measured as signal peak to peak height. Overmodulation is manifested in lineshape distortion which can alter double integrated areas used to quantify radicals.

2.4.3.3 Parameters

After investigating the power and modulation amplitude settings, the parameters outlined in Table 2.1 are used to collect spectra of paramagnetic species in these studies. The receiver gain is adjusted as necessary to magnify the signal and does not have an effect on the lineshape or linewidth.

Table 2.1: Parameters for EPR Spectra Collection of Nitroxide and Carbon-Centered Free Radicals in UHMWPE		
Parameter	*Setting*	*Units*
Power	5	mW
Modulation Amplitude	3.12	G
Modulation Frequency	100	kHz
Time Constant	20.48	ms
Conversion Time	20.48	ms
Resolution	1024	--

2.5 UV-Visible Spectrophotometry

2.5.1 Introduction and Theory

Spectroscopy in the ultraviolet (UV) and visible range is often used to identify chemical species. UV and visible wavelength lamps project a beam with 200 nm – 800 nm through a sample of a specified pathlength, *l*. According to the Beer-Lambert Law, the absorbance of a species of *c* concentration, with ε molar absorptivity, is equal to (equation 2.8):

$$A = l \cdot c \cdot \varepsilon \qquad (2.8)$$

The Beer-Lambert principle is used to obtain the absorbance and change in absorbance at specific wavelengths. This method is used to measure the absorbed dose by Far West dosimetry (section 2.3.1) as well as confirm the nitroxide radical concentration for the EPR calibration curve (section 3.3).

2.5.2 Experimental Method

The Varian Cary 3 (Palo Alto, CA) UV-visible spectrophotometer is used to identify the absorbance of solutions or thin films. The instrument is set to a specific

wavelength and a control cuvette placed in the reference position. An empty cuvette of 1 cm path length is placed in the experimental position and the reading is zeroed. The absorbance of an experimental sample is recorded at a fixed wavelength or a spectrum taken from 200 – 800 nm. Sample absorbance can be used for dose calculations or for calibrations.

2.6 Pulse Radiolysis

2.6.1 Introduction and Theory

Pulse radiolysis is used to identify transients and radiolysis events on time scales less than 10 ms. As the electron beam is pulsed, electrons incite transient species in the specimen whose absorbance is measured with a photomultiplier and xenon light. A computer and oscilloscope system are used to capture traces of the build-up or decay of a species at a specified wavelength, depending on the time-scale of the reaction. A series of optical lenses are used to focus the light through the sample holder to the photomultiplier. Reactions occurring just after the electron pulse are observed. For example, absorbance of rapid reactions that occur on time scales less than nanoseconds will be obscured by the Cherenkov radiation gap, where the photomultiplier is unable to capture a signal due to Cherenkov light emission. Therefore, shorter electron beam pulses are necessary to capture such events. To capture rapid alkyl radical decay, the pulse radiolysis system at Notre Dame Radiation Laboratory is used which utilizes a variable pulse width (from 2 ns to 1.5 μs), as described in section 2.2.3. The 6 MeV Linear Accelerator employs a computer system that collects data on ten time-frames simultaneously.

To investigate the kinetics of TEMPO reaction with UHMWPE carbon-centered free radicals, octane is used as a liquid hydrocarbon model. TEMPO is dissolved in octane and the build-up and decay of transients are recorded with and without the antioxidant.

2.6.2 Experimental Method

Dosimetry using potassium thiocyanate (KSCN) aqueous solution (section 2.3.3) is performed prior to collecting data. This dose per pulse data is then used for the experimental samples. Solutions containing 0.01 mM, 0.05 mM, 0.1 mM, 0.2 mM, 1.0 mM TEMPO/octane are mixed. Electronic grade octane (Aldrich, St. Louis, MO) is purged with nitrogen for 5 – 10 minutes in the sample cell.

The neat octane and TEMPO/octane solutions are pulsed with 30 ns pulses with approximately 10 Gy/pulse. Transient absorbance is collected over a range 230 nm – 350 nm. Time frames of data collection are 100 ns, 200 ns, 500 ns, 1 μs, 2 μs, 5 μs, 10 μs, 20 μs, 50 μs, and 100 μs with each longer scale consisting of averaged points from the previous scale. The same point averaging is used to record 100 μs, 200 μs, 500 μs, 1ms, 2 ms, 5 ms, 10 ms time scales. Some points consist of four or five pulse averages, as indicated. The data are then fit to first or second order kinetics.

2.7 Thermomechanical Analysis (TMA)

2.7.1 Introduction and Objective

The introduction of antioxidants into UHMWPE prior to irradiation can reduce the extent of crosslinking. This is due to the reaction of antioxidants with

carbon-centered free radicals in UHMWPE, competing with the bimolecular crosslinking reaction (see section 1.2.2 and 5.2). With increasing ionizing radiation dose, more alkyl radicals will immediately bimolecularly crosslink which produces a three-dimensional gel that cannot be dissolved. To measure the extent of crosslinking, TMA uses a linear variable differential transformer (LVDT) to mechanically measure the changes in sample height before and after swelling. This swelling is performed at 140°C in decahydronaphthalene (decalin).

2.7.2 Experimental Method

UHMWPE pucks are machined into 1 mm thick strips. Samples of 1 mm diameter are drilled from these strips, forming a cylindrical pellet with 1:1 height-to-width aspect ratio. Pellets are packaged in argon, and irradiated to varying total absorbed doses, using a 7 MeV pulsed electron linear accelerator (LINAC) and ^{60}Co gamma. The electron beam irradiations are performed using 60 pulses·s^{-1}, with ~8 Gy·pulse^{-1}. The gamma irradiations are performed at 27.5 kGy·h^{-1} dose rate. Four to five samples are used for each irradiation dose and annealing condition. In an adaptation of ASTM Standard F2214, the samples are swelled in decalin in a Mettler Toledo TMA/SDTA841e Thermomechanical Analyzer until equilibrium is reached within 100 minutes. The swell ratio, q_s, crosslink density, ν_d, and molecular weight between crosslinks, M_c, are calculated for each sample as described in section 5.2. A schematic showing how the swell ratio is measured is shown in Figure 2.9b while a photograph of the quartz sample holder is shown in 2.9a.

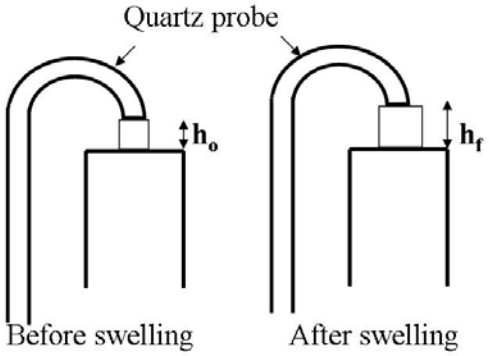

(a) (b)

Figure 2.9: A photograph of the quartz specimen holder and probe of the Mettler Toledo TMA/SDTA 841e (a) and schematic of specimen height measured by TMA before and after swelling to calculate the swell ratio (b) after swelling in decalin solvent at 140 °C. The swell ratio is then used to calculate the crosslink density and molecular weight between crosslinks.

2.8 Differential Scanning Calorimetry (DSC)

2.8.1 Introduction and Theory

The thermal properties and crystallinity of UHMWPE are measured by DSC. The crystallinity of a polymer sample are measured by the difference in heat flow between the sample and a blank reference pan as the temperature is increased or decreased across the sample's melting point, T_m, or the glass transition temperature, T_g. For UHMWPE, the T_g is -160°C so the polymer exhibits plastic flow rather than being glassy (as below the T_g). A typical DSC experiment measures the melting of UHMWPE crystals past the T_m and then cooling to measure the crystallization temperature, T_c. Through the heat flow divided by sample mass, ΔH_s (J/g), the percent crystallinity, φ, can be calculated by equation 2.9:

$$\varphi = \frac{\Delta H_{s,J/g}}{289.3 J/g} \cdot 100 \qquad (2.9)$$

Each series of heating and cooling cycles identifies different polymer properties. The first melt determines crystallinity and T_m due to thermal processing of the specimen. Cooling from the melt at a standard rate recrystallizes the polymer. A second melting cycle measures the inherent polymer properties by erasing the thermal history.

2.8.2 Experimental Method

A TA Q100 Differential Scanning Calorimeter is used to measure the T_m and the φ, percent crystallinity of UHMWPE specimens. A die with a 3.5 mm inner diameter is used to cut samples from bulk-processed material. These 3.5 mm diameter cores are then cut into thin sections, weighed with a microbalance having 0.0001 g resolution, and crimped in an aluminum DSC pan. This sample pan is placed in the DSC with an empty reference pan. Nitrogen (50 ml/minute) is used to purge the system before and during measurements. To measure the ΔH_s, a flat baseline is extrapolated from 50 ºC to 160ºC and the area under the curve is integrated and divided by the sample weight. The following thermal cycles are used:

First heat: 40ºC to 200ºC at 10ºC/minute, held at 200ºC

Cool: 150ºC to 40ºC cooled at 10ºC/minute, held at 40 ºC

Second heat: Repeat first heat and then quench to room temperature

Statistical analysis is performed with StatPlusMac LE software to calculate *p*-values of significance. The Student's T-test compares heteroscedastic means (uneven variances) with a two-tailed distribution calculated with a reliability level $\alpha = 0.05$.

2.9 Fourier Transform Infrared (FTIR) Spectroscopy

2.9.1 Introduction and Theory

Changes to UHMWPE specimen chemistry are analyzed using FTIR spectroscopy. IR exploits molecule absorption at specific wavenumbers. Various vibrational modes are IR active, such as symmetrical and anti-symmetrical stretching, rocking, wagging and scissoring of the bond between two atoms. The absorption data for UHMWPE specimens is collected in transmission mode through a thin film of the material. The formation of *trans*-vinylenes from absorbed radiation dose, the formation of oxidation products such as carbonyls and concentrations of diffused antioxidants are quantified using this technique. The species of interest, shown in Table 2.2, relate to these chemical changes. The area under each species absorbance is used to identify and quantify changes to UHMWPE. While the NO moiety (1340 cm^{-1}) would be useful to identify nitroxide concentrations, the peak overlaps too much with the skeletal absorbance at 1370 cm^{-1}. Also, the C-N stretch has a low molar absorptivity, ε, and does not yield quantitative results for low concentrations. Thus, EPR is a more sensitive method to identify the concentrations of nitroxides.

Table 2.2: Chemical Species Identified by Fourier Transform Infrared (FTIR) Spectroscopy for UHMWPE Irradiated by Ionizing Radiation and Diffused with Antioxidants

Species	Occurance	Center (cm^{-1})	Start (cm^{-1})	End (cm^{-1})
Skeletal C-H[68, 69]	Backbone	1370	1394	1330
CH_2 Rocking	Backbone	1895	1940	1866
Carbonyl	Oxidation	1718	1847	1670
Trans-vinylene[70]	Absorbed Dose	965	979	946
α-tocopherol[8]	Diffused Vit E	1275	1278	1230
NO Moiety[68, 69, 71, 72]	Nitroxides	1340	-	-
C-N Stretch[68]	Nitroxides	1130	1149	1122

2.9.2 Sample Preparation

Cubes used for FTIR analysis after accelerated aging are microtomed (Leica RM2255) by trimming material until the desired 1.0 cm^3 size. After irradiation, processing and accelerated aging, the cubes are cut from one side in 100 μm sections. The first (top surface) 100 μm, 10^{th} (1 mm depth), 25^{th} (2.5 mm depth), and 50^{th} films (5.0 mm depth) are collected and analyzed by FTIR analysis (Thermo Nicolet 4700 FTIR with Microscope Attachment and MCT/A detector). An average of 64 scans is collected with 1.928 cm^{-1} data spacing, a resolution of 4 and with data collection from 4000 cm^{-1} to 650 cm^{-1}. Scans are corrected for H_2O and CO_2 presence.

Several thin films are lined up on the microscope stage. The x-y coordinates of each film are recorded and scans are collected every 100 μm, creating a spectral map of the films. This produces approximately 100 points per film (total width of 10 mm). FTIR of the 3 mm puck cross-sections (section 7.4.1) are collected with a 50 μm data spacing and 5 mm puck cross-sections (section 6.4) are collected with 75 μm data spacing. The FTIR absorbance data are processed by the OMNIC software. This data is then converted into individual spectra and processed by TQ Analyst software which automatically integrates the areas under the peaks of interest in Table 2.2.

2.10 Accelerated Aging

2.10.1 Introduction and Objective

Accelerated aging of UHMWPE samples for comparing materials used in surgical implants is thoroughly described in ASTM Standard F2003. This method uses an elevated temperature and oxygen pressure, to accelerate oxidation in

UHMWPE and to evaluate long-term chemical and mechanical stability. Although this method cannot estimate a material shelf life or possible lifetime in the patient, it is an effective method for ranking materials according to their oxidation-resistance. Thus, the objective of this method is to evaluate the long-term effects of oxygen and oxidation on UHMWPE and to rank the oxidation resistance between virgin UHMWPE, nitroxide-infiltrated and vitamin E-infiltrated specimens.

2.10.2 Experimental Method

After irradiation and processing, the 1 cm^3 cube specimens are conditioned at room temperature for at least 24 hours. Aging is performed in a vessel called an oxygen bomb (Millipore XX6700P10, Billerica, MA), which was validated according to ASTM F2003. This validation protocol requires a temperature of 70 ± 1°C and internal pressure ± 1°C over the course of the 336 hours. The validation process also shows that each specimen set has to be aged separately because of evidence of nitroxide contamination in control specimens (section 6.4.4). A photograph of the specimens in the oxygen bomb is shown in Figure 2.10a and the oxygen bomb in the oven is shown in Figure 2.10b. The vessel is closed and purged with 60 psi of O_2 three times. Finally, the oxygen bomb is pressurized with oxygen to 62 psi, heated at 1°C/minute to a maintained temperature of 70 ± 1°C to accelerate the aging process that would normally occur on the shelf. The pressure is increased to 73 ± 1 psi and maintained within this range for 14 days (336 ± 1 h). The specimens are placed in a metal gauze box constructed to separate samples and to allow for oxygen contact with all specimen sides for homogenous aging. The oxidation index, as calculated by

ASTM standard F2102 (section 6.1), increases as the material becomes oxidized. Measurement of the oxidation index through the depths of the specimen ensures the oxidation profiles are evaluated. These methods can determine if the antioxidants are effective in reducing oxidation levels and hence minimize mechanical property changes.

(a) (b)

Figure 2.10: The oxygen bomb (Millipore, Billerica, MA) set-up used to pressurize specimens with O_2 gas at an elevated temperature. This artificial aging process accelerates the aging and oxidation process. Accelerating aging occurs at 70 ±1 °C at 73 ± 1 psi O_2 for 14 days (336 ± 1h) as according to ASTM Standard F2003. The specimens are placed inside the oxygen bomb (a) which is placed in the oven (b) where the temperature and pressure are closely monitored.

2.11 Tensile Testing

2.11.1 Introduction and Theory

The addition of antioxidants can affect mechanical properties, either by acting as a plasticizer and increasing polymer chain movement, or by blunting the propagating fatigue crack. While there are many mechanical testing methods that can be used to evaluate the effect of antioxidants and thermal processing methods, some

like fatigue testing take months and require specialized equipment. Therefore, the most expedient method to measure quantitative changes in mechanical properties is tensile testing.

Testing the polymer in uniaxial tension allows the exploration of a number of different mechanical properties of UHMWPE. First when the tensile specimen is pulled in tension, a linear elastic region (Young's modulus or the modulus of elasticity) is exhibited on a plot of stress versus strain, which can be calculated from equation 2.10, where engineering stress, σ_{eng}, is the load divided by initial area, and the engineering strain, ε_{eng}, is the change in sample length divided by the initial length:

$$E = \frac{\sigma_{eng}}{\varepsilon_{eng}} = \frac{load/area_i}{\Delta length / length_i} = \frac{P/A_o}{\frac{l_f - l_o}{l_o}} \tag{2.10}$$

After this linear elastic behavior, the polymer reaches the yield strength, σ_{YS}, and begins to deform plastically where the polymer structure becomes oriented. Finally, the polymer will fail at the ultimate tensile strength, σ_{UTS}. The area under the curve represents the toughness of the material.

2.11.2 Experimental Method

To test the tensile properties of UHMWPE, specimens are cut from the materials received from Biomet, Inc. Specimens are machined to a thickness of 3 mm from the 5 mm UHMWPE pucks received. These specimens are then cleaned with acetone and sonicated in deionized H_2O for 10 minutes each. Dried specimens are packaged in N_2 in the LabMaster 130 glove box (MBraun, Stratham, NH) using

aluminized polyethylene foil (MIL-B-131H, Bell Fibre Products Corp., Columbus, GA). Specimens are irradiated to 62 kGy and 110 kGy using the low dose rate ^{60}Co γ. Specimens are then remelted at 150 °C, doped with α-tocopherol or TEMPO or Tempol at 100 °C. After processing, samples are aged (section 2.10). After aging, dog bone specimens are cut with a custom die. The specimens are tested with an Instron 33R4465 material testing machine at 5 mm/min ramp rate and 1 kN load cell.

Statistical analysis is performed with StatPlusMac LE software. Basic statistics comparing means between two sample groups, with uneven variances (heteroscedastic) are used to calculate *p*-values of significance. The Student's T-test with a two-tailed distribution is calculated with a reliability level $\alpha = 0.05$.

Chapter 3: Nitroxide Methods Development

3.1 Introduction

To develop a novel UHMWPE containing nitroxide antioxidants and to evaluate the resulting property changes, the diffusion of the molecule into the polymer should be performed in a controlled manner. Vitamin E has been successfully diffused into UHMWPE using two methods. The first is consolidation with the polymer resin prior to compression molding, irradiation or machining.[73] While this produces a homogeneous distribution of antioxidant at a predetermined concentration, the degree of crosslinking is reduced,[33, 35, 74] along with wear-resistance. The second method of introducing α-tocopherol into UHMWPE is through diffusion at an elevated temperature.[8, 75] Pre-determined quantities of vitamin E diffuse into the polymer immersed in pure liquid α-tocopherol at a controlled temperature and diffusion time, according to preliminary work by Oral *et al*. The vitamin E will be concentrated at the surface and so a homogenization step is used to distribute the α-tocopherol throughout the bulk, by heating for some time in an inert environment or in vacuum. For nitroxide diffusion, the doping method is used because the UHMWPE provided by Biomet, Inc. is compression molded bar stock, ready for irradiation and machining into an acetabular liner. This chapter explores the possible methods to infiltrate UHMWPE with nitroxides and the resulting concentrations that are produced.

Additionally, in order to quantify the concentrations of nitroxide radicals in UHMWPE, the molar absorptivity, ε, of TEMPO in any of the solvents used is

determined. The ε is used in conjunction with UV-visible spectroscopy to quantify and confirm the concentration in solutions used for infiltration and to build a calibration curve for EPR spectroscopy. The latter involves correlating the absorption of TEMPO concentration in xylene to the paramagnetic signal observed in the EPR.

3.2 Molar absorptivity, ε, of nitroxides

Using the Beer-Lambert law (equation 2.8) and the molar absorptivity, ε, of TEMPO in a given solution, the concentration can be calculated from the UV-visible absorbance. The molar absorptivity is determined for TEMPO solutions in octane, *p*-xylene, and d-H_2O at various concentrations. Once the ε is known, those solutions can be used for calibration curves for EPR and doping solutions.

3.2.1 TEMPO in d-H_2O

One of the doping methods used to diffuse TEMPO into UHMWPE, as described in section 3.4.2, is an aqueous solution-based method. TEMPO is mixed into deionized-H_2O to any given concentration up to the saturation point. The molar absorptivity, ε, has been evaluated to be 14.0 mol L^{-1} cm^{-1} at 426 nm, by UV-visible spectroscopy (described in section 2.5), calculated from a series of solutions mixed with different concentrations of TEMPO, shown in Figure 3.1. There was some degree of error in weighing the TEMPO powder but each solution had very high reproducibility in UV-visible absorbance. Three measurements for each solution mixed at a concentration higher than 5.0 mM did not vary by more than 1.2%. Overall the degree of error in the measurements was 0.5 %.

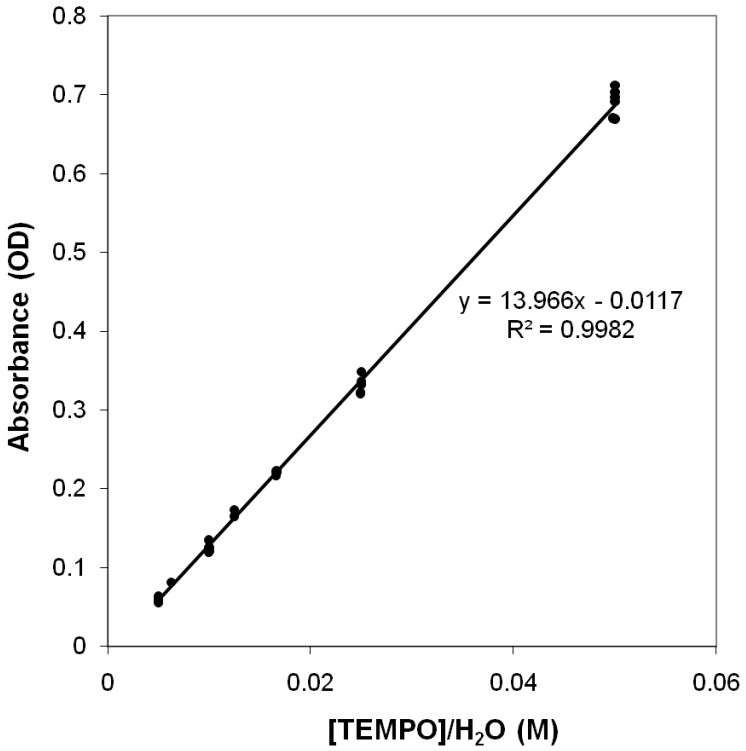

Figure 3.1: A plot of absorbance versus TEMPO/H_2O solution concentration mixed to obtain the molar absorptivity of TEMPO in H_2O at 426 nm, ε_{426nm}=14.0 mol L^{-1} cm^{-1}.

3.3.2 TEMPO/octane

For pulse radiolysis studies of the reaction rates and kinetics between nitroxides and carbon centered free radicals, TEMPO is mixed into electronic grade octane, free from impurities. To quantify the resulting species concentrations, the molar absorptivity of TEMPO in octane is measured to be 9.7 mol L^{-1} cm^{-1} at 471 nm by UV-visible spectroscopy (section 2.5). Figure 3.2 shows a series of solutions of TEMPO/octane from which the molar absorptivity is calculated. These measurements are preliminary yet showed good correlation according to the Beer-Lambert law, with a R^2 of 0.9996.

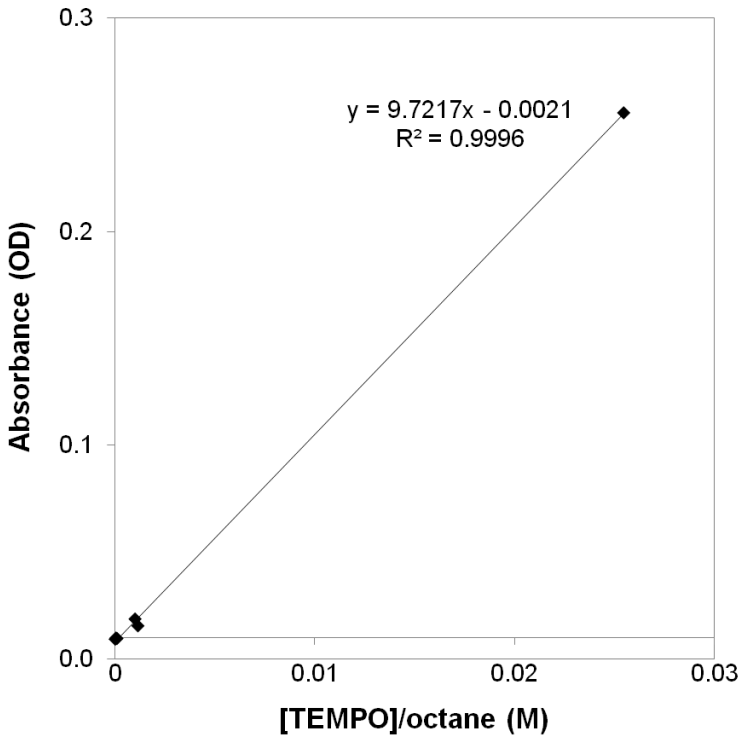

Figure 3.2: A plot of absorbance versus TEMPO/octane solution concentration mixed to obtain the molar absorptivity of TEMPO in octane at 471 nm, ε_{471nm}=9.7 mol L^{-1} cm^{-1}.

3.2.3 TEMPO/*p*-xylene

The EPR calibration curve of TEMPO radicals in *p*-xylene is built using a series of solutions of 0.0125 mM – 100 mM TEMPO/*p*-xylene concentration. From solution absorbance, the molar absorptivity of TEMPO in *p*-xylene is determined to be 10.9 mol L^{-1} cm^{-1} at 471 nm, by UV-visible spectroscopy (section 2.5). Figure 3.3 shows the absorbance versus TEMPO concentration curve used to determine the molar absorptivity. Some error was incurred in weighing the TEMPO powder and maintaining it homogenously distributed in xylene. However, each solution had very high UV-visible absorbance reproducibility. The three measurements for each solution mixed at a concentration higher than 1.0 mM did not vary by more than

1.0%. For 1.0 mM – 100 mM solutions, the overall the degree of error in the measurements was 1.9%.

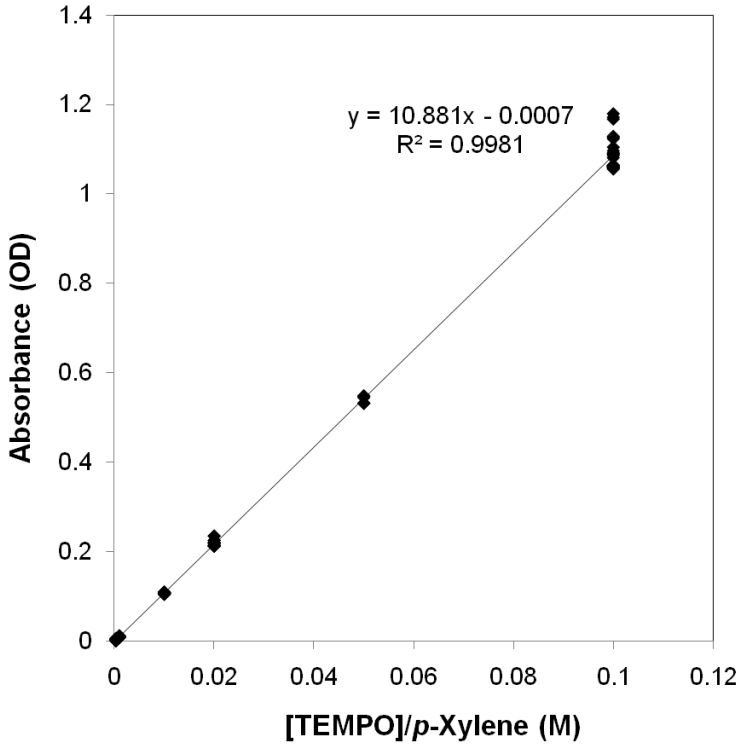

Figure 3.3: A plot of absorbance versus TEMPO/*p*-xylene solution concentration mixed to obtain the molar absorptivity of TEMPO in *p*-xylene at 471 nm, ε_{471nm}=10.9 mol L^{-1} cm^{-1}. This molar absorptivity is used to quantify the concentrations of solutions used to build a paramagnetic calibration curve for EPR spectroscopy of nitroxide and carbon-centered free radicals.

3.3 Paramagnetic Calibration Curve

An important aspect of observing the free radical processes that occur when nitroxides scavenge carbon-centered free radicals is quantifying the radicals in spins per gram. Additionally, the concentration of the nitroxides should be known for optimization of the material. This can be performed either with UV-visible, FTIR, or EPR spectroscopy. While there were several identified absorbance wavenumbers that

can be used to quantify nitroxides by FTIR (Table 2.2) and although UV-visible spectroscopy has shown demonstrated linear absorbance-concentration dependence (section 3.2), both of these methods are limited by the measurement sensitivity. The EPR is a very sensitive technique to quantify very low concentrations of nitroxides, or any other paramagnetic molecule or species. Hence, EPR is used to quantify the nitroxide concentration in UHMWPE. For accuracy and to compare one spectra to another, a calibration curve is necessary to relate the experimental sample concentration to a known value.

A series of solutions of TEMPO/*p*-xylene are mixed, according to Bruker Technical Note 3. A 100 mM TEMPO/ *p*-xylene solution is mixed, then diluted to 10 mM, which is then diluted to 1 mM. This 1 mM solution is diluted to 300 μM, 200 μM, 100 μM, 75 μM, 50 μM, 25 μM and 12.5 μM TEMPO/*p*-xylene. The advantage of the sensitivity of EPR over UV-visible and FTIR spectroscopies is immediately clear when only the 100 mM, 10 mM, 1 mM and 300 μM solutions show measurable absorbance in UV-visible spectroscopy, while all dilutions (even below 12.5 μM TEMPO/*p*-xylene) can be clearly quantified by EPR. These solutions are mixed and their concentration is confirmed with UV-visible spectroscopy. According to the molar absorptivity, $\varepsilon_{471nm} = 10.9$ mol L^{-1} cm^{-1}, calculated in section 3.2, the concentration of each solution is adjusted to account for the mixing error. A volume of 100 μL of each solution mixed is pipetted into an EPR tube and analyzed by EPR spectroscopy using the same collection parameters as for UHMWPE. The calculated concentrations are used to develop a calibration curve for each set of EPR parameters. The calibration curve for 10 mW power, 3.12 G modulation amplitude is shown in

Figure 3.4a, while the curve for 5 mW power and 3.12 G modulation amplitude is shown in Figure 3.4b.

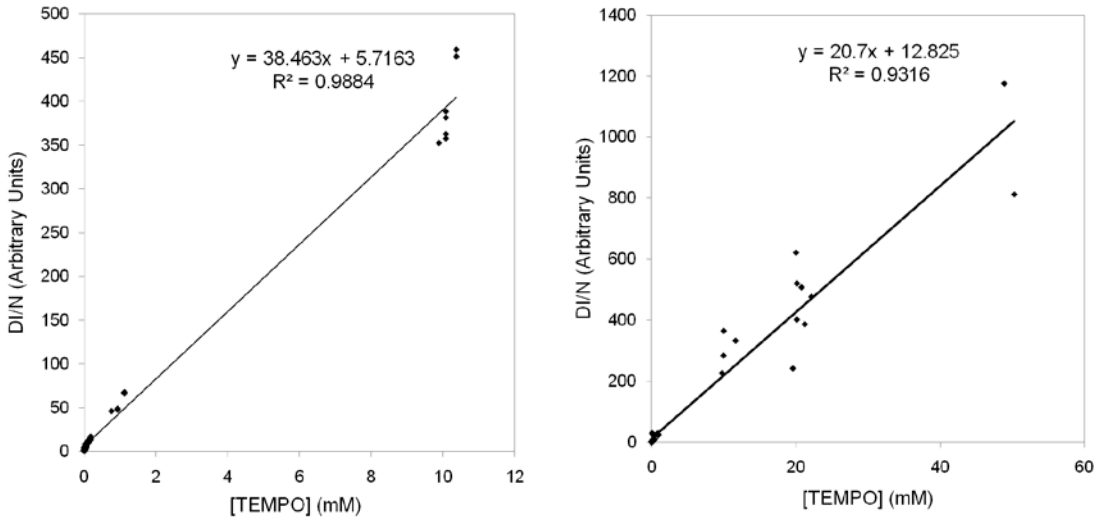

(a) (b)

Figure 3.4: EPR calibration curves for TEMPO radicals in *p*-xylene, normalized to solution volume and density difference between xylene and UHMWPE. Calibration curve for spectra collected with 10 mW power, 3.12 G modulation amplitude (a) and calibration curve for spectra collected with 5 mW power, 3.12 G modulation amplitude (b).

The calibration curves in Figure 3.4 are collected by normalizing each spectrum double integration value to three factors. There was some small variation in 100 μL of each solution was pipetted into the EPR tubes so the first normalization factor takes into account solution volume. The second normalization factor is the response of the EPR spectrometer, normalized to the relative signal intensity of a standard DPPH specimen. The last normalization factor is the density of the *p*-xylene to UHMWPE. Since the density of the solvent and polymer are different, the same volume will contain a different concentration of radicals of TEMPO. The

concentration of TEMPO radicals in Molar concentration or spins/g in the calibration curves are calculated according to equation 3.1:

$$DI/N_{UHMWPE} = DI/N_{p-xylene} \times \frac{\rho_{UHMWPE}}{\rho_{p-xylene}} = DI/N_{p-xylene} \times \frac{930 g/L}{860 g/L} \quad (3.1)$$

The calibration curve collected with 5 mW, in Figure 3.4b, includes a greater range of TEMPO/*p*-xylene concentrations because the signal in the EPR grows with the square root of the power, so higher concentrations yield saturated signals with a 10 mW power setting. The TEMPO triplet becomes a single peak at saturation. More concentrations can be measured with the 5 mW curve. Yet there is a great degree of error at such high concentrations (R^2 = 0.932 for 5 mW curve, while R^2 = 0.988 for the 10 mW curve). The homogeneity of the solution is very important to the measurable signal and this is more evident in the spread of measured intensities of 10 mM, 20 mM and 50 mM TEMPO/*p*-xylene solutions.

In addition, the slope of each calibration curve can be used to calculate the concentration of radicals in experimental specimens. For the entire curve, the calibration factors are F_{cal}= 38.5 and 20.7 for the 10 mW curve and 5 mW curve, respectively. On the other hand, at lower concentrations, the general linear trend does not fit as well. Figure 3.5 shows the same calibration curves at lower concentrations, less than 1 mM. This expanded calibration curve can be helpful to quantify small concentrations of nitroxide in UHMWPE. For dilute concentrations ≤ 1 mM TEMPO/UHMWPE, the calibration factors that can be used to relate the intensity of experimental signal in UHMWPE to a known concentration of TEMPO

radicals in *p*-xylene are F_{cal}= 55.8 and 27.3 in the 10 mW and 5 mW power calibration curves.

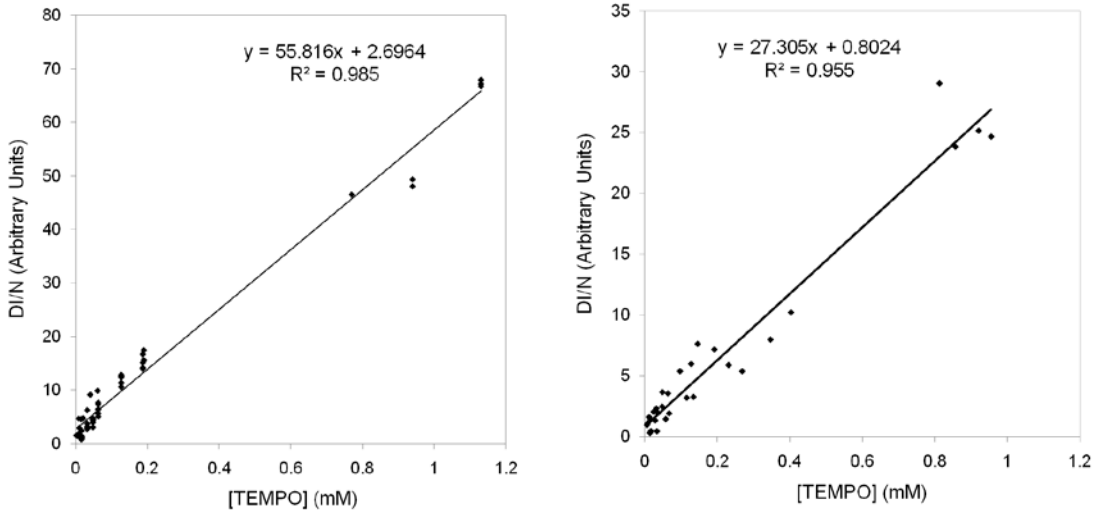

(a) (b)

Figure 3.5: EPR calibration curves for TEMPO radicals in *p*-xylene at low concentrations under 1 mM, normalized to solution volume and density difference between xylene and UHMWPE. Calibration curve for spectra collected with 10 mW power, 3.12 G modulation amplitude (a) and calibration curve for spectra collected with 5 mW power, 3.12 G modulation amplitude (b).

Using these calibration curves, the experimental concentration of nitroxides and carbon-centered free radicals in UHMWPE can be identified. Using the molar-concentration calculated from the calibration curve according to the calibration factors, a number of spins per grams can be calculated by multiplying by Avogadro's number, N_A, according to equation 3.2:

$$\frac{spins}{g} = DI/N_{UHMWPE} \times F_{Cal} = M \times N_A / \rho_{UHMWPE} = \frac{mol}{L} \times \frac{6.022 \times 10^{23}\, spins}{mol} \times \frac{L}{930 g} \quad (3.2)$$

where the density of UHMWPE, ρ_{UHMWPE} = 0.93 g/cm^3 or 930 g/L.

3.4 Infiltration Methods

3.4.1 Previous Work

The diffusion of TEMPO or nitroxides into polymers has been investigated by several authors. Syndiotactic polystyrene is infiltrated with TEMPO using a guest exchange procedure.[69] Kaneko *et al*. showed that TEMPO molecules entered the semi-crystalline polymer and completely replaced the original guest molecules using a guest exchange process with chloroform and a TEMPO-chloroform solution. In addition, a recently published paper details how nitroxides can be diffused into UHMWPE by heating in a glass container in an oven.[76]

3.4.2 Solution-Based Diffusion Method

Because α-tocopherol is liquid at room temperature and diffused into UHMWPE as a liquid, a solution-based technique mimicking this method was first attempted. A solution of TEMPO/H_2O was used in order to create a hydrophilic environment to encourage the hydrophobic TEMPO into the hydrophobic polymer. These solutions were mixed to maximum solubility of 65.4 mM ± 0.43 mM TEMPO/H_2O, as calculated from the measured molar absorptivity, as described in section 3.2.1.

Solutions of 65 mM TEMPO/H_2O were mixed and UHMWPE specimens soaked in this solution on a hotplate at 50°C. Although some nitroxide infiltrated into UHMWPE, the liquid evaporated quickly, and the nitroxide concentration varied during the doping process. As a result, the solution-based diffusion method proved to be unreliable and time consuming. It was determined that the nitroxide could easily

penetrate into UHMWPE if vaporized so a vapor-based method of heating in a glass vial is used to transfer nitroxides into UHMWPE, as described below.

3.4.3 Vapor Based Method

The vapor based diffusion method is a more consistent method of nitroxide transfer into UHMWPE. Although some nitroxide is occasionally lost, perhaps through the vial cap or due to thermal degradation, the resulting concentration of nitroxides in UHMWPE is largely controlled by the amount of nitroxide powder used and the doping time and temperature.

3.4.3.1 Experimental Set-up

A range of temperatures and diffusion times can be used to incorporate TEMPO and Tempol into the polymer. Tempol, being more hydrophilic is more difficult to diffuse through UHMWPE. However, because TEMPO has such a high affinity for UHMWPE, this may be a disadvantage since the diffusion of the hydrophilic Tempol molecule is slower and more controlled.

Temperatures of 40°C, 60°C, 80°C, and 100°C are used to diffuse TEMPO and Tempol into UHMWPE at 1 h, 2 h, 4 h, 8 h, 12 h, and 24 h time periods. Approximately 0.01 millimole of each antioxidant is weighed out and placed in a small 10 mL glass vial. UHMWPE pellets are machined with a custom designed 1/8 inch diameter plug cutter, to fit into EPR quartz tubes. Because of the affinity of TEMPO for polymers, the aluminum underside of aluminized-polyethylene was used to seal the top of the vial, and then topped with a metal cap. The goal of this method is to eliminate any other material that could absorb the nitroxide inside the vial, to

maximize nitroxide deposition in UHMWPE. Opening of the oven is minimized during these diffusion periods to increase repeatability.

After each diffusion period, the specimen vials are immediately removed from the oven. The specimens are then rinsed with acetone three times, then with water twice, and sonicated in H_2O for 20 minutes. Afterwards, the specimens are dried and placed into a vacuum desiccator for storage. The Bruker ESP 300 EPR is used to quantify the nitroxide content in UHMWPE pellets. A double integration normalized to the weight of the pellet, and related to the calibration curves in section 3.3, is used to calculate nitroxide content.

3.4.3.2 Doping Curves

The double-integrated free radical content is normalized to a calibration curve, by a calibration factor, F_{cal}, presented in section 3.3, to calculate a free radical concentration. These concentrations increased with time and temperature for both TEMPO and Tempol diffusion into UHMWPE. Plots of the nitroxide concentration as a function of time, over 40°C, 60°C, 80°C, and 100°C doping temperatures are presented in Figure 3.6. The two plots show that both TEMPO and Tempol concentrations increase logarithmically approaching a saturation point. The 60°C and 80°C doping show nitroxide concentrations only up to 4 hours and the plots are limited to 24 hour time frames due to instrument malfunction and time limitations, so the longer-term behavior cannot be observed. However, the general trends of nitroxide diffusion into UHMWPE can still be identified. Figure 3.6a shows that the TEMPO concentration is much higher at all temperatures, even at 1 hour time frames.

All the doping temperatures show an increase in concentration with increasing temperature, except 100°C. The 100°C doping of 8 hours or more show a very large standard deviation in the acquired signal. This could be due to one of two factors. First, the specimens may have been packaged in manner where some of the TEMPO was able to escape from the vial, if the cap was not secured firmly. Another possibility is that 100 mM is the saturation point of TEMPO in UHMWPE. These specimens, having reached this concentration within 4 - 8 hours, may be in equilibrium. This is not observed in Figure 3.6b, where Tempol doping exhibits a logarithmic increase in concentration which appears to continue to increase after 24 hours.

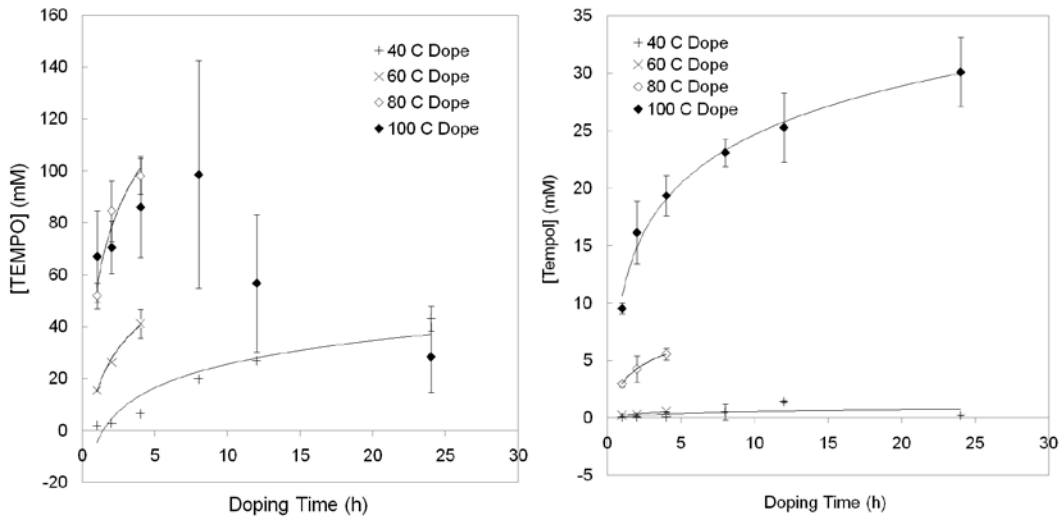

(a) (b)

Figure 3.6: UHMWPE nitroxide doping with increasing time and temperature as measured by a double integration of EPR signal, correlated to a calibration factor, F_{cal} to calculate a nitroxide concentration. TEMPO doping (a) and Tempol doping (b) both exhibit increasing concentrations with higher diffusion temperature and time. Logarithmic concentration increase is indicated with the trend lines. Longer doping points are not collected due to instrument malfunction and time constraints.

The difference in concentration with doping time and temperature between TEMPO and Tempol is significant. Figure 3.7 shows a plot of the nitroxide concentration after 4 hours of doping at a range of doping temperatures. At 4 hours, the TEMPO molecule exhibits a dramatic increase in concentration at 80°C doping. Once again, the potential saturation and equilibrium conditions at 100°C can be observed with no significant increase in concentration between 80°C and 100°C. The different nitroxide concentrations for the two molecules can be explained by their different hydrophobicity. TEMPO is similar in hydrophobicity to the polymer and its diffusion is thermodynamically favorable. Since Tempol is slightly more hydrophilic, its diffusion is much slower.

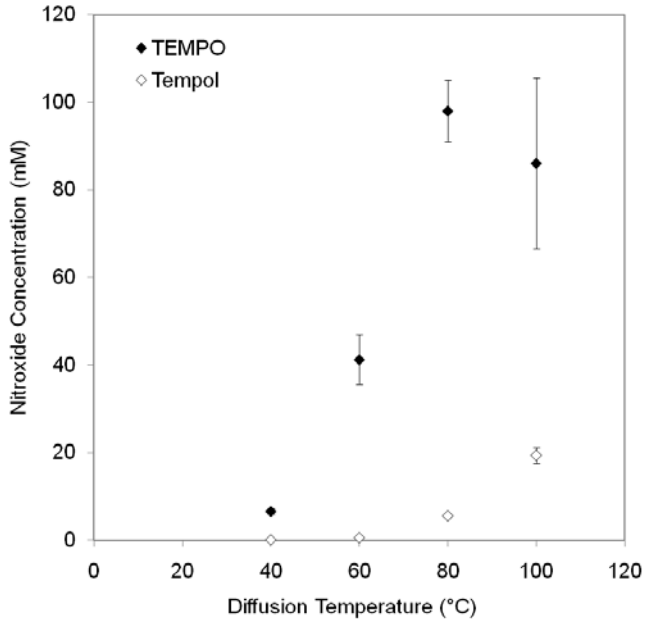

Figure 3.7: The nitroxide concentration of TEMPO and Tempol after 4 hours of doping at 40°C, 60°C, 80°C and 100 °C doping temperatures. The TEMPO molecule exhibits a significant increase in concentration at 80°C doping, and a potential saturation and equilibrium between 80°C and 100°C doping temperatures. The difference in concentration is due to the hydrophobicity of TEMPO, making it favorable for diffusion through the polymer.

3.5 Lower Detection Limit

The calibration curves created in section 3.3 are very helpful tools to identifying the spins per gram or concentration of nitroxide free radicals and carbon-centered free radicals in UHMWPE. The lower limit of EPR free radical detection is also important for identifying lowest concentrations at which antioxidants prevent oxidation. Very low concentrations of nitroxides have been identified while trying to eliminate contaminants in a pressure vessel used for accelerated aging. This involved the use of paraffin (ρ= 0.8 g/cm^3) to absorb any remaining TEMPO in the vessel after aging a set of UHMWPE-TEMPO samples. Due to the low vapor pressure of TEMPO when heated, it easily vaporizes and deposits on any surface upon cooling. This makes it easy to diffuse into UHMWPE, but also deposits TEMPO throughout the oxygen bomb used to age samples. The concentration of TEMPO absorbed into the paraffin film decreases with time. The lowest TEMPO concentration, detected by adding EPR spectra intensity from 50 scans, is 1-2 μM TEMPO. With more than 50 added scans, it may be possible to probe lower concentrations. This is helpful to identifying very low concentrations of radicals, but may not be applicable if the concentration of those radicals is changing with time, as each scan takes 20 seconds. A 1 – 2 μM TEMPO concentration correlates to less than 1 ppm. In contrast, vitamin E can only be detected to 135 ppm by FTIR. The sensitivity of the EPR technique is a great advantage to the use of nitroxides.

3.6 Conclusions

This chapter has provided a base for not only how the nitroxide molecules are diffused into UHMWPE, but how the resulting concentrations are quantified. By relating the molar absorptivity of nitroxides in solutions by UV-visible spectroscopy, a paramagnetic calibration curve can be compiled to quantify the number of radicals in a given specimen volume. As a result, the relation between specimens of different sizes can be made, although this is subject to error due to the sensitivity of the EPR signal to sample shape. Regardless, a baseline has been developed to which paramagnetic signals can be related to calculate radical concentration. Most importantly, the concentration of antioxidants in experimental specimens can be quantified with ease.

Chapter 4: Free Radical Scavenging by Nitroxides

4.1 Introduction

In this chapter, the nitroxide 2,2,6,6-tetramethylpiperidine-1-oxyl (TEMPO) is used to investigate radical-radical interactions between nitroxides and carbon-centered free radicals in UHMWPE. The first study investigates the reaction rate constants of radical-radical interactions between the nitroxide and radiolytically-produced alkyl free radicals. This interaction is observed in octane, a liquid linear alkane used to model UHMWPE. Pulse radiolysis is used to observe transient species through their absorption at the ultraviolet range of wavelengths and measure the kinetics of species absorption build-up and decay on microsecond and millisecond time scales after a 30 nanosecond electron pulse. Differences in the kinetics of the formation of reaction transients in the presence and absence of the nitroxide TEMPO are identified. In the second study, EPR spectroscopy is used to observe the paramagnetic reactions that occur between nitroxides and radiolytically-produced radicals in UHMWPE. The free radicals in UHMWPE containing TEMPO are observed before and after irradiation. Through identification of the characteristic lineshapes of each type of radical, a reaction scheme is inferred. This chapter focuses on the mechanisms of reaction between free radicals in UHMWPE and nitroxides. These reaction mechanisms give insight into how nitroxides can prevent oxidation and embrittlement in a UHMWPE joint replacement.

4.2 Pulse Radiolysis Study of Nitroxide Radical Reaction

4.2.1 Background and Theory

Pulse radiolysis is a common technique used to identify the fast transients and build-up or decay kinetics of species formed in an electron-pulsed solution or material. The time scale of investigation is typically controlled by the nature of the system set-up, i.e. the width of the electron pulse and the optical and data processing capabilities. For successful species identification, the target species must clearly absorb at an ultraviolet wavelength, the species must be produced within the correct time scale, the molar absorptivity, ε, must be substantial enough for the absorption to be distinguishable from noise and the optical system must have a high signal to noise ratio. Given these factors, once the target wavelength is identified, the build-up or decay of that wavelength absorbance can be monitored and related to the species concentration and reaction kinetics using a computer system integrating a monochromator and photomultiplier.

Although some authors have studied solid Low Density Polyethylene (LDPE) by pulse radiolysis at low temperatures,[77] such work would be difficult with UHMWPE because of the higher opacity of the polymer. Pulse radiolysis studies of molten LDPE has also been reported,[78, 79] but the viscosity of UHMWPE would make a molten study challenging. Thus, in order to investigate the reactions of carbon-centered free radicals in UHMWPE, the liquid linear hydrocarbon octane is used. A liquid allows for more accurate nitroxide solution compositions, yielding a homogenous distribution of the antioxidant that would be nearly impossible to achieve in semi-crystalline UHMWPE.

Furthermore, pulse radiolysis studies of alkanes like cyclohexane and isooctane have been extensive,[80-82] although most authors focus on the production of radical cations and excited states. Some authors have published studies of the pulse radiolysis of neat hydrocarbons and antioxidants in linear alkanes. Tagawa *et al*., 1989, observed a near-infrared absorption band in *n*-alkanes (*n* = 6, 8, 9, 13, 14, 15, where *n* = 8 is isooctane (2,2,4-trimethylpentane)), that was assigned to radical cations.[82] Visible absorption bands were assigned to excited states. Ultraviolet absorption bands, with 240 nm maxima, were assigned to secondary and tertiary alkyl radicals. It was observed that alkyl radicals had formed within the 20 ps time resolution of the instrumentation. It was concluded that alkyl radicals were formed from a contribution of singlet excited molecules and radical cations, although alkyl radical formation occurred faster than decay of cations or excited states.[82] Allyl radicals have been observed to absorb at approximately 258 nm.[22] While Tagawa *et al*. observe radical cations and excited states, they do not discuss the fate of disproportionation, vinyl unsaturations or allyl radicals.

Previous pulse radiolysis studies with nitroxides have shown TEMPO and TMIO (1,1,3,3-tetramethylisoindoline-2-oxyl) to combine with carbon-centered radicals in issoctane.[52] The resulting coupling product of carbon-centered radicals, $R^{\bullet}$ and nitroxides, $>NO^{\bullet}$ is a >NOR complex or structure. Beckwith *et al*. proposed that nitroxides may react with carbon-centered radicals up to the diffusion limit, but noted solvent polarity and viscosity, as well as chain molecular weight, reduced the reaction rate constant. Therefore the reaction rate constants gathered for liquid alkanes are typically extrapolated using molecular weight approximations to estimate

reaction rate constants for UHMWPE. In polyethylene, the formation of allyl free radicals has widely been attributed to the alkyl radicals encountering vinyl unsaturations formed through disproportionation,[83-85] (equation 1.5) discussed in section 4.2.4. These vinyl unsaturations will also absorb at 230 – 240 nm[86] so the observed absorbance in this range will be indicative of alkyl radicals and unsaturations formed in the solvent. Consequently, three alkyl radicals are required to form one allyl radical.

4.2.2 Objective

Although there have been some similar pulse radiolysis studies of nitroxides in hydrocarbon solvents, this work examines how carbon-centered radicals produced on a linear alkane chain react with TEMPO. The aim of this study is to observe the decay of alkyl radicals and the build-up and decay of allyl radicals in the presence and absence of the nitroxide TEMPO. According to previous studies, when alkyl radicals react with nitroxide radicals an intermediate should form and this reaction should occur very rapidly.[52] Elucidated kinetics of this reaction can be compared to the same process containing α-tocopherol. If the reaction rate constant for TEMPO is much larger than for α-tocopherol, it can be proposed that the nitroxide is more effective at scavenging alkyl radicals.

This study differs from previous work in the use of linear octane to model the linear UHMWPE, while other authors use isooctane and various other alkane solvents. The time-scale of investigation is in the nanosecond-microsecond range, while others like Tagawa *et al*. use picosecond pulses. The nanosecond pulse is

appropriate for this work because alkyl radical production has already been identified and the reactions of interest here occur on the microsecond time frame. Additionally, this study does not involve the purification steps used by Tagawa *et al.* but impurities can be considered negligible because the electronic-grade octane procured is 99.999+ % pure, and the concentrations of impurities are likely to be much lower than the concentrations of TEMPO or of alkyl radicals. UV-visible spectra of this solvent show a very clean absorption, aside from a small shoulder in the 200 – 230 nm range. Thorough bubbling of solutions (5-10 minutes) with nitrogen gas also eliminates any dissolved oxygen.

4.2.3 Experimental Method

The build-up and decay of low wavelength transients (230 nm – 280 nm) in the presence and absence of nitroxide antioxidant was investigated at the Notre Dame Radiation Laboratory. Neat octane (99.999+% metals basis, Aldrich Chemical, Milwaukee, WI), and TEMPO/octane solutions of 1.0 mM, 0.2 mM, 0.1 mM, and 0.05 mM concentrations were covered with paraffin film and bubbled with nitrogen gas for 5-10 minutes in a 1 cm wide quartz cuvette. Four to five pulse averages were collected for each spectrum, with a dose of 10 Gy per pulse, for a total dose of 40 – 50 Gy per trace. The wavelength of each subsequent pulse average is shifted by 10 nm, ultimately collecting data between 230 nm – 350 nm. Each time scale consists of 200 points. Data at time scales of 100 ns – 10 ms are collected with each succeeding time point consisting of averages of previous time-scales.

4.2.4 Results and Discussion

4.2.4.1 Conversion of Alkyl Radicals to Allyl Radicals in Neat Octane

The transient absorption of neat octane produced after a 30 ns pulse exhibits fast transient build-up followed by a slower decay. The absorption at the 230 – 240 nm wavelength region is attributed to alkyl radicals[82] while the 250 – 270 nm region corresponds to allyl radicals.[22] The build-up of allyl radicals and the decay of alkyl radicals can be observed in neat octane to occur within 5 μs after the 10 Gy, 30 ns electron pulse, averaged over four pulses, over a range of wavelengths. At this time, the absorbance of transients at 230 – 240 nm (alkyl radicals) is in decay while the absorbance at 250 nm – 280 nm (allyl radicals) is increasing (species build-up or growth), shown in Figure 4.1a. The corresponding decay of absorbance at these wavelengths over 10 ms is shown in Figure 4.1b.

As stated by Tagawa *et al*. the alkyl radical has already formed within 20 ps[81] and so it will begin to decay during the 30 ns pulse. In neat octane, the alkyl radicals can decay to i) bimolecularly crosslink, ii) form vinyl unsaturations through disproportionation (equation 1.5), iii) react with the vinyl groups to form allyl radicals (equation 1.6), or iv) react with oxygen in the solvent. Since the solutions are thoroughly bubbled with nitrogen, the oxygen concentration can be assumed to be negligible. Alkyl radicals are produced with a *G*-value of 3.3 – 4.4 molecules per 100 eV ionizing radiation energy,[18, 19] and in this study the $G(R^{\bullet})$ will be approximated to be 4. So for each 10 Gy pulse there will be approximately 3 μM of alkyl radicals produced. Next, the alkyl radicals will either bimolecularly crosslink or form vinyl unsaturations through disproportionation. The *G*-value of crosslinks is ~$G(X)$=3[23]

and the *G*-value for formation of vinyl unsaturations is approximately 2.2.[20] These two *G*-values do not add to the $G(R^{\bullet})$ because these are experimental observations and highly depend on irradiation conditions, like the polymer/solvent type, enviornment and dose rate. Nevertheless, these two *G*-values give a rough estimate for the ratio of crosslinking to disproportionation in the absence of oxygen.

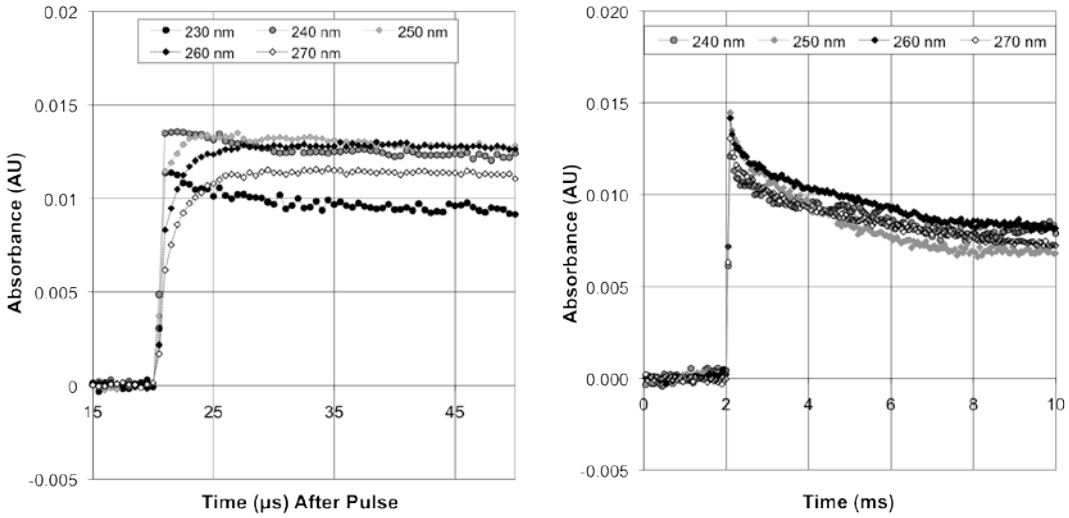

(a) (b)

Figure 4.1: The decay of alkyl radicals at 230 nm and 240 nm occurs simultaneously with the build-up of allyl radicals in neat octane at 250 nm, 260 nm and 270 nm after the 30 ns pulse (a). The decay of 240 nm – 270 nm absorbance and corresponding species occurs over 10 ms (b). Each absorbance trace consists of four averaged pulses, each with a 10 Gy dose per pulse. The build-up of allyl radicals (250 nm – 270 nm) is complete within 10 μs and they continue to decay 10 ms after the pulse.

The transient absorbances shown in Figure 4.1 are averages of four or five pulses. The first and second pulse will produce alkyl radicals that form crosslinks, according to equation 1.3 and simultaneously, other alkyl radicals will form vinyl unsaturations, through disproportionation by equation 1.5:

$$R^{\bullet} + R^{\bullet} \rightarrow R\text{-}R \qquad (1.3)$$

$$\begin{array}{c} RCH_2C^{\bullet}HCH_2R \\ + \\ RCH_2C^{\bullet}HCH_2R \end{array} \rightarrow \begin{array}{c} CH_2CH_2CH_2CH_2 \\ + \\ RCH_2CH=CHR \end{array} \qquad (1.5)$$

The bimolecular crosslinking and disproportionation reactions are mostly not observed in Figure 4.1. Alkyl radicals are formed within 20 ps, and the crosslinking and disproportionation processes will begin between 20 ps and the first 10 ns after the pulse, not observed by the optical system at Notre Dame. In fact, Johnson *et al*. reported that alkyl radical decay is a composite of two first order reactions, one occurring must faster than the other.[19] The "fast" process will encompass the formation of unsaturations and crosslinks, which are not observed by the traces in Figure 4.1. The second "slow" process encompasses the reaction of alkyl radicals with unsaturations to form allyl radicals, as well as some crosslinks and unsaturations still forming. After the fast crosslinking and disproportionation reactions begin, any remaining alkyl radicals react to form allyl radicals, by equation 1.6, which is dependent on the presence of vinyl unsaturations:[20, 21, 87]

$$R^{\bullet} + CH_2CH=CHCH_2 \rightarrow CH_2CH=CHC^{\bullet}H + RH \qquad (1.6)$$

Hence, within 10 μs of the pulse, allyl radicals are produced and the corresponding absorbance (~258 nm) builds up. The *G*-value of allyl radical production is ~0.25, as most of the radicals form crosslinks and unsaturations. Five alkyl radicals will react to form three products: two alkyl radicals form a crosslink, two alkyl radicals form a vinyl unsaturation through disproportionation and one more alkyl radical is necessary to form the allyl radical by hydrogen abstraction from the C-H chain.

Through disproportionation, the concentration of unsaturations becomes much larger than the concentration of O_2 or any impurities, and the remaining alkyl radicals formed in the final pulses of the four pulse average react with the vinyl unsaturations to form allyl radicals, as observed by the build-up at 250 nm – 280 nm. These allyl radicals then decay on a millisecond time-scale. This can also be observed through a spectral plot of absorbance. Since each species is identified at a characteristic wavelength, reactions can be observed as the spectral plot shifts from the reactant towards the reaction product. Figure 4.2 shows spectral absorbance observed between 230 nm – 350 nm in neat octane, 1 μs – 50 μs after the pulse (4.2a) and 1 μs – 8 ms after the pulse (4.2b). This figure demonstrates how species absorbance changes with time. The spectral absorbance peak shifts from 240 nm at 1 μs after the 30 ns electron pulse, to a peak centered at 250 nm after 5 μs and a peak centered at 260 nm, 50 μs after the pulse. The shift of the absorbance peak corresponds to the decay of alkyl radicals and the build-up of allyl radicals, as described previously, through the reaction of alkyl radicals with vinyl unsaturations that have formed through disproportionation.[83-85]

These allyl free radicals continue to decay 8 ms after the electron pulse, as shown in Figure 4.2b. Consequently, in neat octane, in the absence of oxygen and antioxidants, the series of events can be proposed to be i) very rapid production of alkyl radicals and vinyl unsaturations that ii) react to form allyl radicals within 50 μs, which iii) begin to decay as they bimolecularly crosslink.

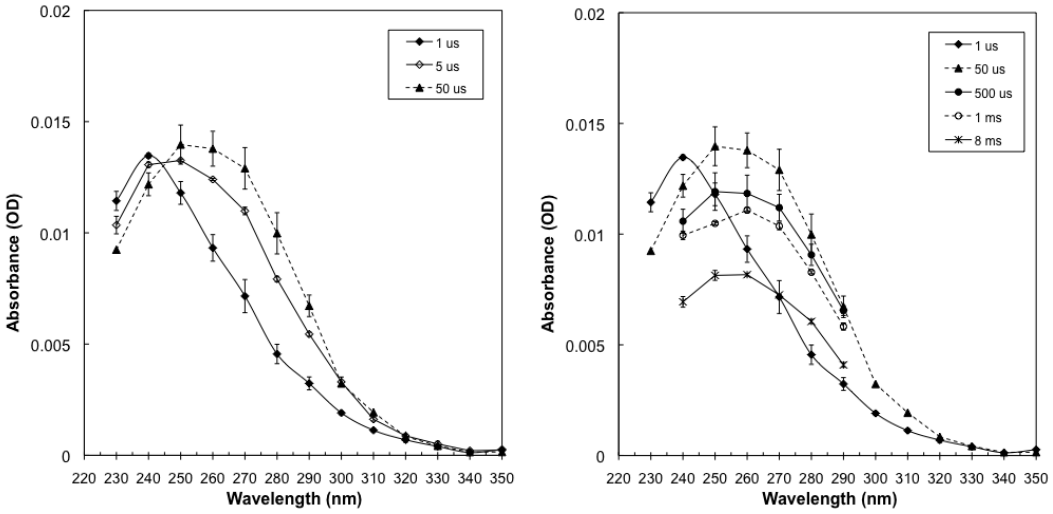

(a) (b)

Figure 4.2: Pulse radiolysis transient species spectral plots of absorbance intensity from 230 nm – 350 nm at different time scales. (a) Neat octane 1 μs – 50 μs after the pulse; (b) neat octane 1 μs – 8 ms after the pulse. A shift from the alkyl (240 nm) peak to the allyl (260 nm) peak indicates reaction of alkyl radicals with vinyl unsaturations to form allyl radicals that then decay over the next 10 ms.

To measure the reaction rate constants of build-up or decay, the change in absorbance and corresponding concentration of the absorbing species can be fit to pseudo-first order or second order kinetics. The theoretical equations used to calculate the observed reaction rate constant, k_{obs}, and the real reaction rate constant, k', as well as an example k_{obs} fit to data are discussed in Appendix A. Again, once the majority of alkyl radicals have formed crosslinks and vinyl unsaturations, in the absence of oxygen, the few remaining residual alkyl radicals will form allyl radicals by reacting with vinyl unsaturations. The observed simultaneous decay of alkyl radicals at 230 nm - 240 nm and build-up of allyl radicals observed at 250 – 290 nm follows the premise that there is a 1:1 conversion[87] of the remaining unreacted alkyl radicals to the allyl radicals (which form with a *G*-value of ~0.25). The reaction rate constants, k_{obs}, for the observed portion of alkyl radical decay to form allyl

radicals, are calculated assuming a pseudo-first order decay in neat octane to be k_{obs}= 1.0×10^5 s^{-1} at 230 nm and 2.3×10^4 s^{-1} at 240 nm. While both of these wavelengths are representative of alkyl radical decay, the rate constant at 240 nm is approximately four times slower than at 230 nm. This is attributed to the fact that the 240 nm absorbance lies in between the decaying 230 nm absorbance and the building absorbance at 250 nm. It is likely that the allyl radicals absorb at 240 – 250 nm as well, and the observed reaction rate constant is reduced. As a result, the k_{obs} at 230 nm will be assumed as the actual rate constant of alkyl decay (1.0×10^5 s^{-1}), although both observed rate constants should be taken into account. This correlates to the findings of Johnson *et al*. indicating that alkyl radicals decay with first order kinetics,[19, 88] with a composite reaction rate constant.

Consequently, the build-up of allyl radicals at 250 nm – 280 nm also occurs with a pseudo-first order build-up reaction rate constant. Similarly, the k_{obs} can be measured at each wavelength: k_{obs}= 1.1×10^6 s^{-1} at 250 nm, 5.3×10^6 s^{-1} at 260 nm, 4.0×10^6 s^{-1} at 270 nm and 3.8×10^6 s^{-1} at 280 nm. The decay of alkyl radicals and build-up of allyl radicals do not occur with the same reaction rate constant for three reasons. First of all, the alkyl radicals react to form three products: crosslinks, vinyl unsaturations, as well as allyl radicals. As a result the observed decay involves all three decay reactions. Secondly, the vinyl unsaturations also absorb at 230 nm,[86] and the decay rate is likely mitigated by the build-up of their concentration. Lastly, the experimental set-up involves the use of four pulses per absorbance trace and the solution used for multiple wavelengths. Thus, the decay and build-up are

complicated by the presence of vinyl unsaturations, which absorb at 230 nm, from previous pulses.

Finally, allyl radicals decay through a bimolecular crosslinking reaction with a second order reaction rate constant that is calculated at each wavelength: $k' = 3.2 \times 10^4$ ε mol $L^{-1}s^{-1}$ at 250 nm, 8.2×10^4 ε mol $L^{-1}s^{-1}$ at 260 nm, 6.4×10^4 ε mol $L^{-1}s^{-1}$ at 270 nm, 6.8×10^4 ε mol $L^{-1}s^{-1}$ at 280 nm and 2.7×10^4 ε mol $L^{-1}s^{-1}$ at 290 nm. This confirms previous work in polyethylene, where allyl radical decay has been estimated to be a diffusion-controlled second-order process,[21] that also has a fast and slow component.[89] This slow decay continues to occur past the observed 10 ms. It is important to note that allyl decay is much slower than the decay of alkyl free radicals because the alternative single and double bond electron conjugation has overlapping p-orbitals. Delocalization of the pi electrons across the adjacent aligned p-orbitals lowers the overall energy and increases stability of this double bond. Moreover, the reaction of allyl radicals with oxygen to form peroxyl radicals is also much slower than with alkyl radicals, because the unsaturation limits peroxyl radical formation. The allyl and alkyl radicals, for that matter, do not decay to an absorbance of zero. This can be attributed to the overlap in absorption wavelengths, and the production of vinyl groups.

Consequently, the presence of vinyl groups in irradiated neat octane can be measured by UV-visible spectroscopy (section 2.5). Electron grade octane is irradiated by ^{60}Co γ to 5 kGy, 15 kGy and 25 kGy and the vinyl group absorption at 230 nm is measured as a function of dose in Figure 4.3. The UV-visible absorption plots are shown in Figure 4.3a and the corresponding absorption versus absorbed dose

plot is shown in Figure 4.3.b. These plots confirm the production of vinyl unsaturations long after the alkyl radicals have reacted. A linear build-up of vinyl groups in octane as a function of radiation dose also reaffirms that alkyl radicals disproportionate to form vinyl unsaturations. From the plot in Figure 4.3.b, the *G*-value of vinyl unsaturations can be calculated. From the slope of the plot, the optical density per kGy dose is 0.0377. Using the molar absorptivity ε_{230nm} = 139 mol $L^{-1}cm^{-1}$,[90] the concentration of vinyl group production can be calculated to be 0.27 mM kGy^{-1}. The *G*-value is calculated according to equation 4.1,[91] where *D* is the dose, ρ is ratio of the density octane and *c* is the concentration of vinyl groups per dose (Gy):

$$G = 9.648 \cdot 10^{6} \times \frac{c}{\rho \times D} = \frac{\frac{2.7 \cdot 10^{-7}\, mol}{L}}{\frac{0.7\, kg}{L} \times 1000\, Gy} = \frac{3.7\, molec.}{100\, eV} \qquad (4.1)$$

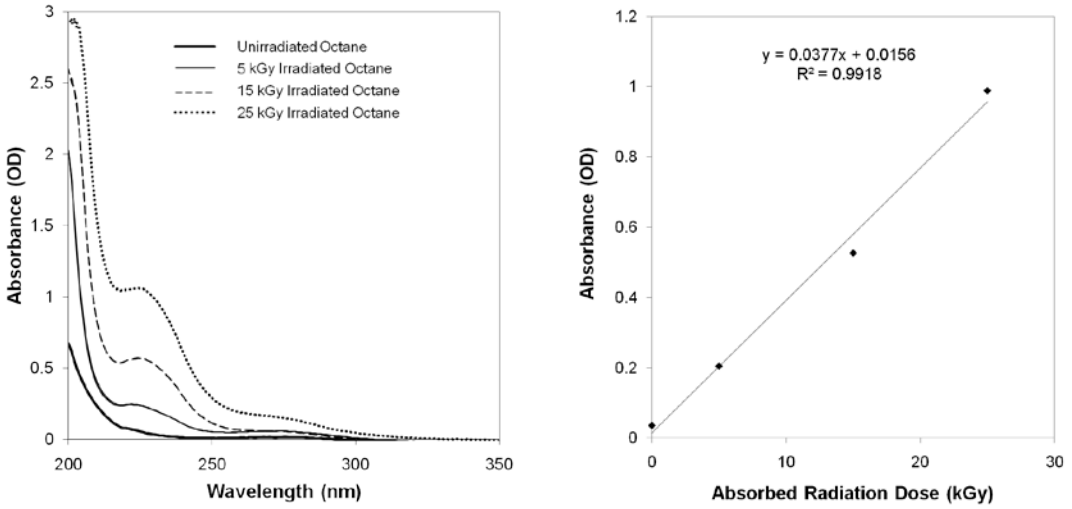

(a) (b)

Figure 4.3: UV-visible spectroscopy of neat octane solutions irradiated with ^{60}Co γ to 5 kGy, 15 kGy and 25 kGy. The solution spectra show absorbance in the 230 nm region representative of vinyl groups (a). A plot of the absorbance at 230 nm of octane solutions versus radiation dose (b) shows linear production of vinyl groups.

As a result, vinyl groups are produced in octane with a *G*-value of 3.7 molecules per 100 eV, while in LDPE the *G*-value ~ 2.2. This value has not been reported in linear octane before, and in fact few studies have evaluated vinyl unsaturation production since 1959. Therefore, this work fills in some important gaps in knowledge about the radiolysis of polyethylene and alkanes. A summary of all measured observed reaction rate constants are summarized in Tables 4.1 and 4.2.

4.2.4.2 Reactions in the Presence of the Nitroxide, TEMPO

Pulse radiolysis of octane containing nitroxides also shows rapid build-up and subsequent decay of absorbance between 230 nm – 290 nm, shown in Figure 4.4. A 0.05 mM TEMPO/octane solution exhibits transient build-up at 270 nm, 280 nm and 290 nm (Figure 4.4a). This plot shows decreasing absorbance with increasing wavelength. The 280 nm wavelength transient build-up in 0.05 mM, 0.1 mM and 0.2 mM TEMPO/octane is shown in Figure 4.4b. The build-up of 0.1 mM absorbance seems to occur faster than the 0.05 mM solution. Overall, solutions of 0.05 – 1.0 mM TEMPO/octane pulsed with four averaged 10 Gy, 30 ns electron pulses show decay of the 240 nm wavelength and build-up of 250 – 290 nm absorbance. The 240 nm wavelength corresponds to the alkyl radicals formed within 20 ps, and a species observed at 250 – 290 nm is building up. While the solutions containing TEMPO exhibits the same decay/build-up characteristics, the 250 – 290 nm build-up occurs within 500 ns in TEMPO/octane versus 1 – 2 μs in neat octane.

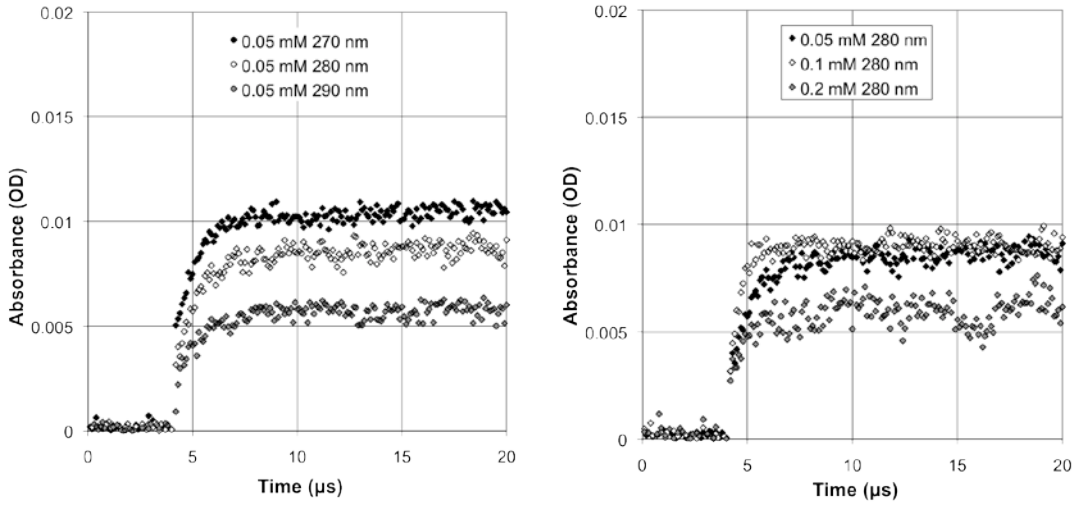

(a) (b)

Figure 4.4: Pulse radiolysis traces of >NOR intermediate build-up recorded at 270 nm, 280 nm and 290 nm in 0.05 mM TEMPO/octane solution (a) and at 280 nm in 0.05 mM, 0.1 mM and 1.0 mM TEMPO/octane solution (b), recorded within 20 µs of the 30 ns electron pulse.

Both neat octane and 0.05 mM TEMPO/octane, for example, exhibit a spectral peak shift to longer wavelengths, but there are subtle differences between these two resulting peaks. The peak observed in 0.05 mM TEMPO/octane after 1 ms, shown in Figure 4.5, is 10 nm red-shifted and this peak appears to be much more narrow than the peak observed in neat octane. Figure 4.6 shows a schematic highlighting the differences in proportions between these two peaks. Proportional differences imply that instead of a reaction of alkyl radicals with unsaturations to form allyl radicals, in the presence of nitroxides the alkyl radicals react to form an intermediate complex. This intermediate decays in Figure 4.5.

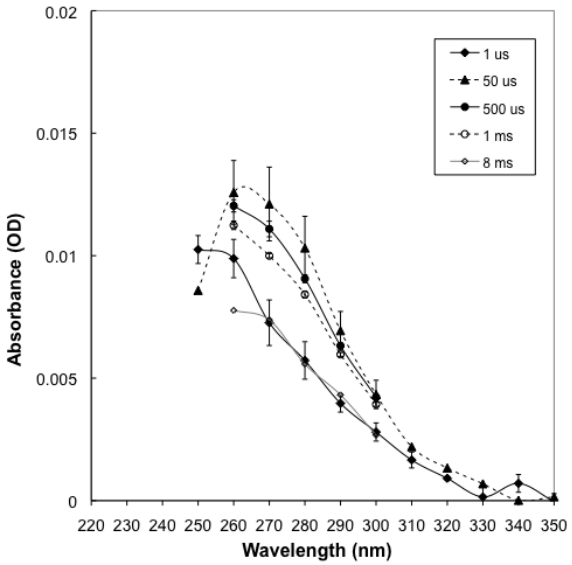

Figure 4.5: Spectral plots of 230 nm – 250 nm absorbance 1 μs – 8 ms after 0.05 mM TEMPO/octane is pulsed with electrons. A shift from 250 nm to 270 – 280 nm occurs four orders of magnitude faster in 0.05 mM TEMPO/octane, than in neat octane, to form an intermediate complex.

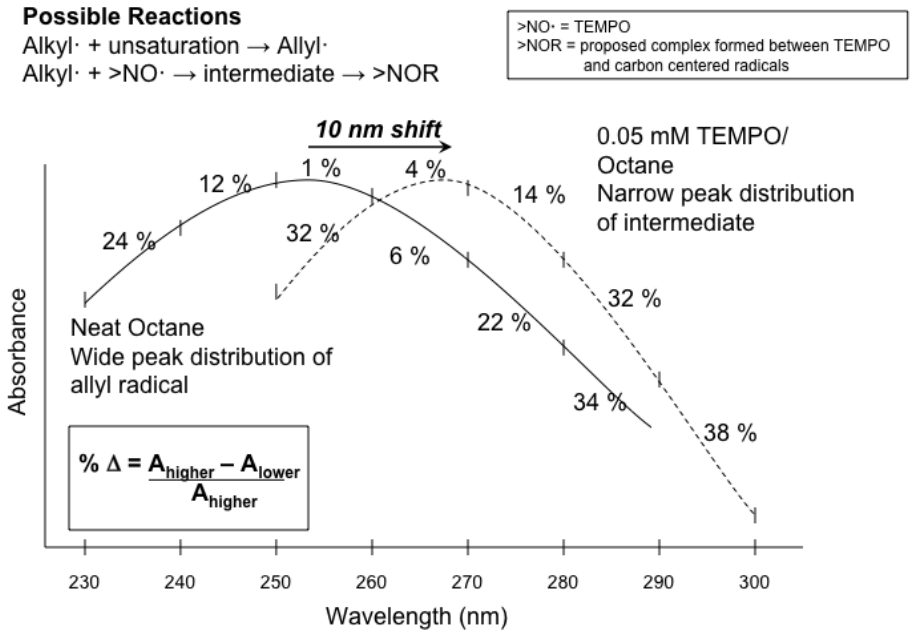

Figure 4.6: A schematic of the proportional differences between the peak appearing at 1 ms in neat octane and 0.05 mM TEMPO/octane. The peak is shifted by 10 nm and appears more narrow in the presence of nitroxide. This peak is proposed to be an intermediate nitroxide complex (>NOR), instead of the allyl radical.

While equation 1.12 may be partly true, the decay or dissociation of the secondary product at 260 – 290 nm indicates that this is an intermediate and not the final product as indicated in equation 1.12 (repeated below):

$$R\cdot + >NO\cdot \rightarrow >NOR \qquad (1.12)$$

It is more likely that carbon-centered alkyl radicals, $R^{\bullet}$, interact with the TEMPO radical, $>NO^{\bullet}$, to form the >NOR complex, that then rapidly dissociates to form $>NO^{-}$ and a cation on the polymer chain, shown in equation 4.2. The polymer chain is then deprotonated and forms a double bond, as shown in equation 4.3:

$$R\cdot + >NO\cdot \rightarrow >NOR \rightarrow >NO^{-} + \ RC^{+}HCH_2R \qquad (4.2)$$

$$RC^{+}HCH_2R \rightarrow \ RCH{=}CHR + H^{+} \qquad (4.3)$$

The deprotonation of the cation is likely to occur because the NO moiety is an oxidizing species and the carbon atom is a reducing species, donating the electron to the NO. The formation of an unsaturation as a result of carbon centered radical reaction with nitroxide indicates that the antioxidant molecule promotes the production of a stable unsaturation, decreasing the chance for peroxyl radical formation. Therefore, in the absence of oxygen, the octane solution will form vinyl unsaturations with or without TEMPO. Importantly, when there is oxygen in the octane solution, the TEMPO molecule may divert the reaction from peroxyl radical formation to the final production of unsaturations. These reactions in the presence of oxygen were not explored here, but would be a very valuable experiment to perform in future work.

The reaction rate constants for alkyl radical decay in the presence of nitroxides, nitroxide intermediate build-up, and its subsequent decay are as follows and are summarized in Tables 4.1 and 4.2. In the presence of 0.1 mM TEMPO, the alkyl radical decays with a pseudo-first order reaction rate constant $k_{obs} = 5.4 \times 10^4$ s^{-1} (at 240 nm). Moreover, the build-up of the nitroxide intermediate complex at 270 nm occurs with a $k' = 1.0 \times 10^9$ mol $L^{-1}s^{-1}$ second order reaction rate constant, as calculated from Figure 4.7. The slope of the k_{obs} versus nitroxide concentration gives the actual reaction rate constant, k'. Decay of the >NOR intermediate occurs with a second order reaction rate constant of $k' = 4.9 \times 10^6$ mol $L^{-1}s^{-1}$ at 270 nm, calculated in the same way from the slope of a plot of observed decay k_{obs} versus [TEMPO].

Table 4.1: Pseudo-First Order Reaction Rate Constants, k_{obs}, of Observed Transient Species Build-Up at 230 – 290 nm by Pulse Radiolysis after a 30 ns Electron Pulse

(s^{-1})	230 nm	240 nm	250 nm	260 nm	270 nm	280 nm	290 nm
Neat Octane			1.1×10^6	5.3×10^6	4.0×10^6	3.8×10^6	4.0×10^5
0.05 mM TEMPO/octane				7.3×10^5	2.9×10^5	5.2×10^5	4.8×10^5
0.1 mM TEMPO/octane				8.4×10^5	5.1×10^5	5.4×10^5	1.0×10^6
0.2 mM TEMPO/octane					3.7×10^5	7.1×10^5	4.1×10^5
1.0 mM TEMPO/octane						1.5×10^6	1.1×10^6

Table 4.2: Pseudo-First Order Reaction Rate Constants, k_{obs}, of Observed Transient Species Decay at 230 – 290 nm by Pulse Radiolysis after a 30 ns Electron Pulse

(s^{-1})	230 nm	240 nm	250 nm	260 nm	270 nm	280 nm	290 nm
Neat Octane– 1st Order	1.0×10^5	2.3×10^4					
Neat Octane– 2nd Order			*3.2×10^4*	*8.2×10^4*	*6.4×10^4*	*6.8×10^4*	*2.7×10^4*
0.05 mM TEMPO/octane			3.5×10^4	1.5×10^3	1.7×10^3	1.0×10^3	5.8×10^2
0.1 mM TEMPO/octane		5.4×10^4	3.2×10^4	2.9×10^3	2.4×10^3	2.2×10^3	3.3×10^3
0.2 mM TEMPO/octane				5.5×10^2	4.8×10^2	3.8×10^2	4.6×10^2
1.0 mM TEMPO/octane					6.5×10^3	7.7×10^3	3.3×10^3

Furthermore, the spectral absorbance plots of solutions containing 0.05 – 1.0 mM TEMPO are plotted 10 μs after the pulse, in Figure 4.8. An increasing concentration of nitroxide (0.05 mM, 0.1 mM, 0.2 mM and 1.0 mM TEMPO) exhibits decreasing absorbance at 10 μs after the electron pulse. This indicates that the reaction of the alkyl radical to form the intermediate complex occurs faster with increasing concentration of TEMPO. The reaction rate constant is the same but with a higher concentration of reactant, the reaction occurs faster. With 1.0 mM TEMPO/octane, there is no sign of the intermediate peak, so the complex may have already formed and dissociated within 10 μs.

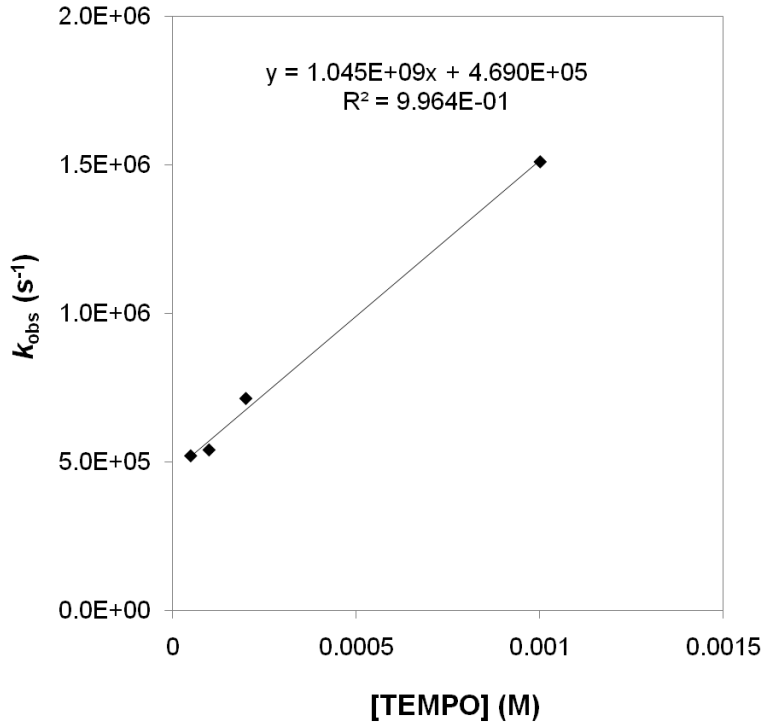

Figure 4.7: The observed pseudo-first order reaction rate constant, k_{obs}, of 270 nm transient species build-up plotted versus TEMPO concentration. The slope gives the real $k' = 1.0 \times 10^9$ mol $L^{-1}s^{-1}$, the reaction rate constant of the alkyl radicals and nitroxide radicals to form the >NOR intermediate.

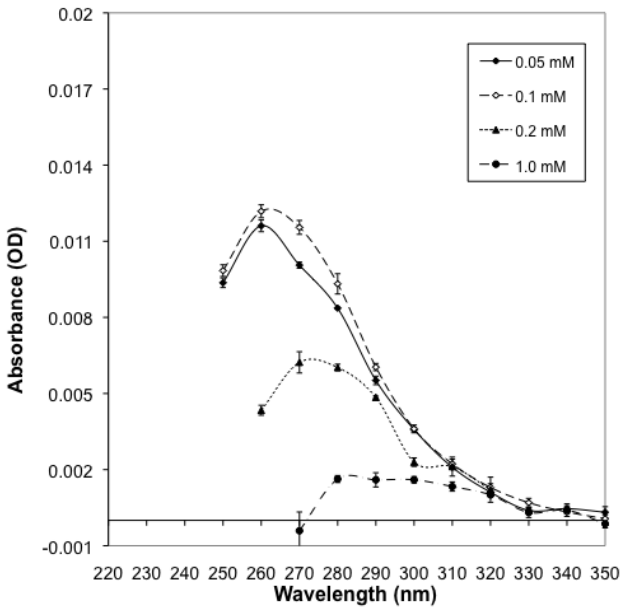

Figure 4.8: Absorbance spectra of TEMPO/octane solutions 10 μs after the electron beam pulse for concentrations of 0.05 mM – 1.0 mM TEMPO/octane. The absorbance of the nitroxide intermediate, centered at 270 nm has already decayed at higher concentrations. The reaction speed of alkyl + >NO$^{\bullet}$ increases with increasing TEMPO concentration.

Beckwith *et al*. reported that nitroxide radical trapping rate constants are 5 - 10 × 10^8 mol $L^{-1}s^{-1}$ for a range of carbon-centered radical structures,[52] which agrees with the data evaluated here. The bimolecular recombination reaction rate constants for the same radicals are 5 – 24 × 10^9 mol $L^{-1}s^{-1}$.[52] Thus the radical scavenging by nitroxides is only one order of magnitude slower than bimolecular crosslinking.[52, 92] On the other hand, the [>NO$^{\bullet}$] > [R$^{\bullet}$], as the alkyl radicals have a G(R$^{\bullet}$) = 4 so ~3 μM radicals are produced per pulse. The nitroxide concentrations are at least 50 μM. While the preferred events are first bimolecular crosslinking (10^{10} mol $L^{-1}s^{-1}$) and then the reaction with the nitroxide (10^9 mol $L^{-1}s^{-1}$) because there are so many more nitroxide radicals, it can be expected the alkyl radicals will encounter a nitroxide before another alkyl radical, to form the >NOR intermediate in the absence

of oxygen. Additionally, with such a high nitroxide concentration, vinyl unsaturations will not form immediately from disproportionation of two alkyl radicals. Instead, they will form after the reaction of the nitroxide and alkyl radical, after the deprotonation of the cation from the reduction of the nitroxide.

Furthermore, previous studies have shown that phenols react with alkyl radicals on the order of 10^5 mol L^{-1} s^{-1},[93] which is four orders of magnitude slower than TEMPO. Consequently, nitroxides prove to be more efficient carbon-centered radical scavengers. The nitroxide reaction with alkyl radicals is very fast, albeit slower than alkyl radical bimolecular crosslinking and the reaction with oxygen to form peroxyl radicals. However, by eliminating oxygen and introducing a high nitroxide concentration, the alkyl radicals react with the nitroxide to eliminate allyl radical production.

For engineering an oxidation-resistant UHMWPE, the goal is for all alkyl radicals to react bimolecularly and crosslink. The speed of the nitroxide radical scavenging reaction reduces the probability that peroxyl radicals will form to cause oxidation. Although the values for the reaction rate constants identified here cannot be directly translated to reaction constants in UHMWPE, the relative orders of magnitude between the competing reactions should still be valid in UHMWPE.

4.2.5 Conclusion

This section shows that the presence of the nitroxide TEMPO can alter the radiation products that are formed in an unsaturated solution. Instead of allyl radical production, an intermediate >NOR complex is formed, which dissociates to form a

stable vinyl unsaturation on the polymer chain. TEMPO has been found to scavenge alkyl radicals on the order of 1×10^9 mol $L^{-1}s^{-1}$ or just below the diffusion controlled limit.[52] Consequently, the nitroxide can be expected to compete with bimolecular crosslinking and to react with alkyl radical slightly slower than oxygen. By eliminating oxygen and introducing nitroxides, the occurring reactions can be controlled. Additionally, a new *G*-value for vinyl group production by γ-radiolysis has been determined to be 3.7, much higher than observed in LDPE.

4.3 Reaction of Nitroxides in UHMWPE Measured by EPR

4.3.1 Introduction

The production of carbon-centered free radicals and their subsequent reactions, as described by the reaction schemes in Chapter 1, can also be observed with EPR spectroscopy. The alkyl radical forms very rapidly, and then quickly reacts in one of five ways: bimolecular crosslinking, disproportionation to form a vinyl group, interaction with a vinyl unsaturation to form the long-lived allyl free radical, reaction with oxygen to form the peroxyl radical or reaction with an antioxidant. Each of the radicals formed has its own characteristic hyperfine structure in the EPR, making it easy to identify each radical type, and at times determine the combination of radicals present. The alkyl radical forms a sextet and its transition to an allyl radical after the interaction with a vinyl unsaturation is observed as a transition to a more narrow septet.[84] The reaction of alkyl radicals with diffused molecular oxygen in UHMWPE or on the surface of the specimen forms peroxyl radicals with a

singlet structure.[94] The nitroxide radical exhibits a characteristic triplet structure. EPR theory explaining how these lineshapes are formed is described in section 2.4.1. These typical radical structures observed in the EPR are shown in Figure 4.9, where the alkyl and allyl radicals overlap (4.9a) producing a complex signal, the peroxyl radicals showing a narrow singlet (4.9b), and the nitroxide triplet (4.9c) that can distort and eventually form a broad singlet at high concentrations due to signal broadening (4.9d). This latter phenomenon does not allow for accurate signal quantification. Through lineshape analysis, the transformation of one radical to another or the disappearance of a species can be observed by EPR.

4.3.2 Objective

In order to develop an effective antioxidant for UHMWPE in joint replacements, the reactions that cause and prevent oxidation should be defined. Elucidation of the reactions by which nitroxides scavenge carbon-centered and oxygen-centered radicals in UHMWPE allows comparison to other antioxidants. This section explores the reaction of carbon-centered radicals with nitroxides by the observation of free radical evolution and reaction with EPR spectroscopy. The lineshapes and radical concentrations of specimens doped and irradiated or conversely, irradiated and doped, are evaluated to determine the most effective strategy of scavenging residual carbon-centered free radicals in UHMWPE. Free radical quantification is performed through a signal double integration and calculated through the techniques and calibration curves determined in section 3.3.

4.3.3 Experimental Method

The consumption of nitroxides by radiolytically-produced free radicals is characterized by EPR. UHMWPE pellets of 1/8 in. diameter and 5 mm length are doped to a concentration of 18.6 ± 2.3 mM TEMPO by the solution-based doping method (section 3.4.2) for 48 – 72 hours at 50ºC and packaged in argon in aluminized-polyethylene (Al-PE) pouches. These specimens are then irradiated to incremental doses between 20 kGy and 100 kGy doses with the 7 MeV LINAC electron beam with 60 pulses s^{-1} and 7 Gy per pulse. At each dose interval, the pellet is transferred from the Al-PE to an argon-flushed EPR tube, and the EPR signal is collected with standard parameters discussed in section 2.4.2, within 20 minutes of irradiation.

Additionally, UHMWPE pellets are irradiated with the 7 MeV LINAC electron beam under the same conditions. The initial carbon-centered radical signal is acquired at incremental doses between 20 kGy and 100 kGy. These specimens are then doped with TEMPO and Tempol for five minutes at 80ºC and 100°C, respectively, to produce a very low concentration with the vapor-based diffusion method (section 3.4.3). In addition, a short five minute 80°C annealing step demonstrates the thermal effect of doping on total free radical content. The resulting lineshapes are recorded within 24 hours of doping.

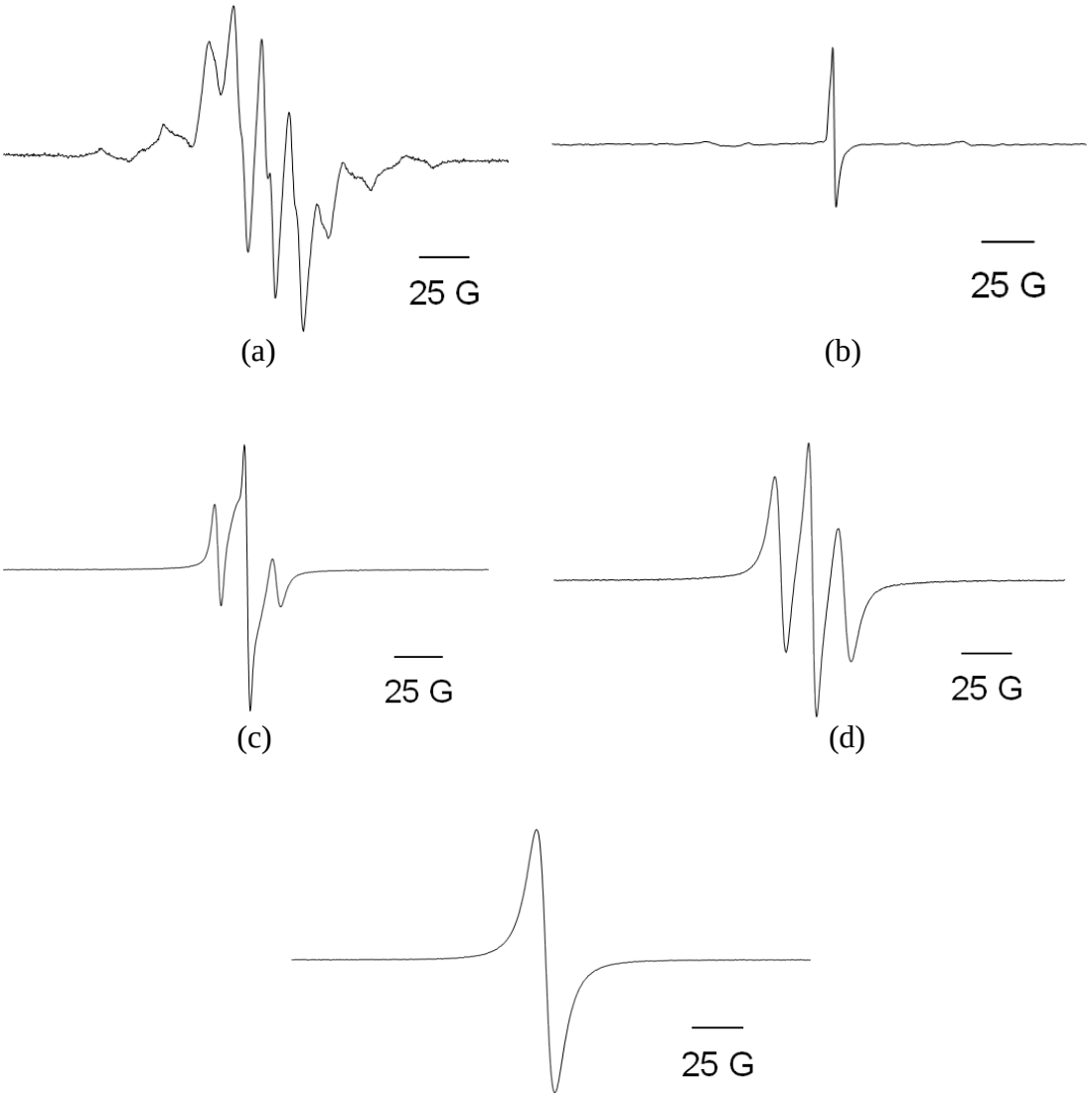

Figure 4.9: Typical hyperfine structures of free radicals observed in UHMWPE. The combination of alkyl (sextet) and allyl (septet) radicals forms a complicated lineshape (a) while the peroxyl radical is observed as a singlet (b). Nitroxides are naturally paramagnetic; Tempol (c) and TEMPO (d) are observed as triplets until a saturated concentration causes lineshape broadening (e). These radicals can be differentiated by the hyperfine structure as well as hyperfine constants, or width of the signal.

4.3.4 Results and Discussion

4.3.4.1 Scavenging of Carbon-Centered Free Radicals During Irradiation

The doping of UHMWPE with TEMPO produces a strong triplet lineshape, as shown in Figure 4.9d. As the TEMPO-UHMWPE is irradiated, this triplet signal begins to decay. With increasing irradiation doses, the triplet signal becomes smaller and eventually a small septet is observed. This signal reduction can be seen in Figure 4.10 where the initial signal is reduced with 30 kGy and 100 kGy of ionizing radiation. Ionizing radiation produces alkyl radicals proportionally to the ionization radiation dose. In the absence of TEMPO and oxygen, most alkyl radicals immediately crosslink. The residual alkyl radicals convert to allyl radicals with a 1:1 conversion,[87] as discussed in section 4.2.4, which are observed to increase linearly to radiation dose in Figure 4.11. But in the presence of TEMPO, some radicals crosslink and remaining alkyl radicals react with the nitroxide radical, as discussed in section 4.2.4. The result is a reduction in the nitroxide paramagnetic signal, as demonstrated by triplet reduction in Figure 4.10 and the double integration value reduction in Figure 4.11.

As carbon-centered free radicals are formed in UHMWPE, the nitroxide radicals, with a high 18.6 mM concentration scavenge the radicals as they are produced. If the $G = 4$ for alkyl radical production,[18] a total of ~30 mM alkyl radicals will be produced with 100 kGy. Since $[R^{\bullet}] \geq [>NO^{\bullet}]$, many of the alkyl radicals will crosslink, but many others will encounter a nitroxide first. Thus, it is feasible for 18.6 mM of TEMPO to be completely consumed and for ~6 mM of crosslinks to form. While crosslinking is not completely prevented, it is likely to be

reduced by the presence of TEMPO. It will be shown in Chapter 5 that high concentrations of antioxidants can scavenge 50% of more of the crosslinks that could form. This *G*(X) is likely to be greatly reduced in the presence of TEMPO. The number of residual alkyl radicals is approximately equal to the concentration of these specimens irradiated up to 100 kGy. The degree of bimolecular crosslinking will vary depending on the ionizing radiation dose rate (electron beam or gamma) and the concentration is dependent on the doping time and temperature (section 3.4).

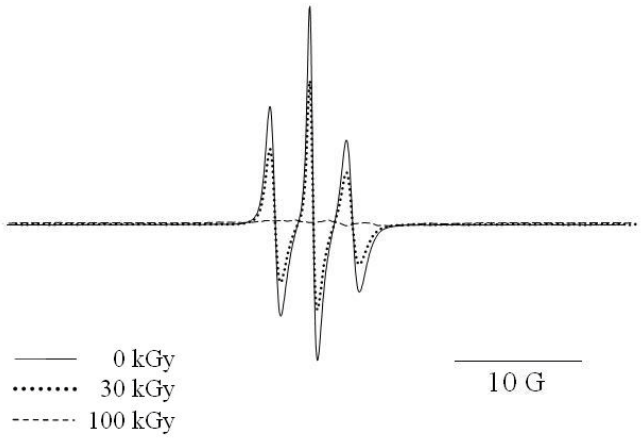

Figure 4.10: The characteristic triplet signal of TEMPO-doped UHMWPE is reduced in intensity with 30 kGy and eventually all nitroxide signal is eliminated and only a septet is observed by EPR after 100 kGy. This triplet signal decays as the nitroxide radicals scavenge the alkyl and allyl radicals as they are radiolytically-produced.

From this triplet signal decay plot, the estimated consumption of nitroxide is 0.02 mM TEMPO/kGy of radiation. This may be used to calculate future concentrations needed to scavenge all residual carbon-centered radicals, depending on dose rate and desired residual nitroxide concentration.

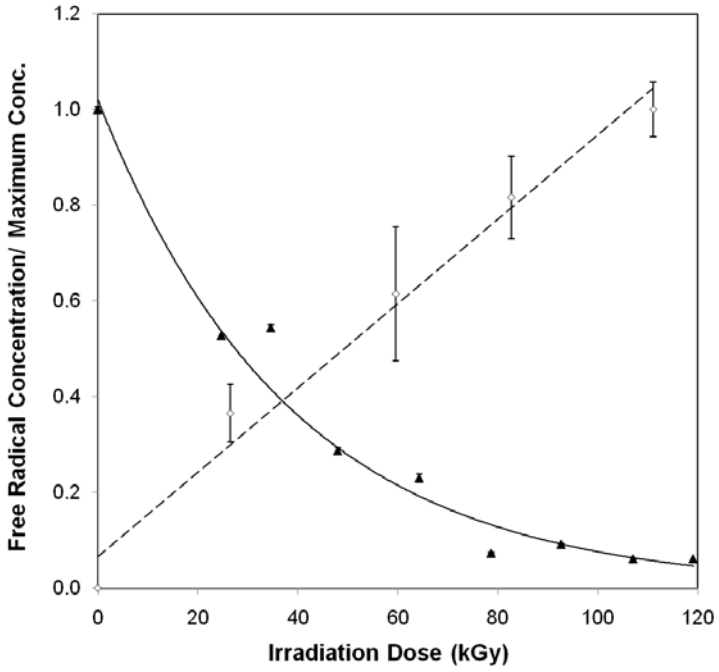

Figure 4.11: The build-up of carbon-centered free radicals (◊) increases linearly with ionizing radiation dose. The TEMPO triplet signal intensity (▲) decays with increasing doses of ionizing radiation, as observed by EPR spectroscopy. The double integration of the signal is normalized to the initial concentration of TEMPO radicals and the allyl radical double integration is normalized to the final concentration of the radicals.

4.3.4.2 Scavenging of Carbon-Centered Radicals After Irradiation

Equally important is the effect of nitroxide-doping on free radical content after irradiation and crosslinking. The doping process not only deposits the nitroxide to scavenge free radicals, but the thermal treatment also reduces residual free radicals. The reduction of allyl radical intensity through the short five minute thermal annealing of a 100 kGy irradiated specimen is shown in Figure 4.12a, as indicated by the dotted line with slightly smaller intensity. A longer annealing or remelting step, as is typical in industry, would reduce the free radical signal almost completely. The final doping concentration, as determined in section 3.4, highly depend on the time

and temperature of doping, as well as the hydrophobicity of the molecule. The addition of nitroxides at high concentrations results in a large residual signal, as demonstrated with the TEMPO triplet signal (16.5 mM) in Figure 4.12b, which is 25 times larger in intensity than the initial carbon-centered radical signal. Figure 4.13 demonstrates the complexity of free radical reactions that occur when depositing a small concentration of antioxidants, as in the doping with 0.5 mM Tempol (Figure 4.13b). This specimen exhibits a complex signal in comparison to a specimen that is unirradiated and doped with the same conditions (Figure 4.13c), where a larger amount of residual radical is left. The initial signal is shown in Figure 4.13a.

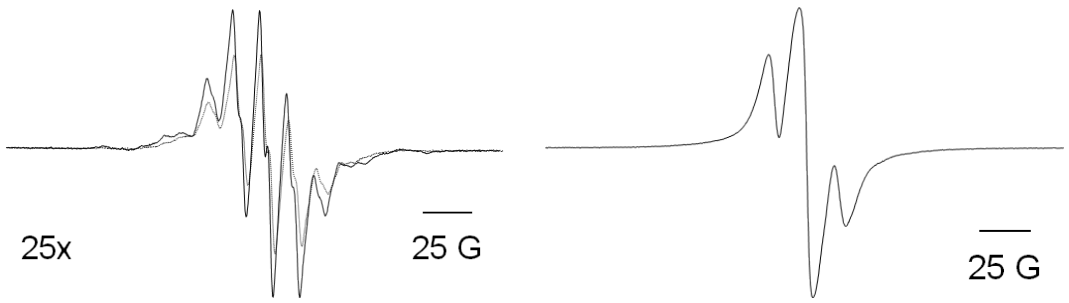

(a) (b)

Figure 4.12: EPR spectra of UHMWPE irradiated and doped with nitroxides. UHMWPE irradiated to 101 kGy with the 7 MeV electron beam (7.6 Gy/pulse) and (a) then annealed for only 5 minutes at 80ºC shows a small reduction in radical intensity (dotted line indicates annealed signal), and (b) doped with TEMPO for 5 minutes 80ºC (16.5 mM). The short dope with TEMPO results in a very large residual radical signal.

The spectra shown in Figures 4.12 and 4.13 are magnified to the same scale if accounting for their multiplication factors. The difference in intensity between the two spectra in 4.13b and 4.13c shows how the paramagnetic lineshapes of carbon-centered radicals and nitroxide radicals will cancel out when reacting, as observed by EPR. While some Tempol reacts to scavenge the carbon-centered radical, Figure

4.13b shows a complex lineshape where some residual carbon-centered radicals remain, most likely in the crystalline phase. It is likely the residual radicals in the crystal do not have enough time to migrate to the crystalline-amorphous interface or to the amorphous region, where the Tempol molecule can scavenge them. However, the complexity of the lineshape in Figure 4.13b indicates that most allyl radicals have not been scavenged and that the observed signal is a combination of residual allyl and Tempol radicals. The difference between 4.13b and 4.13c is likely to be the scavenging of alkyl radicals that are migrating to the crystalline-amorphous interface. Although alkyl radicals are easily scavenged by nitroxides, the stability of the unsaturation through electron conjugation limits the allyl radical reaction with antioxidants.

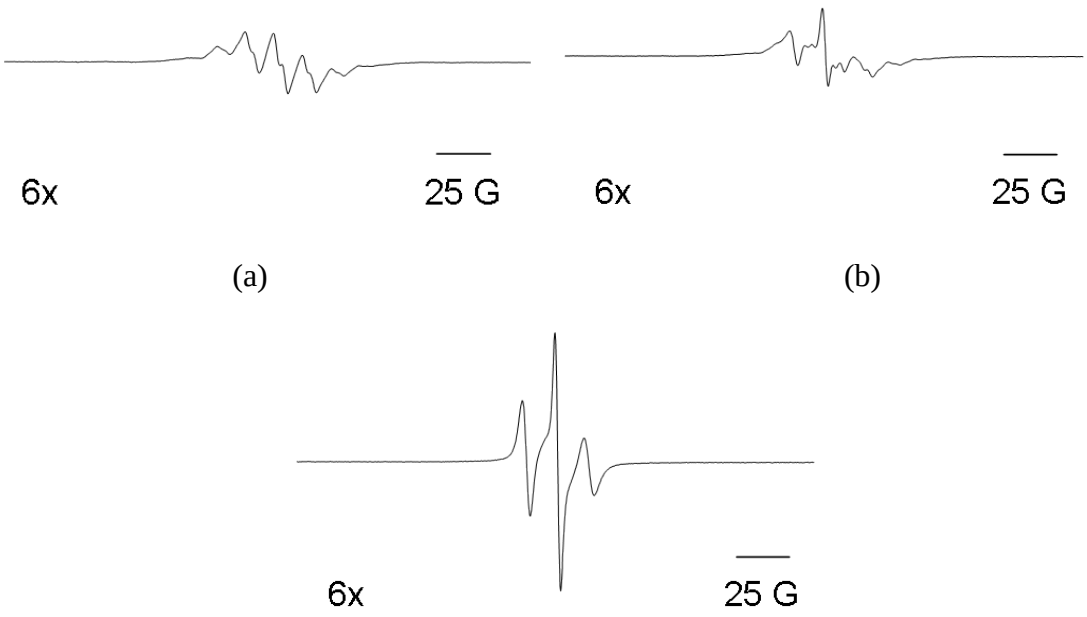

Figure 4.13: EPR spectra of 101 kGy (7 MeV electron beam, 7.6 Gy/pulse, 60 pulses per second) irradiated UHMWPE with (a) no thermal treatment and (b) a 5 minute 100°C Tempol doping. The same doping of an unirradiated specimen (c) produces a much higher nitroxide triplet intensity. While some alkyl radicals are scavenged by the nitroxide, the allyl radical signal remains, resulting in the complex lineshape (b).

4.3.5 Conclusion

The EPR investigation of nitroxide-infiltrated UHMWPE illustrates that TEMPO and Tempol are efficient alkyl radical scavengers. While alkyl radicals are scavenged rapidly, allyl radicals are more stable and remain in the presence of nitroxides. However, the goal is to prevent oxidation and not the formation of allyl radicals. Therefore, nitroxide doping can still be used after irradiation, to scavenge any residual alkyl radicals. The optimal concentration can be attained, by fine tuning the doping time and temperature, before or after irradiation. A small amount of residual nitroxide radical may be beneficial, as to be available to scavenge any remaining radicals that may slowly migrate from the crystals. Assessing the necessary antioxidant concentrations for long term oxidative protection may be an important topic for future work. Mechanically-generated radicals during wear in the joint may need to be scavenged as well, and this presents a challenge to the quantification of total radicals produced over the UHMWPE liner lifetime.

4.4 Conclusions

This chapter has illustrated the free radical reactions that occur in the presence of nitroxides. In the absence of oxygen and at high nitroxide concentrations, the TEMPO free radicals scavenge carbon-centered radicals through radical-radical interactions. This is illustrated by EPR spectroscopy showing a decreasing nitroxide triplet signal where the radical lineshapes eventually cancel-out, as well as by the production of the >NOR intermediate on the microsecond time scale after irradiation by pulse radiolysis. The formation of this intermediate is reported here to be a second

order reaction rate constant $k' = 1 \times 10^9$ mol $L^{-1}s^{-1}$. Additionally, the *G*-value of 3.7 for the vinyl unsaturation production in octane by γ-radiolysis is first reported here.

The calculated reaction rate constants, if extended to TEMPO/octane solutions containing oxygen, can be used to create a kinetic model for the resulting products depending on the initial species concentration. Additionally, picoseconds pulse width studies can be used to measure the full alkyl radical decay reaction rate constants. With this crucial piece of the reaction puzzle, radiation chemical yields can be calculated for the alkyl radical, allyl radical, peroxyl radical and nitroxide intermediate complex for this specific set of parameters.

The kinetic differences between alkyl radical reactions in neat octane and TEMPO/octane solutions are expected to extend to UHMWPE. Though, to obtain predicted reaction rate constants in UHMWPE, the constants calculated for octane need to be extrapolated for the molecular weight and viscosity of the polymer. Regardless, the presence of the nitroxide alters the reaction scheme to produce a nitroxide-polymer complex that introduces a fifth competing reaction path for alkyl radicals. By controlling the presence of oxygen, alkyl radicals can be persuaded to bimolecularly crosslink and react with the nitroxide, eliminating oxidative degradation of the polymer.

Chapter 5: Effect of Nitroxides on UHMWPE Structure

5.1 Introduction

The addition of antioxidant can have both positive and negative effects on UHMWPE. While they prevent oxidation, antioxidants can cause UHMWPE to become plasticized, allowing the polymer chains to reptate and slide more easily.[8, 95] This phenomenon occurs because the antioxidant swells the polymer, increasing the free volume and reducing the activation energy for disentanglement.[37] Therefore, the polymer chain moves more easily. Plasticization by vitamin E will increase the tensile strength, elongation at failure,[33] fatigue strength and crack propagation resistance of vitamin E-impregnated UHMWPE.[66] While this seems to be a benefit, the full plasticization effects are not known. For example, antioxidants can reduce the degree of crosslinking, as reported with vitamin E blended into UHMWPE.[33, 35, 74] Highly crosslinking UHMWPE prevents wear[96] and this property should be balanced with oxidation and fatigue-resistance. A viable option is to diffuse or add the antioxidant after radiation crosslinking.[8, 95] Since UHMWPE performance is so closely tied to its structure, this chapter evaluates the effect of nitroxides on the microstructure (crystallinity) and bulk crosslink density. These two properties have been identified as the largest contributing factors to mechanical performance.[97] Inherent to the nitroxides' ability to prevent oxidation is the scavenging of carbon-centered free radicals. The effect of such scavenging on the crosslink density, which prevents wear debris production, should be elucidated. This chapter evaluates the effect of adding nitroxides on the crosslink density of

UHMWPE before and after irradiation. Additionally, the effect of nitroxides on the crystal structure, in percent crystallinity, φ, and melting temperature, T_m, is examined.

5.2 Crosslinking of Nitroxide-Doped UHMWPE

5.2.1 Background and Theory

Bimolecular crosslinking of a polymer occurs through the addition of two alkyl radicals,[16] as shown in equation 1.3. Alkyl radicals are produced with a *G*-value[†] of 3.3 – 4.4 molecules per 100 eV deposited ionizing radiation energy.[18, 19] For this study, the $G(R^{\bullet})$ will be assumed to be 4. Crosslinking is a dominant process with a $G(X)$ of crosslink formation ≈ 3.[23] However, this value highly depends on the radiation dose rate and on the presence of radical scavengers, like oxygen and antioxidants. The number of crosslinks can be maximized with a very high dose rate, as with electron beam irradiation. If a radical scavenger is present during crosslinking, some proportion of the alkyl radicals produced will not crosslink but will react with the radical scavenger. The presence of oxygen is minimized to prevent the formation of peroxyl radicals, formed in equation 1.7, but there will be some diffused oxygen that cannot be eliminated. Antioxidants are added to compete with oxygen for residual free radicals. Accordingly, the antioxidant will also compete with bimolecular crosslinking reactions. The effect of nitroxides on the crosslink density is evaluated using Thermomechanical Analysis (TMA), as described in section 2.7. The change in sample height during solvent swelling over a temperature range of

[†] *G*-value is defined as the number of molecules/units produced per 100 eV of ionizing radiation.

25 – 140 °C is used to calculate the swell ratio, crosslink density and molecular weight between crosslinks. The swell ratio of polymer can be measured from the initial height, H_o, and the final height, H_f, by equation 5.1:

$$q_s = \left(H_f / H_o\right)^3 \tag{5.1}$$

From the swell ratio, the crosslink density, υ_d, can be calculated by equation 5.2, using 0.225 + (0.56/q_s) for the Flory polymer-solvent interaction parameter, χ_1, and 174.5 cm^3/mol for the molar volume of solvent, ϕ_1:[98]

$$v_d = -\frac{\ln\left(1 - q_s^{-1}\right) + q_s^{-1} + \chi_1 q_s^{-2}}{\phi_1\left(q_s^{-1/3} - q_s^{-1}/2\right)} \tag{5.2}$$

Finally, the molecular weight between crosslinks, M_c, can be calculated by equation 5.3, using 930 g/L as the specific volume of polymer, $\bar{v}$:

$$M_c = \bar{v} v_d^{-1} \tag{5.3}$$

These three calculations comprise the parameters determined to assess network crosslinking of UHMWPE. The effect of antioxidants and thermal treatments on the swell ratio, crosslink density and molecular weight between crosslinks is explored in this section.

5.2.2 Objectives

It has been observed that the addition of vitamin E before crosslinking reduces the crosslink density (ν_d) dramatically.[33, 66, 74] The changes to UHMWPE bulk gel structure, or crosslink density, due to the introduction of nitroxide antioxidants are evaluated here. Nitroxides can be infiltrated prior to consolidation or after radiation crosslinking, by diffusion. One objective is to determine which processing scenario will yield the most optimal crosslink density. Since crosslinking, oxidation and radical stabilization through antioxidants compete for the radiolytically-produced alkyl radicals, it is important to evaluate the best processing practices and the effect each processing scenario will have on crosslink density. Additionally, these measurements should be compared to literature values of the crosslink densities obtained with vitamin E. Determining the effect of nitroxides on crosslinking plays a part in qualifying the molecules for use in joint replacement bearings. The effect of the following areas on the crosslink density of UHMWPE will be evaluated:

- Antioxidant added before or after crosslinking
- Concentration of antioxidant
- Effect of ionizing radiation dose rate

From these observations, conclusions about the reaction mechanisms between carbon-centered free radicals and nitroxides can be made. The time scale of crosslinking will be elucidated. Lastly, the effect of processing conditions on the molecular weight between crosslinks formed will be evaluated.

5.2.3 Experimental Method

A description of the irradiation and infiltration conditions of samples for TMA analysis is summarized in Table 5.1. Samples of 1 mm diameter are drilled from 1 mm thick strips of UHMWPE, as described in section 2.7.2, forming a cylindrical pellet with 1:1 height-to-width aspect ratio. Pellets of 1 mm thickness are either packaged in argon, and irradiated according to Table 5.1, or doped/pre-annealed first and then packaged and irradiated. The 30 minute doping was estimated from initial data from Figure 3.6 to produce a low concentration of antioxidant that would be equivalent to typical vitamin E diffusion concentrations.

Table 5.1: TMA Crosslinking Measurement Sample Processing Matrix

Sample Processing	*Irradiation Doses*	*Thermal Treatment, Temperature*
Irradiated and Annealed (Control)	10, 30, 50, 55, 75 100, 120kGy	Annealed, 110°C 48 hours
Pre-annealed and Irradiated	50, 75, 100 kGy	Annealed, 70°C 30 minutes
TEMPO and Irradiated	25, 50, 100 kGy	TEMPO Infiltrated, 70°C, 30 min.
Tempol and Irradiated	50, 75, 100 kGy	Tempol Infiltrated, 70°C, 30 min.
Irradiated and TEMPO	50, 75, 100 kGy	TEMPO Infiltrated, 70°C, 30 min.
Irradiated and Tempol	50, 75, 100 kGy	Tempol Infiltrated, 70°C, 30 min.

5.2.4 Results and Discussion

While antioxidants may prevent oxidation, blending these additives with UHMWPE resin and consolidating prior to irradiation may reduce crosslinking more than desired.[33, 35, 74] On the other hand, the desired degree of crosslinking may be maintained by first crosslinking, followed by absorption of antioxidant to achieve oxidation stabilization. It is hypothesized that the extent of crosslinking will be largely affected by whether antioxidants are added before or after irradiation. Similarly, it is important to understand the mechanisms by which antioxidants may

prevent crosslinking. It is expected that crosslink density of the polymer will increase linearly with increasing dose, and then level off to a crosslink saturation.[99] The irradiation doses used here lie in the linear portion of such a plot and the crosslink densities are loosely approximated with a linear trendline, as shown in Figures 5.1 – 5.4. These trendlines are not meant to fit the data, nor to indicate that the crosslink density versus dose relationship is completely linear.

5.2.4.1 Crosslink Density of UHMWPE Irradiated Prior to Antioxidant Doping

The calculated crosslink densities, υ_d, of UHMWPE specimens thermally treated or doped with antioxidants before irradiation are shown in Figure 5.1. Specimens are doped with TEMPO and Tempol at 70°C for 30 minutes to mimic typical vitamin E diffusion concentrations. Due to differences in hydrophobicity, TEMPO diffuses more easily into UHMWPE so these specimens contain 5.8 mM TEMPO, while under the same conditions, only 87 μm of Tempol is absorbed. These concentrations are measured by EPR spectroscopy and the effect of hydrophobicity on absorbed nitroxide concentration is further discussed in section 3.4.3. One set of TMA specimens simulates this 70°C, 30 minute doping without the antioxidant to assess the effect of the 70°C thermal treatment alone. Specimens are then irradiated with ionizing radiation doses of 15 – 120 kGy with the 7 MeV electron beam, with 60 pulses per second and approximately 7.2 Gy per pulse for a high dose rate that maximizes crosslinking. Conversely, the control specimens were irradiated (with 7 MeV electron beam, 60 pulses per second and 7.2 Gy per pulse) and then annealed at 110°C for 48 hours, an approach similar to typical industry annealing, such as used to

manufacture the Crossfire^{TM} UHMWPE hip liner (Stryker Howmedica Osteonics, Mahwah, NJ). Lastly, data adapted from Oral *et al*., 2005, of vitamin E consolidated specimens to 0.1 wt% and 0.3 wt%, gamma-irradiated to 100 kGy[33] provide a measure for the degree of crosslinking-inhibition by vitamin E.

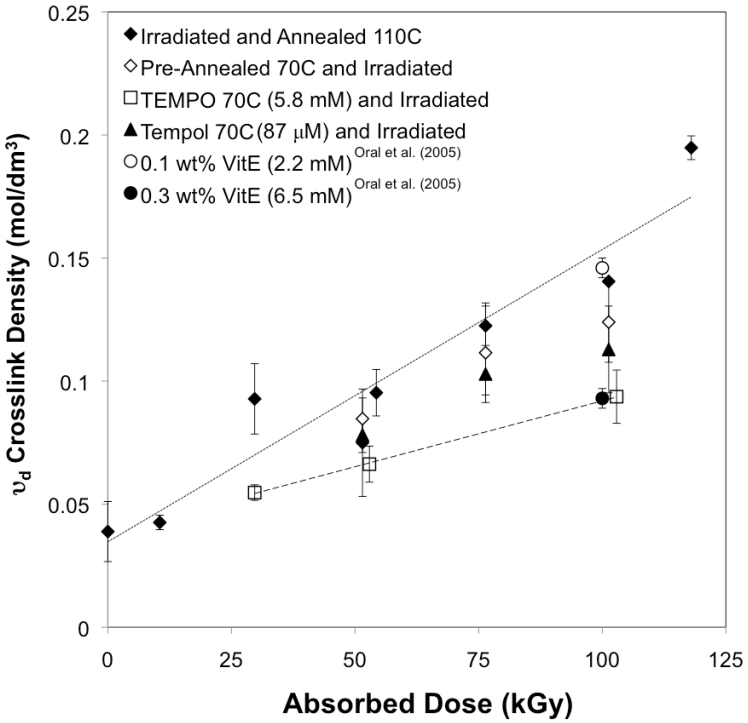

Figure 5.1: Crosslink density, υ_d (mol/dm^3) of UHMWPE doped with nitroxide antioxidants prior to crosslinking with 7 MeV electron beam (60 pulses s^{-1}, 7.3 Gy per pulse). Specimens doped with TEMPO and Tempol are compared to specimens that incurred the same thermal history (pre-annealed 70 °C) and control specimens processing by irradiation and subsequent 110 °C annealing. Additionally, crosslink densities of specimens consolidated with 2.2 mM and 6.5 mM vitamin E are also shown.[33] The addition of antioxidants prior to crosslinking inhibits some crosslinking, as can be expected. Three to five specimens are used per data point.

Figure 5.1 indicates that the addition of any antioxidant prior to irradiation inhibits crosslinking to some degree. There is an approximately 40 – 50% reduction in crosslink density of TEMPO-doped and irradiated specimens compared to the irradiated and 110°C annealed control. In addition, the sample series that is pre-

annealed and irradiated also shows a slightly reduced crosslink density (ν_d). Of course, due to the high $G(R^{\bullet})$=4 of alkyl radical production[18, 19] during high dose rate electron beam irradiation, crosslinking cannot be inhibited completely by the addition of a radical scavenger. While some crosslinking is maintained, higher doses of ionizing radiation must be utilized to achieve the same crosslink density. The pre-annealed (70°C for 30 minutes) and irradiated specimens without antioxidant also show a reduced crosslink density compared to the control (specimens irradiated and annealed for 110°C for 48 hours), demonstrating that the 70°C thermal treatment contributes to a morphological change that causes crosslinking inhibition.

5.2.4.2 Crosslink Density of UHMWPE Irradiated Prior to Antioxidant Doping

Conversely, antioxidants infiltrated after irradiation do not impact the degree of crosslinking, as shown in Figure 5.2. This plot shows UHMWPE samples irradiated with both 7 MeV electron beam and ^{60}Co gamma doped with the nitroxide TEMPO at 70°C for 30 minutes (5.8 mM). Both the electron beam and gamma-irradiated TEMPO-doped specimens show similarly high degrees of crosslinking equivalent to the industry-similar annealing processing (irradiated and 110 °C annealed). The dose rate for electron beam irradiation is 430 Gy s^{-1}, while for gamma it is 6.9 Gy s^{-1}. Regardless of dose rate, the post-irradiation addition of nitroxides does not reduce the degree of crosslinking. Since the time frame of radical production and crosslinking is much shorter than the time to diffuse antioxidants, all crosslinking has already completed in the time frame between irradiation and doping, and minimal residual radicals remain. Therefore, any antioxidants can be added after irradiation to yield the same crosslink density, dependent only on dose.

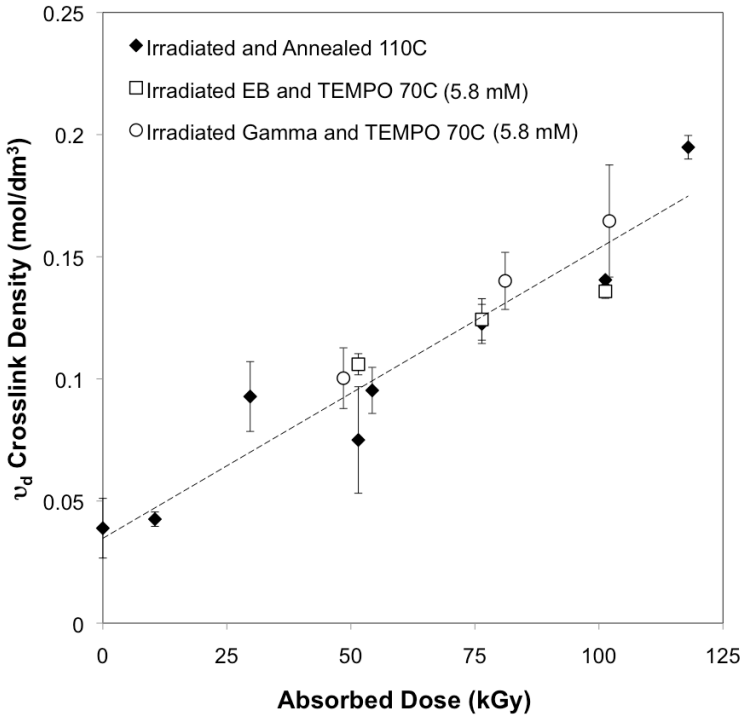

Figure 5.2: Crosslink density, υ_d (mol/dm^3) of UHMWPE doped with the nitroxide TEMPO after crosslinking with both 7 MeV electron beam (430 Gy s^{-1}) and ^{60}Co gamma (6.9 Gy s^{-1}). Specimens doped with TEMPO are compared to processing by EB irradiation and 110 °C annealing. Both gamma and electron beam crosslinking of UHMWPE produce a similar crosslink density. The addition of the nitroxide TEMPO after irradiation does not impact the crosslink density. Three to five specimens are used per data point.

5.2.4.3 Effect of Ionizing Radiation Dose Rate on Crosslinking

However, the impact of ionization radiation dose rate during crosslinking is significant. Specimens doped with TEMPO prior to irradiation are expected to exhibit lower degrees of crosslinking, as shown in Figure 5.1. Moreover, the doping of UHMWPE with TEMPO and subsequent slow ^{60}Co gamma irradiation almost completely prevents crosslinking, as shown in Figure 5.3. The minimal level of crosslinking is a result of the low 6.9 Gy s^{-1} dose rate at which alkyl radicals are produced, where they are more likely to encounter a TEMPO radical than one

another. In the course of the 20 – 50 hour irradiation, all of the alkyl radicals produced have been scavenged by TEMPO. Yet at a high dose rate, many of the alkyl radicals will find one another to bimolecularly crosslink, prior to encountering a TEMPO radical. The high 430 Gy s^{-1} electron beam dose rate produces all of the alkyl radicals within 1 – 5 minutes. It has been shown that the reaction rate constant of bimolecular crosslinking is one order of magnitude faster than nitroxide radical scavenging (see section 4.2.1).[52] However, [>NO$^{\bullet}$] > [R$^{\bullet}$] and while many of the radicals will crosslink, the remaining alkyl radicals may be scavenged by the TEMPO radical. The high dose rate maximizes crosslinking during the irradiation, in the absence of oxygen and antioxidants. Therefore, the electron beam irradiated and 110°C annealed specimens exhibit the highest level of crosslinking. The specimens irradiated by electron beam (EB) after doping exhibit a slightly lower crosslink density, while those irradiated by ^{60}Co gamma after doping show a relatively flat line or almost no increase in crosslink density with irradiation dose.

5.2.4.4 Time Frame of Crosslinking

By infiltrating UHMWPE with nitroxide antioxidants immediately after irradiation, it is possible to elucidate the time scale of polymer crosslinking. The difference in crosslink density between the two nitroxide doped curves in Figure 5.3 shows that half of the crosslinking occurs immediately during irradiation, and the remaining portion occurs on a slower time scale. The electron beam produces free radicals very rapidly and the nitroxide cannot scavenge them before they crosslink, hence there is a noticeable level of crosslinking above the unirradiated baseline. Alkyl

radicals that have not encountered other alkyl radicals are scavenged by the nitroxide. The proportion of crosslinking that typically occurs during irradiation, υ_d^{irr}, and the proportion that occurs after irradiation, υ_d^{post} can be differentiated, as labeled in Figure 5.3. In total, the degree of crosslinking will equal, υ_d^{total}, in equation 5.4:

$$\nu_d^{total} = \nu_d^{irr} + \nu_d^{post} \tag{5.4}$$

The complete crosslinking-inhibition by adding antioxidant prior to low dose rate gamma radiation has not been reported previously. Furthermore, the nitroxide carbon-centered radical scavenger has also not been used for this purpose in UHMWPE, highlighting the novelty of this work. Also, the low dose rate used here may be much lower than typically used in commercial irradiation facilities. This may enhance the effect of carbon centered-radical scavenging by nitroxides. It is important to note that the crosslinking-inhibition is not a function of gamma versus electron irradiation but that of the dose rate. Also, the high TEMPO concentration are likely to be contributing factors, if [>NO$^{\bullet}$] > [R$^{\bullet}$] > [O_2]. Considering a *G*-value of 4 for alkyl radical production, for a 100 kGy dose, 3 mM of alkyl radicals will be produced during the irradiation duration. From EPR, the observed paramagnetic concentration of TEMPO is 5.8 mM. The oxygen concentration can be calculated from the solubility in UHMWPE, S_{O_2} = 0.00881 mL (stp)/mL atm.[25] If the partial pressure of O_2 is 0.2 atm, the ρ_{UHMWPE} = 0.930 g/mL and the molecular weight of O_2 is 32 g/mol, then the concentration of O_2 in UHMWPE is calculated (equation 5.5):

$$[O_2] = \frac{S \cdot P_{O_2} \cdot \rho_{UHMWPE}}{MW_{O_2}} = \frac{(0.00881 mL(stp)/mL(atm)) \cdot 0.2 atm \cdot (0.930 g/mL)}{32.0 g/mol} = 51.2 \mu M \tag{5.5}$$

Therefore, [>NO$^{\bullet}$] ≈ [R$^{\bullet}$] >>[O_2] and the production of peroxyl radicals can be assumed to be negligible. Consequently, the reactions observed in Figures 5.1 – 5.3 do, in fact, represent carbon-centered radical scavenging by nitroxides. Thus, a nitroxide concentration of 5.8 mM can scavenge all of the alkyl radicals produced with a very low dose rate, if the concentration of oxygen is low.

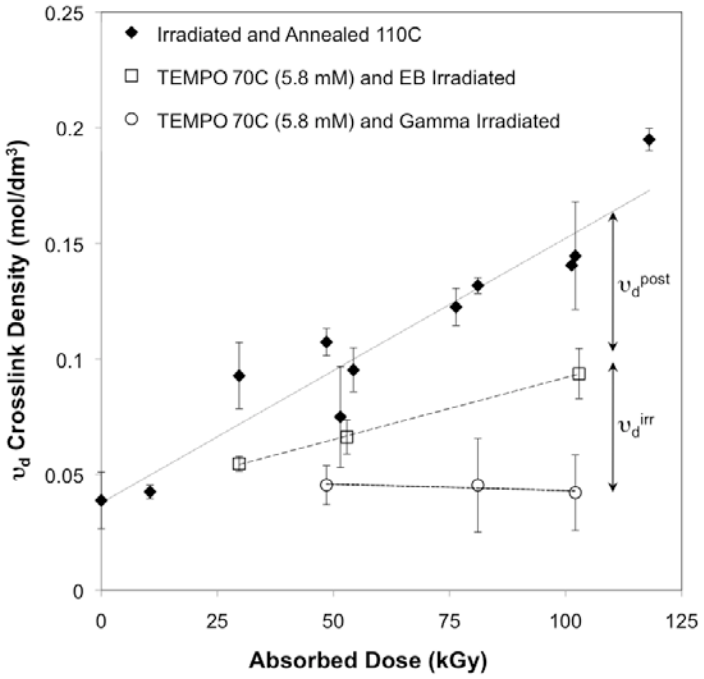

Figure 5.3: Crosslink density, υ_d (mol/dm^3) of UHMWPE doped with nitroxide antioxidants before crosslinking with both 7 MeV electron beam and ^{60}Co gamma. Specimens doped with TEMPO and Tempol are compared to standard specimens processing by electron beam irradiation and 110 °C annealing. Crosslinking with ^{60}Co gamma with a low dose rate (6.9 Gy s^{-1}) shows a near complete prevention in crosslinking, as the free radicals are produced at such a slow rate that the nitroxides can scavenge them before bimolecular crosslinking can occur. ν_d^{irr} indicates the proportion of crosslinking occurring during irradiation and ν_d^{post} is the proportion crosslinking after irradiation. Data points consist of three to five specimens each.

5.2.4.5 Molecular Weight Between Crosslinks

The molecular weight between crosslinks, M_c, calculated according to equation 5.3, for specimens containing nitroxide antioxidant is shown in Figure 5.4.

This corresponds to the molecular weight (g/mol) on average that will lie between two interchain or intrachain crosslinks. This distance decreases with increasing ionizing radiation dose and degree of crosslinking. The M_c for an irradiation dose of approximately 50 kGy is 26,700 g/mol ±1800 g/mol for 110°C annealed UHMWPE, and 43,200 g/mol ± 4600 g/mol for TEMPO-doped UHMWPE. The data in Figure 5.4 show that all specimens lie on a single general trendline, regardless of pre-irradiation processing. Apparently, the ionizing radiation dose has a more significant impact on the M_c, than the addition of nitroxides. Antioxidant inhibition of crosslinking does not significantly affect the distance between crosslinks. Ultimately, the dose of irradiation determines the M_c.

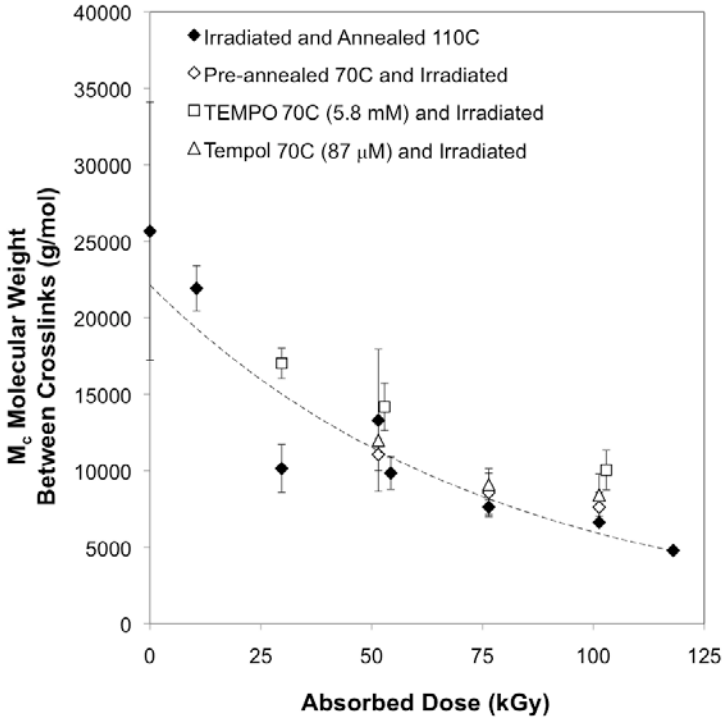

Fig. 5.4: The molecular weight between crosslinks, M_c, as calculated from the crosslink density. The impact of ionizing radiation dose is more significant than the effect of carbon-centered radical scavenging by nitroxides. Data points consist of three to five specimens each.

5.2.4.6 Antioxidant Concentration

As discussed in the previous sections, antioxidants can scavenge all of the alkyl radicals in UHMWPE to prevent the formation of bimolecular crosslinks. The concentration of antioxidants has a significant impact on what proportion of alkyl radicals will be scavenged. The Tempol doping procedure in thirty minutes introduces an approximately 87 μM residual concentration, as identified by EPR spectroscopy. TEMPO, being more hydrophobic and compatible with polyethylene, diffuses rapidly into UHMWPE up to a 5.8 mM residual concentration. TEMPO doping prior to irradiation exhibits the lowest ν_d in Figure 5.1, by scavenging more radicals, thereby preventing crosslinking. Because the concentrations are drastically different for TEMPO and Tempol, scavenging efficiency between the two molecules cannot be compared. Only a statement of the effect of nitroxide concentration to scavenge alkyl radicals can be made.

The comparison of nitroxide crosslink densities to vitamin E shows that the vitamin E consolidated UHMWPE also shows concentration-dependent radical scavenging. Although less effective at scavenging alkyl radicals (see section 4.2.4), phenols like α-tocopherol still do so in the absence of oxygen. The crosslink density adapted from Oral *et al*. show a much lower ν_d with 6.5 mM α-tocopherol (0.093 mol/dm^3) consolidated before irradiation than 2.2 mM α-tocopherol (0.146 mol/dm^3).[33] Again, 6.5 mM α-tocopherol consolidated specimens show the same degree of crosslinking as 5.8 mM TEMPO irradiated to the same dose (0.093 mol/dm^3). In brief, crosslink density inhibition is dependent mostly on antioxidant concentration and to some extent the processing temperatures used.

5.2.5 Conclusions

Antioxidants, such as the nitroxides, TEMPO and Tempol, can have a substantial effect on the microstructure and bulk crosslink density. If the antioxidants are added after crosslinking, the resulting crosslink density will be equivalent to typical processing (irradiated and annealed). The dose rate at which the specimens are irradiated will not change the crosslink density, providing it is in the absence of oxygen. Contrarily, if the nitroxide is consolidated with the UHMWPE or diffused into the polymer prior to irradiation and crosslinking, the crosslink density will be compromised. The degree to which the crosslink density is reduced will depend on the concentration of the nitroxide, the ionizing radiation dose and most importantly the radiation dose rate. If the nitroxide is added before irradiation and the dose rate is low, as with ^{60}Co gamma, crosslinking can be completely prevented.

One limitation of this work is the relation of the control specimen, irradiated and 110 °C annealed to industry-typical processing. Most UHMWPE tibial inserts and articular liners are currently crosslinked and remelted. However, the control set here approximates an irradiated and annealed processing methods, which has somewhat been rejected for its *in vivo* oxidation. The control set used loosely approximates industry annealing similar to those to manufacture Crossfire^{TM}, although the irradiation and annealing conditions are not exactly equal. Crossfire^{TM} is irradiated in air and annealed at 130 – 135°C. At these temperatures, many of the smaller crystals have remelted. The 110°C annealing lies well below most crystalline melting. While a lower annealing temperature is likely to allow less recombination of radicals, the inert irradiation environment will increase the initial crosslinking. For

this reason, the irradiated and 110°C annealed specimen set can loosely approximate an industry processing method.

An important advantage of using nitroxides versus vitamin E is the shorter duration and lower doping temperature. Standard thermal processing can be adapted to include a shorter, lower-temperature diffusion with TEMPO or Tempol into UHMWPE, resulting in a highly crosslinked material that is resistant to oxidation.

5.3 Effect of Nitroxides on Crystallinity

5.3.1 Introduction

The crystallinity of a semi-crystalline polymer, like UHMWPE, has a high impact on the mechanical properties. Crystals in the polymer blunt fatigue crack propagation,[7] enhancing fatigue strength, which is crucial in total knee arthroplasties. The percent crystallinity, φ, is defined in equation 5.7, as the ratio of the specimen's heat of fusion, ΔH_s divided by the theoretical heat of fusion of 100% crystalline polyethylene (289.3 J/g), ΔH_f:

$$\varphi(\%) = \frac{\Delta H_s}{\Delta H_f} \times 100 = \frac{\Delta H_s}{289.3 J/g} \times 100 \qquad (5.7)$$

The melting point is determined as the peak of the melting endotherm, with a baseline defined between 50°C and 160°C (ASTM Standard F2625). Additionally, the shape of the melting endotherm can be evaluated to detect degradation products or the presence of additives that may be detected as a separate peak or shoulder on the main melting peak. The larger the crystals and higher the crystallinity of UHMWPE,

the higher the melting point because thermodynamically, larger crystals take longer to melt at higher temperatures.

The modification of UHMWPE with ionizing radiation and thermal treatments during annealing, remelting or diffusion of antioxidant will alter the crystallinity of the polymer. The rate of crystallization will determine the crystallinity and morphology, which in turn determines mechanical properties.[100] Therefore, the initial consolidation and subsequent processing temperature and rate of cooling will change the crystal morphology of the polymer. Previous studies have indicated that percent crystallinity of UHMWPE increases with radiation dose,[97, 101] as crosslinking plays a role enhancing the crystal structure. Correspondingly, the melting point also increases with radiation dose due to increasing crystallinity.[97] The introduction of antioxidants involves a thermal treatment to diffuse the antioxidant into the polymer and homogeneously distribute it throughout the thickness of the material. Temperatures up to 120°C have been used to diffuse vitamin E into UHMWPE,[75] which is above the α-transition temperature of 90 – 95 °C. The introduction of vitamin E into crosslinked UHMWPE at these temperatures does not reduce the crystallinity but will allow crystal relaxation, while remelting the polymer will reduce the crystalline percentage.[102]

5.3.2 Objectives

In this section, the objective is to evaluate the changes that nitroxides and vitamin E (α-tocopherol) have on the crystallinity and melting point of UHMWPE. These changes are compared to UHMWPE irradiated and remelted specimens. Differential Scanning Calorimetry (DSC) is used to evaluate the effect of radiation

crosslinking on the thermal properties of UHMWPE. The experiment also determines how antioxidants further affect the crystallinity and melting point of radiation crosslinked UHMWPE.

5.3.3 Experimental Method

Processing for DSC specimens involves packaging 2 inch diameter pucks, with 5 mm thickness, in nitrogen gas and irradiating with ^{60}Co gamma (dose rate of 2.7 kGy h^{-1}). Doping is performed either by soaking UHMWPE in α-tocopherol for 2 hours at 100°C and homogenizing for 72 hours at 100°C (0.0071 wt% or 15.3 mM) or doping with TEMPO or Tempol at 100°C for 72 hours (17.0 mM and 15.3 mM, respectively). Remelted specimens are heated at 148°C for 2 hours. Gravimetrically measured resulting antioxidant concentrations for each specimen absorbed dose are shown in Table 6.2 in section 6.4.2. Specimens are then cleaned and placed in an oxygen bomb for accelerated aging (section 2.10) at 70°C for 14 days. Specimen cores with a 3.5 mm diameter are drilled from these bulk specimens from which tensile specimens are cut (section 7.3). Samples of 3 – 10 mg weight are cut from each core, weighed and packaged in a hermetic DSC pan. The first heat, melt, and second heat are measured according to the method described in section 2.8.2, according to ASTM D3418. The percent crystallinity and melting temperature are evaluated according to ASTM F2625.

Statistical analysis is performed with StatPlusMac LE software. Basic statistics comparing means between two sample groups, with uneven variances (heteroscedastic) are used to calculate *p*-values of significance. The Student's t-test with a two-tailed distribution is calculated with a reliability level $\alpha = 0.05$. *P*-values

that are greater than 0.05 are considered not significant, $0.05 < p < 0.01$ are significant, $0.01 < p < 0.001$ are very significant, and $p < 0.001$ are extremely significant.

5.3.4 Results and Discussion

A table of the thermal properties of UHMWPE with a range of processing conditions is shown in Table 5.2. Virgin UHMWPE, that has not been irradiated, serves as a control. The melting point, T_m, and percent crystallinity, φ, of UHMWPE specimens irradiated and remelted or doped are shown for the first and second melt. The first melt is indicative of the thermal history of the polymer. The melting endotherms of 62 kGy irradiated and remelted, vitamin E-doped, TEMPO-doped and Tempol-doped UHMWPE are shown in Figure 5.5. The second melt provides a measure of the material's inherent thermal properties, recrystallized under conditions specified by ASTM D3418. The corresponding second melt endotherms are shown in Figure 5.6.

The first melt indicates that the presence of the three antioxidants increases the melting temperature versus remelted UHMWPE. Additionally, the melting peak of antioxidant containing specimens is more narrow and the area under the peak is larger than the remelted specimens. This indicates that the crystals are larger and the crystal size distribution is more narrow, because smaller crystals melt first at lower temperatures,[103] so a distribution shifted up indicates larger crystal size.

Table 5.2: Thermal Properties of UHMWPE: Virgin, Remelted, or Doped with the Antioxidants Vitamin E, TEMPO, Tempol									
	Radiation Dose (kGy)	1st Melt				2nd Melt			
		T_m (°C)		φ (% crystallinity)		T_m (°C)		φ (% crystallinity)	
Virgin	0	137.47	±0.52	66.61	±3.59	134.27	±1.73	61.56	±3.01
Remelted	0	137.26	±0.31	67.38	±1.62	136.47	±0.47	68.85	±1.78
	62	137.31	±1.05	62.97	±1.79	134.88	±0.96	61.51	±1.16
	110	137.58	±0.45	69.05	±0.70	133.58	±0.64	63.83	±0.82
VitE	0	139.54	±0.88	69.02	±2.31	136.11	±0.89	62.75	±0.43
	62	142.07	±0.71	70.69	±1.34	135.07	±0.55	58.81	±1.01
	110	142.45	±0.52	77.10	±2.32	134.63	±1.65	62.90	±2.37
TEMPO	0	138.87	±1.14	66.34	±0.79	135.51	±1.06	60.86	±0.49
	62	142.83	±0.38	71.30	±2.26	134.84	±1.53	59.15	±1.84
	110	143.72	±0.32	70.82	±2.11	138.63	±0.20	56.99	±1.79
Tempol	0	138.55	±0.48	65.55	±1.53	135.98	±0.51	60.64	±1.21
	62	142.47	±0.20	71.13	±1.46	134.98	±0.31	59.42	±0.97
	110	143.75	±0.64	72.28	±1.75	137.95	±0.53	58.93	±0.44

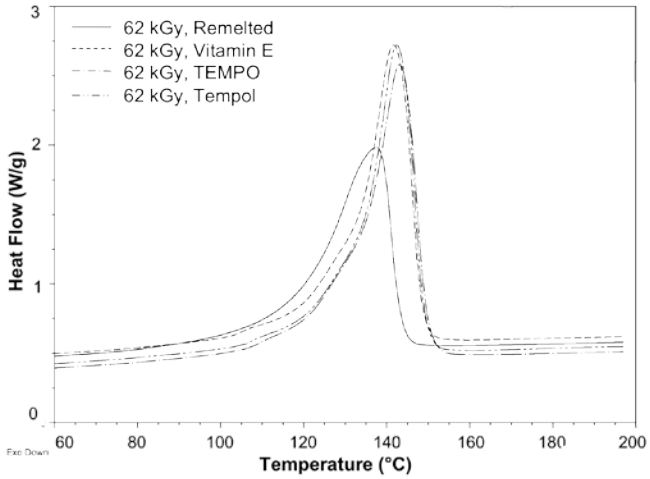

Figure 5.5: The first melting endotherms for UHMWPE irradiated to 62 kGy in nitrogen and remelted 148°C (2 hours), doped with Vitamin E 100°C (2 hours) and homogenized for 100°C (72 hours), doped with TEMPO or Tempol 100°C (72 hours). Specimens of 3 – 10 mg weight are packaged in DSC pans and heated from 40°C - 200°C at 10°C per minute. The overlaid endotherms indicate that the addition of antioxidant increases T_m and the heat flow. The remelted sample T_m and area under the curve are lower than that of the antioxidants due to the smaller crystals that resulted from the remelted processing.

On the other hand, the second melt endotherm shows very similar traces for all four sample groups irradiated to 62 kGy because the thermal history is erased by

melting and recrystallizing. The four processing groups were all crosslinked with the same ionizing radiation dose, presumably producing the same crosslink density. Once the thermal history is erased, the crosslink density governs the properties observed in the second melt. The second melt endotherms have a smaller heat flow and crystallinity than the first melt because the crosslinking has inhibited recrystallization after the first melt.

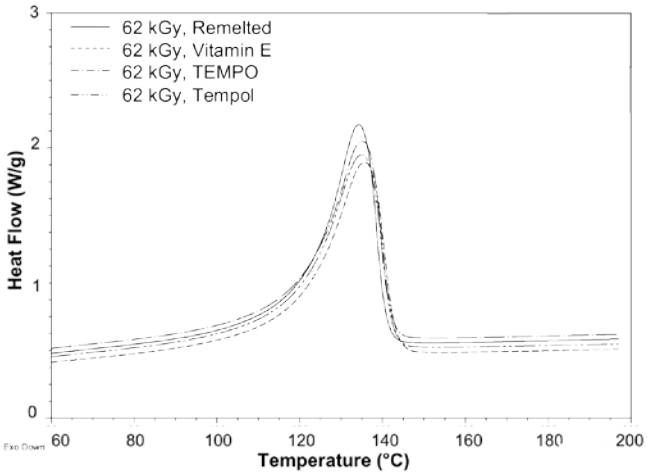

Figure 5.6: The second melting endotherms for UHMWPE irradiated to 62 kGy in N_2 and remelted 148°C for 2 hours, doped with Vitamin E 100°C for 2 hours and homogenized for 72 hours (100°C), doped with TEMPO 100°C, 72 hours or doped with Tempol 100°C 72 hours. These specimens, of 3 – 10 mg weight, have been heated to 200°C, recrystallized (cooled) at 10°C per min., and heated again from 40°C to 200°C at 10°C per min. to produce these second melt endotherms. The overlaid endotherms indicate that once the thermal history is erased, degree of crosslinking at 62 kGy allows equal recrystallization measured by these endotherms.

With increasing radiation dose, the remelted UHMWPE shows no change in T_m. On the other hand, the crystallinity significantly decreases from 67.4°C of unirradiated, remelted UHMWPE to 63.0°C (p = 0.0108) in 62 kGy irradiated, remelted UHMWPE. From 62 kGy, the crystallinity then increases to 69.0°C in the 110 kGy irradiated and remelted UHMWPE (very significant, p = 0.00322). However the change from unirradiated to 110 kGy irradiated and remelted UHMWPE

is not significant ($p > 0.13$). Overall, it can be stated that the percent crystallinity does not change. The thermal remelting should reduce the crystallinity, but in this case, the remelting simply offsets the increase that should occur with increasing radiation dose. The second melt shows a decreasing melting point and crystallinity with increasing dose, as shown in Figure 5.6, which is a result of the crosslinks. Once the polymer is melted, the crosslinks prevent recrystallization to the same degree. Consequently, the increasing crosslink density reduces the crystallinity.[99, 104]

On the other hand, the diffusion of vitamin E after crosslinking increases the melting point and percent crystallinity in the first melt. First of all, the degree of crosslinking should be similar between the remelted and antioxidant-doped samples because the diffusion is performed after crosslinking is complete. It is possible that the remelted specimens have a slightly higher degree of crosslinking because the 150°C temperature would allow more radicals to recombine than 100°C. However, the addition of vitamin E after crosslinking increases the melting point from approximately 137.3°C ± 0.3°C to 139.5°C ± 0.9°C (very significant, $p = 0.0081$) between unirradiated specimens. Although the crystallinity is not significantly higher in the vitamin E containing specimens ($p > 0.30$), the plasticization effect creates larger crystals that take more energy to melt, hence a higher melting point. Additionally, the doping is performed above the α-transition temperature, allowing crystals to relax and possibly crystallize to a higher degree due to swelling and plasticization. All things being equal, the difference lies in the temperature of thermal treatment and the addition of the antioxidant plasticizer. The φ increases from 69.0% ± 2.3% for unirradiated to 77.1% ± 2.3% for 110 kGy irradiated and vitamin E doped

specimens (very significant, $p = 0.0026$). The melting point increases from 139°C ± 0.9°C to 142.5°C ± 0.5°C with the increase in radiation dose from 0 kGy to 110 kGy (very significant, p = 0.0023). These changes can be attributed to the degree of crosslinking, the doping above the α-transition temperature and the nucleation effect of vitamin E as a result of plasticization. The second melt indicates that the melting point decreases and the crystallinity is somewhat reduced in vitamin E-containing UHMWPE. The crosslinks produced would prevent recrystallization to the same degree and this effect can be observed in all the second melting endotherms.

UHMWPE specimens containing the nitroxides TEMPO and Tempol also exhibit an increase in melting temperature, but no significant increase in crystallinity from the remelted specimens, in the first melt. The difference in T_m between the unirradiated, remelted and nitroxide-doped specimens is not as dramatic, yet the increase within each group with radiation dose is more substantial. The melting point increases from 138.9°C ± 1.1°C to 143.7°C ± 0.3°C in TEMPO containing samples. Tempol containing samples, the melting point rises from 138.6°C ± 0.5°C to 143.8°C ± 0.6°C (very significant, $p = 0.0037$). The crystallinity increases slightly in TEMPO containing specimens, 66.3% ± 0.8% for unirradiated to 70.8% ± 2.1% for 110 kGy irradiated specimens (significant, $p = 0.0286$). In Tempol, the increase in crystallinity is more dramatic with radiation dose, 65.6% ± 1.5% to 72.3% ± 1.8% (extremely significant, $p = 0.00003$). Both TEMPO and Tempol exhibit decreasing crystallinities in the second melt, to as low as 57.0% ± 1.8% in 110 kGy irradiated and TEMPO-doped samples. The decrease in crystallinity indicates a substantial amount of crosslinking in these specimens.

An important point is that the degree of crystallinity is not significantly different between 110 kGy irradiated and remelted UHMWPE, and the 110 kGy irradiated and nitroxide-doped specimens. This implies that the addition of the nitroxide molecules, TEMPO and Tempol, does not significantly disturb the inherent morphology of the polymer. While the crystal size is slightly higher, due to the higher melting point, the material does not lose its crystallinity or its overall inherent strengths that make the material a good candidate for total joint replacement.

Crystallinity is indicated to play a large role in fatigue-crack resistance and this study shows there is a 3 – 11% increase in crystallinity with increasing dose and addition vitamin E. On the other hand, the nitroxides do not impact the crystallinity of the polymer. It is possible the addition of the larger vitamin E molecule contributes to plasticization that allows a higher degree of crystallinity. Swelling of the polymer by the antioxidant molecule above the α-transition temperature may increase chain motion and crystallization due to the vitamin E. The smaller size of the nitroxides may not have this dramatic effect. Nevertheless, addition of nitroxides after crosslinking produces an increase in crystal size and T_m, as well as no change to the crystallinity of the polymer. Therefore the intrinsic properties of UHMWPE are not disturbed, although the ultimate effect will be observed in mechanical properties. The tensile properties of these materials will be evaluated in chapter 7.

5.4 Conclusions

Antioxidants, such as the nitroxides, TEMPO and Tempol, can have a substantial effect on the microstructure and bulk crosslink density of UHMWPE. The addition of an antioxidant and the thermal treatments to introduce the molecule affects the crystalline structure. The crystal size and the melting point increases with the addition of nitroxide and vitamin E antioxidants. Additionally, the percent crystallinity is not disturbed by the presence of nitroxides. Theoretically, this is a benefit to the polymer because higher crystallinities will blunt a propagating crack tip, increasing fatigue resistance.[7]

Consolidation of antioxidants into UHMWPE before irradiation will reduce the crosslink density especially if using a low dose rate. The reduction in crosslink density is also antioxidant concentration dependent. Conversely, antioxidants will not affect the degree of crosslinking if added after irradiation. Accordingly, antioxidants like nitroxides can be diffused into UHMWPE after crosslinking in an inert environment, to produce a high degree of crosslinking and typically high crystallinity, and as a result, possible increase in wear- and fatigue-resistance.

Chapter 6: Nitroxides Reduce Oxidation in UHMWPE After Accelerated Aging

6.1 Introduction

The most significant measure of antioxidant efficiency is resistance to oxidation. Accelerated aging is performed in a pressurized oxygen environment to assess if a material will oxidize under aggressive conditions. The two week process simulates *in vivo* or shelf aging that would occur over several years.[105] This technique has been used to evaluate the oxidative-stability of highly crosslinked UHMWPE[106, 107] as well as vitamin E-doped UHMWPE.[8, 33] Accelerated aging is used to validate new prosthesis materials, as well as the efficacy and performance of packaging materials.[108] While some authors expand the two week aging process to 4 weeks or more, ASTM standard F2003 recommends using a pressure vessel (oxygen bomb) pressured to 73 psi O_2 at 70 °C, held for 14 days. Because some oxygen is diffused throughout the polymer,[109] inevitably oxidation will occur to a degree when the material is irradiated. Therefore, the goal is to minimize oxidation, either through thermal treatments or by introducing a homogeneous distribution of antioxidant through diffusion into UHMWPE after irradiation or by blending with UHMWPE prior to consolidation. The resistance of nitroxide-doped UHMWPE to oxidative degradation is assessed in this chapter.

Oxidation occurs when alkyl radicals react with oxygen to form the peroxyl radicals, as shown in equation 1.9, repeated below. The peroxyl radical then abstracts a hydrogen from the polymer chain, producing a hydroperoxide (ROOH) (equation

6.1).[5] The hydroperoxides then undergo further reactions that produce ketones, alcohols, esters and acids, or degradation products that cause chain scission and loss of mechanical properties.

$$R^{\bullet} + O_2 \rightarrow RO_2^{\bullet} \quad (1.9)$$

$$RO_2^{\bullet} + \sim CH_2CH_2CH_2\sim \rightarrow R^{\bullet} + ROOH \quad (6.1)$$

These hydroperoxides can dissociate to form an alkoxyl radical, $RO^{\bullet}$, and a hydroxyl radical, $^{\bullet}OH$ (equation 6.2).[25, 107] The alkoxyl and hydroxyl radicals can produce a dialkyl ketone and water (equation 6.3), abstract a hydrogen from the polymer chain producing an alcohol and alkyl radical (equation 6.4), or react with a ketone to form an ester (equation 6.5).[25, 107]

$$ROOH \rightarrow RO^{\bullet} + {}^{\bullet}OH \quad (6.2)$$

$$\sim CH_2CHO^{\bullet}CH_2\sim + {}^{\bullet}OH \rightarrow \sim CH_2(C=O)CH_2\sim + H_2O \quad (6.3)$$

$$RO^{\bullet} + \sim CH_2CH_2CH_2\sim \rightarrow ROH + R^{\bullet} \quad (6.4)$$

$$RO^{\bullet} + \sim CH_2(C=O) \rightarrow \sim CH_2(C=O)OR \quad (6.5)$$

Accordingly, there are many other reactions that produce carboxylic acid, methyl alkyl ketones, gamma-lactone, as well as other products and radicals.[107] These reactions are not discussed here in detail because the goal is not to differentiate between the reaction mechanisms, but to quantify the content of these carbonyl groups that are indicative of oxidation of UHMWPE.

The resistance of UHMWPE to oxidation is evaluated by FTIR spectroscopy (section 2.9) by determining the oxidation index (OI). This index consists of the ratio

of the carbonyl groups that are indicative of oxidative degradation (centered at 1718 cm^{-1}) to the skeletal backbone (centered at 1370 cm^{-1}). The ratio of the areas under these peaks comprises the oxidation index, as in equation 6.6:

$$OI = \frac{Carbonyl}{Skeletal} = \frac{Area_{1718\,cm^{-1}}}{Area_{1370\,cm^{-1}}} = \frac{(1847\,cm^{-1} - 1670\,cm^{-1})}{(1394\,cm^{-1} - 1330\,cm^{-1})} \qquad (6.6)$$

Within the carbonyl peak are many contributing signals.[107] Other groups like unsaturated ketones (1687 cm^{-1}),[110] carboxylic acids (1700 cm^{-1}),[111] dialkyl ketones (1714 cm^{-1}),[5] alkyl methyl ketones (1720 cm^{-1}),[5] aldehydes (1730 cm^{-1}),[110] esters (1740 cm^{-1}),[5] γ-lactones (1778 cm^{-1})[111] and other carbonyls contribute to this signal that either appears as one or two peaks (1718 cm^{-1} and 1740 cm^{-1}).

The oxidation index can be calculated as a function of depth through a specimen to obtain an oxidation profile. Additionally, profiles of the α-tocopherol content and *trans*-vinylenes can be determined in the same fashion. The α-tocopherol index (α-TI) is generated as a ratio of the characteristic vitamin E absorbance (1275 cm^{-1}) to CH_2 rocking (1895cm^{-1}), also representative of the skeletal backbone.[8, 95] The CH_2 rocking absorbance is used for this index because the α-tocopherol absorbance overlaps with the skeletal backbone at 1370 cm^{-1}. Nevertheless, the α-TI provides a measure of the α-tocopherol content as a function of depth in a specimen, as shown in equation 6.7:

$$\alpha - t, index = \frac{\alpha - tocopherol}{CH_2 Rocking} = \frac{Area_{1275cm^{-1}}}{Area_{1895cm^{-1}}} = \frac{(1278cm^{-1} - 1230cm^{-1})}{(1940cm^{-1} - 1867cm^{-1})} \qquad (6.7)$$

A challenge identified in FTIR spectrum collection is obtaining a flat baseline for α-TI measurements. The index as defined generates values shifted slightly lower than zero, both for doped and undoped samples. Thus, the α-TI published here involves an adjustment of α-TI + 0.1, or the baseline identified with undoped specimens.

Additionally, the *trans*-vinylene content, which is linearly related to the absorbed radiation dose, is typically reported as the *trans*-vinylene index (TVI) which is the ratio of the *trans*-vinylenes (965 cm^{-1}) to the skeletal backbone (1370 cm^{-1}) (ASTM Standard F2381) as shown in equation 6.8:

$$TVI = \frac{trans - vinylene}{skeletal} = \frac{Area_{965cm^{-1}}}{Area_{1370cm^{-1}}} = \frac{(979cm^{-1} - 946cm^{-1})}{(1394cm^{-1} - 1330cm^{-1})} \qquad (6.8)$$

In this study, the TVI is used as a measure of a specimen's absorbed radiation dose. A caveat to collecting quantitative FTIR spectra, especially for the TVI, is a flat FTIR spectrum baseline. A smooth specimen surface will cause Fourier rippling in regions under 1200 cm^{-1}.[112] To eliminate Fourier rippling, a flat baseline is achieved by roughening the microtomed sample surface with sandpaper or a sharp object like laboratory tweezers.

6.2 Objectives

Using FTIR and accelerated aging techniques, the oxidation-resistance of UHMWPE in the presence of α-tocopherol, TEMPO and Tempol is evaluated and compared to irradiated and remelted UHMWPE, as well as to a group of irradiated and aged samples without antioxidant, that serves as a positive oxidized control. This

control group exhibits the maximum level of oxidation because the residual free radicals have not been eliminated by thermal treatment or antioxidant infiltration. The irradiated and remelted specimen set simulates the oxidation-resistance of what was considered state of the art "highly crosslinked" processing prior to use of α-tocopherol antioxidant. Specimens irradiated and doped with α-tocopherol serve as a measure of the oxidation-resistance of the first widely utilized antioxidant (E-Poly^{TM}, Biomet Inc, Warsaw, IN), and a comparison point for the oxidation stabilization of nitroxides. Ultimately, the goal of this chapter is to evaluate the oxidation resistance and antioxidant efficiency of the nitroxides, TEMPO and Tempol.

6.3 Experimental Method

As mentioned in section 3.5, the low vapor pressure of TEMPO allows the molecule to easily vaporize and deposit on other surfaces, especially when heated. An oxygen bomb (Millipore, Billerica, MA) was used to pressurize the specimens in O_2. Specimens were placed in metal mesh boxes so oxygen contacts all sides during aging. One of the metal mesh boxes was contaminated from the solution-based diffusion method. When this box was used for aging the first control specimens, it was determined that the nitroxide deposited on the mesh had vaporized and diffused into the control specimens, contaminating them with a low level of TEMPO. The contaminated samples contained a residual 66.6 μM ± 8.5 μM TEMPO, as evaluated by EPR spectroscopy. Once this was determined, a separate pressure vessel (oxygen bomb) was used to age control and α-tocopherol-doped specimens and another for the

nitroxides TEMPO and Tempol. Four sets of specimens were used to collect oxidation profiles are described in Table 6.1.

Table 6.1: Description of Processing of Sample Sets Used in FTIR Analysis of Accelerated Aged UHMWPE

	Processing	*Conditions*
"Age 1": Contaminated Control Set – Low Antioxidant Concentration (66 μM ± 8.5 μM TEMPO)	1 cm^3, Irradiated 42 kGy, 77 kGy, 90 kGy	γ in Air, N_2 (27-45 kGy h^{-1})
	Conditioned for 5 days	Room Temperature and Atmosphere
	Aged in Contaminated Vessel	14 days, 70°C, 73 psi O_2 but power failed twice
"Age 2": Positive Oxidation Control Set – No Thermal Treatment	1 cm^3 Irradiated 59 kGy, 110 kGy	γ in Air and N_2 (23.3 – 25.7 kGy h^{-1})
	Conditioned for 80 days	Room Temperature and Atmosphere
	Aged in New Vessel	14 days, 70°C, 73 psi O_2
"Age 3": Cross-section of Tensile Specimen Bulk Material – High Level of Antioxidants	5 mm Thick 2" Puck Irradiated 62 kGy, 110 kGy	γ in N_2 (2.26 kGy h^{-1})
	1) Remelted	148°C – 2 hours
	2) Doped with Vitamin E	100°C – 2 hours in Liquid, 72 hours 100°C Homogenization (Oven)[8]
	3) Doped with TEMPO	100°C – 72 hours, 0.336wt% TEMPO powder
	4) Doped with Tempol	100°C – 72 hours, 0.37wt% Tempol powder
	Accelerated Aged in Two Vessels	14 days, 70°C, 73 psi O_2
"Age 4": Intermediate Antioxidant Concentration	1 cm^3 Irradiated 30 kGy, 90 kGy	γ in N_2 (2.26 kGy h^{-1})
	1) Remelted	148°C – 2 hours
	2) Doped with Vitamin E	100°C – 30 minutes in Liquid, 72 hours 100°C Homogenization[8]
	3) Doped with TEMPO	100°C – 72 hours, 0.022 wt% TEMPO powder
	4) Doped with Tempol	100°C – 72 hours, 0.036 wt% Tempol powder
	Accelerated Aged in Two Vessels	14 days, 70°C, 73 psi O_2

After aging, as described in section 2.10, specimens were microtomed for FTIR analysis, viz., 100 μm thin films from the 1 cm^3 cube (Age 1, 2, 4) surface, 1 mm depth, 2.5 mm depth and 5.0 mm depth. For Age 3, the bulk specimens, from

which tensile dog bones were cut, were microtomed until a 3 mm and 5 mm cross-section was collected. FTIR analysis was performed as described in section 2.9.

6.4 Results and Discussion

6.4.1 Oxidation with Conventional Processing Techniques

Conventional industry processing techniques involve crosslinking UHMWPE with 25 – 100 kGy in an inert environment, followed by a thermal treatment held above the melting point, T_m, so residual free radicals can recombine. Remelting has been reported to eliminate oxidation *in vivo*, although it also results in a reduction of crystallinity and fatigue resistance. The introduction of antioxidants like vitamin E aims to increase oxidation resistance by eliminating free radicals so remelting is not necessary. The efficiency of three antioxidants, vitamin E, TEMPO, Tempol is evaluated here.

The oxidation profiles of the control samples which were irradiated and aged, with no thermal or antioxidant treatment to eliminate residual free radicals (Age 2 samples), exhibit high levels of oxidation on the surface of the 1 cm^3 cubes, shown in Figure 6.1. Both specimens irradiated in air (6.1a) and in N_2 gas (6.1b) oxidized equally when aged under aggressive conditions without a thermal remelting step to eliminate residual free radicals. Both the surface and bulk material exhibit elevated carbonyl absorption in FTIR analysis, as calculated by the oxidation index. The surface shows high oxidation that decreases to a plateau level in the bulk, slightly less than OI = 1, at a quarter of the specimen width. Gamma radiation penetrates the entire thickness of the specimen and free radicals are produced throughout the entire cross-

section. Oxidation and bimolecular crosslinking are in direct competition, as described in section 1.2.3. Hence, regions with higher diffused oxygen will oxidize, and regions with lower diffused oxygen will both crosslink and oxidize. Oxidation is highest at the surface since oxygen diffuses into the bulk from the surface. Similarly, the bulk will oxidize to an extent, but will have a higher degree of crosslinking.[113]

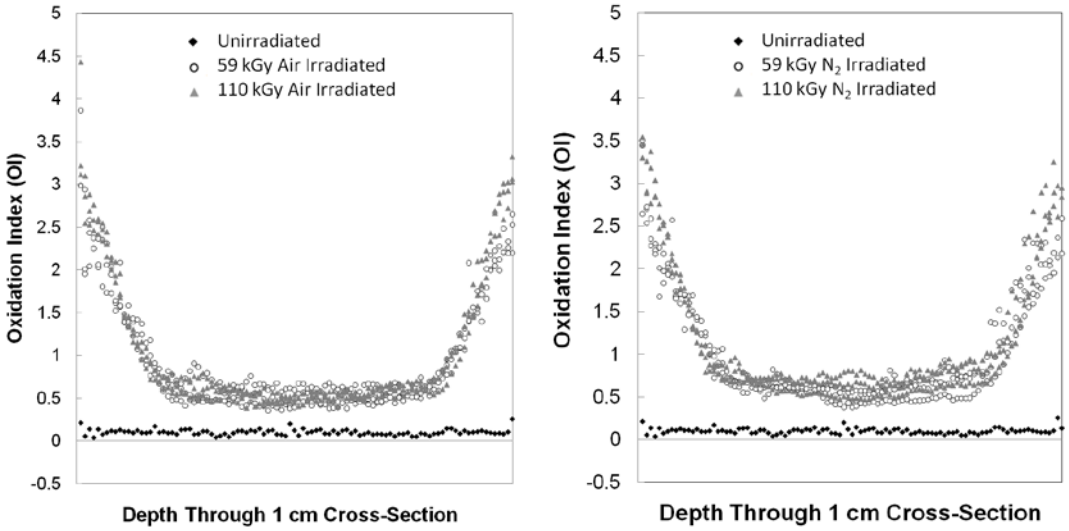

Figure 6.1: Oxidation index (OI) depth profiles through the cross-section of 1 cm^3 cubes without antioxidant or remelting, irradiated both in air (a) and in N_2 gas (b). Specimens are aged for 14 days at 73 psi O_2 at 70°C. Irradiations in inert and oxygen-containing environments both exhibit high levels of oxidation at the cube surface where diffused oxygen is higher. The bulk material also shows elevated oxidation levels, compared to the unirradiated control specimens. Each irradiation condition consists of three specimens.

In comparison, Figure 6.2 shows specimens irradiated and remelted, above the melting point of the polymer, T_m, exhibit much higher oxidation resistance. The OI depth profiles of 1 cm cross-sections of irradiated and remelted specimens are shown in Figure 6.2a. Additionally, 5 mm cross-sections of material processed in the same manner are shown in Figure 6.2b. The latter 5 mm thick specimen set is collected from the bulk material from which tensile dog bones were cut (section 7.3). Both

oxidation profiles in Figure 6.2 show good oxidation resistance throughout the depth of each specimen. Only the 5 mm cross-sections indicate oxidation levels above OI = 0.5 on the sample surfaces. Although the OI is normalized to specimen thickness, surfaces can often yield high oxidation artifacts, since the level of diffused oxygen is higher. For example, the local maximum in the unirradiated sample set in Figure 6.2a is interpreted to be a scratch through the film that produced an artificial oxidation point.

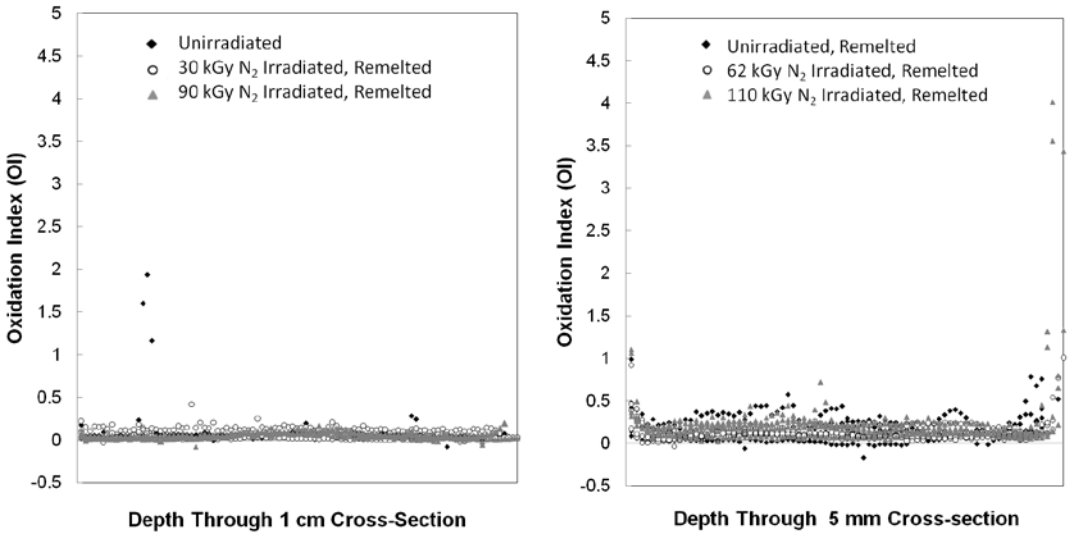

(a) (b)

Figure 6.2: Oxidation index (OI) depth profiles of UHMWPE specimens irradiated and remelted at 150°C for two hours and aged for 14 days at 70ºC, 73 psi O_2. OI profiles of a) cross-sections of 1 cm^3 cubes (consisting of three specimens per each irradiation condition) and b) 5 mm cross-section of bulk material, from which tensile specimens were cut (consisting of five specimens per each irradiation condition), show good resistance to oxidation.

Additionally, melting and recrystallization at the surface may incorporate oxygen during the remelting step to produce higher oxidation levels. These plots show that the remelting step is, in fact, sufficient to prevent oxidation despite a 14

day accelerated aging at 73 psi O_2 at 70°C. While remelting after irradiation may prevent wear due to oxidative embrittlement, the remelting step sacrifices fatigue crack resistance because the remelted polymer has a lower crystallinity (section 5.3). Nevertheless, oxidation is largely avoided by remelting the crosslinked polymer, by irradiating between 30 kGy and 110 kGy.

6.4.2 Oxidation Resistance with High Antioxidant Concentrations

It has been demonstrated that antioxidants, like vitamin E, can reduce oxidation and wear debris production in UHMWPE.[8, 33, 95] The concentrations at which oxidation resistance can be maintained for long term implantation remains debated. Three antioxidant concentrations were used for FTIR analysis of accelerated aging in this study. The concentrations for the two doping groups are shown in Table 6.2, while the third is the accidentally "contaminated group" in Age 1. The weight percentages are determined taking the difference in weight before and after doping and so represent the total concentration in each sample, irrespective of the distribution. Molar concentrations are calculated based on antioxidant molecular weights. The first vitamin E doped concentrations (Age 3) were not measured gravimetrically but rather estimated based on a trial dope with diffusion time estimated from previous data by Oral *et al*., 2007,[75] where the authors plot concentration versus diffusion time and temperature.

Table 6.2: UHMWPE Antioxidant Doping Concentrations Used in Accelerated Aging					
		wt %		**Molar Concentration (M)**	
Age 3 - High Antioxidant Concentration					
Vitamin E		0.7100	-	0.01533	-
TEMPO	Unirradiated	0.2912	± 0.0075	0.01733	± 0.00045
	62 kGy	0.2639	± 0.0135	0.01571	± 0.00081
	110 kGy	0.2998	± 0.0106	0.01785	± 0.00063
Tempol	Unirradiated	0.3326	± 0.0098	0.01796	± 0.00053
	62 kGy	0.2555	± 0.0271	0.01379	± 0.00146
	110 kGy	0.2609	± 0.0944	0.01409	± 0.00510
Age 4 - Intermediate Antioxidant Concentration					
Vitamin E	30 kGy	0.1730	± 0.0293	0.00374	± 0.00063
	90 kGy	0.1610	± 0.0135	0.00348	± 0.00029
TEMPO	30 kGy	0.0220	± 0.0107	0.00131	± 0.00064
	90 kGy	0.0215	± 0.0002	0.00128	± 0.00001
Tempol	30 kGy	0.0539	± 0.0184	0.00291	± 0.00100
	90 kGy	0.0183	± 0.0065	0.00099	± 0.00035

The specimens doped with high antioxidant concentrations (15.3 mM – 18.0 mM) after irradiation exhibit high resistance to oxidation. This is demonstrated in Figure 6.3 where the specimens doped with 0.7 wt% or 15.3 mM vitamin E (α-tocopherol) (Figure 6.3a), 17.0 mM ± 1.1 mM TEMPO (Figure 6.3c) and 15.3 mM ± 3.5 mM Tempol (Figure 6.3d) show OI <0.5 across the 5 mm specimen cross-sections.

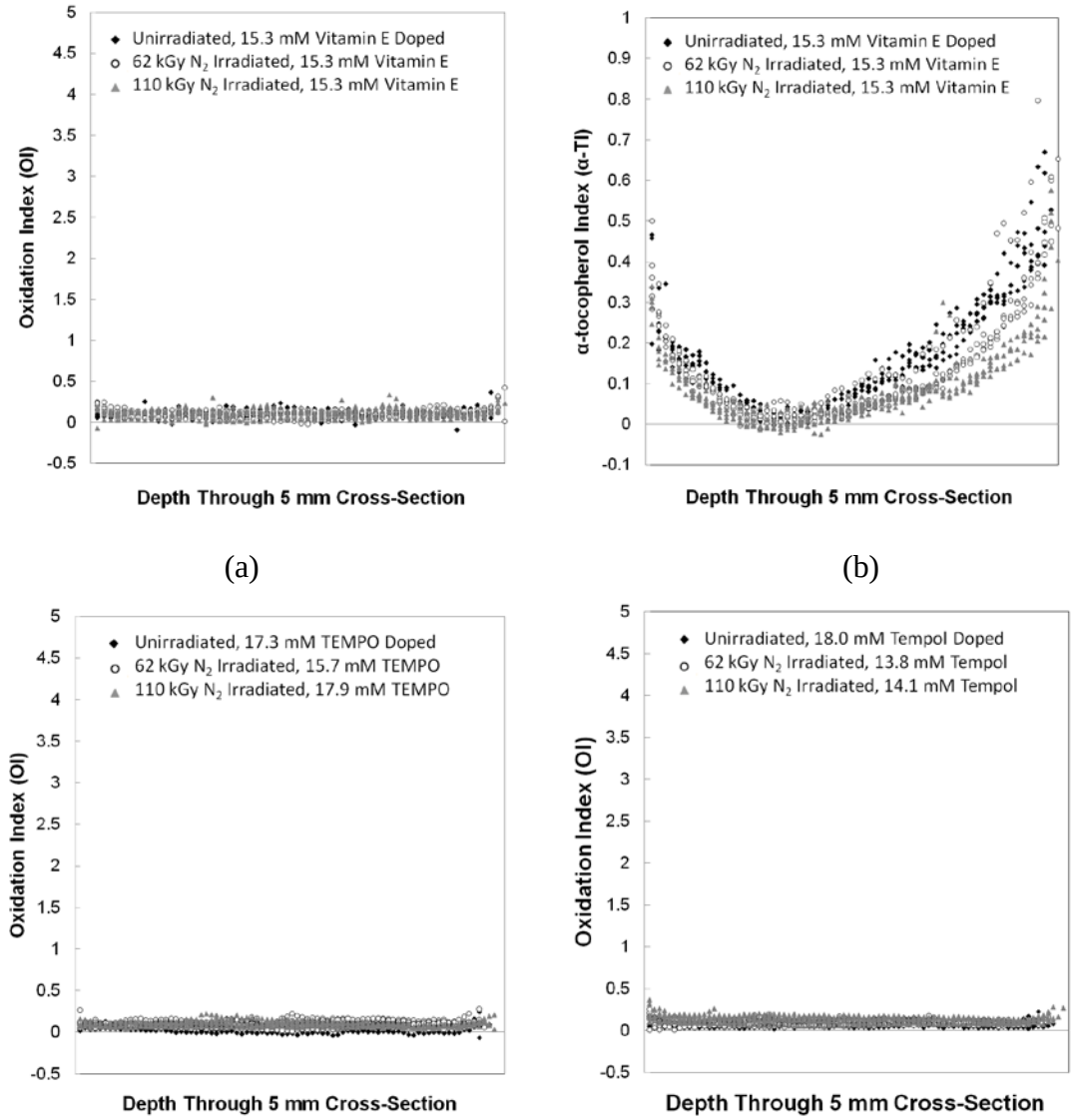

Figure 6.3: Oxidation index (OI) depth profile of 5 mm thick UHMWPE specimens doped with high concentration of antioxidants. a) α-tocopherol doped (15.3 mM) showing (b) an inhomogeneous distribution of α-tocopherol as measured by the α-T index. In addition to vitamin E, c) 17.0 mM ± 1.1 mM TEMPO and d) 15.3 mM ± 3.5 mM Tempol UHMWPE all show OI < 0.5 and very good oxidation-resistance after irradiation and accelerated aging. Each sample set in these plots contains five specimens.

A profile of the α-tocopherol index (α-TI) through the cross-section of the vitamin E-doped specimens, shown in Figure 6.3b provides a measure of the α-tocopherol concentration distribution. The figure indicates that the distribution of

vitamin E is not homogeneous through the thickness of the sample, despite a 72 hour homogenization step. One surface has a higher vitamin E concentration possibly because of the specimen orientation in the doping beaker., i.e., the side facing down and pressed against the beaker would have had a lower exposure to the vitamin E liquid. Regardless of the uneven distribution, the OI depth profiles indicate that TEMPO, Tempol and vitamin E antioxidants at 15 – 18 mM concentrations prevent oxidation during 14 days of accelerated aging at 73 psi O_2 at 70°C.

6.4.3 Oxidation in the Presence of Intermediate Antioxidant Concentrations

While higher antioxidant concentrations can be expected to prevent oxidation, the efficiency of the antioxidants can be more closely scrutinized at lower concentrations. An intermediate level of antioxidants (1 – 4 mM) also shows some resistance to oxidation. Both TEMPO and Tempol, infiltrated to 1.3 mM ± 0.4 mM and 1.9 mM ± 1.2 mM, respectively, show very low oxidation levels, in Figure 6.4. The calculated OI for TEMPO (Figure 6.4a) and Tempol (Figure 6.4b) are both less than 0.5. While all irradiated specimens in this study exhibit OI > 0.1, the method is sensitive to low levels of oxidation. For example, specimens with high concentrations (section 6.4.2) have lower OI values than UHMWPE stabilized with lower antioxidant concentrations. This is demonstrated in Figure 6.5, which shows the enlarged oxidation profiles of UHMWPE with 15.3 mM ± 3.5 mM Tempol (Figure 6.3d) and 1.9 mM ± 1.2 mM Tempol (6.4b). On a smaller OI scale, it is clear that the concentration of antioxidants is important in reducing the degree of oxidation, as higher concentrations exhibit less carbonyl absorbance. Lastly, the unirradiated and

aged specimens have OI between 0.0 and 0.2, indicating that the aging process itself can induce some small degree of oxidation in UHMWPE.

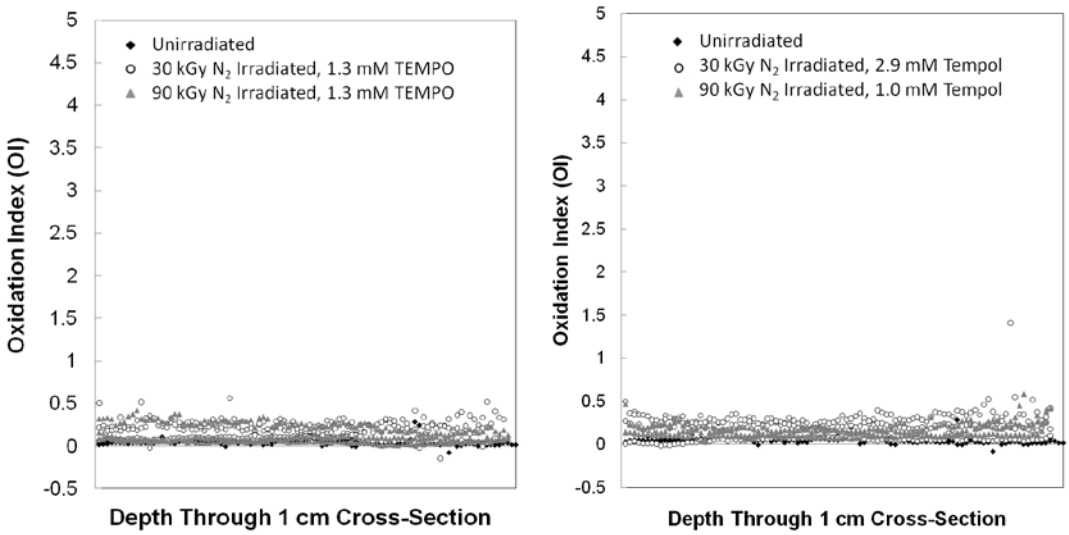

(a) (b)

Figure 6.4: Oxidation index (OI) depth profile of 1 cm^3 UHMWPE specimens doped with an intermediate-level of antioxidants. a) 1.3 mM ± 0.4 mM TEMPO and b) 1.9 mM ± 1.2 mM Tempol-doped UHMWPE show OI < 0.5 and good oxidation-resistance after irradiation and accelerated aging.

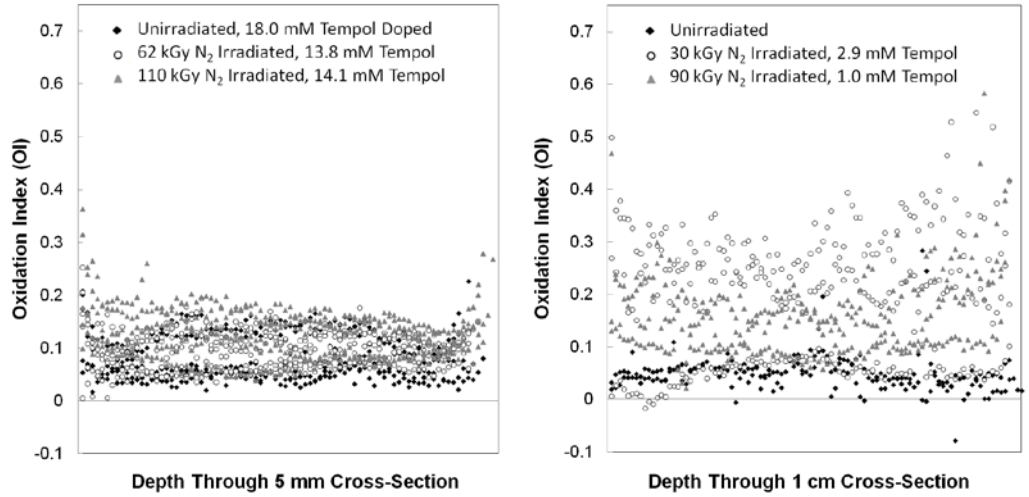

(a) (b)

Figure 6.5: Depth profiles with the oxidation index (OI) axis expanded to show 1 cm^3 UHMWPE specimens doped with a) 15.3 mM ± 3.5 mM Tempol (from Figure 6.3d) and b) 1.9 mM ± 1.2 mM Tempol (Figure 6.4b). While both Tempol concentration levels limit OI to < 0.5, the specimens with higher concentrations limit OI < 0.2.

On the contrary, UHMWPE cubes doped with 3.6 mM ± 0.5 mM vitamin E (α-tocopherol) show good oxidation-resistance on the surface, yet higher OI levels in the bulk, as shown in Figure 6.6a. UHMWPE irradiated to 90 kGy and doped with low levels of vitamin E has a bulk OI slightly less than 1.0, approximately the same OI as shown in irradiated and aged specimens in Figure 6.1. Furthermore, the α-tocopherol index (α-TI) profile for these specimens can be seen in Figure 6.6b. The α-TI index indicates that the α-tocopherol distribution in the 1 cm^3 specimen is not homogeneous, despite a 72 hour homogenization step. Regardless, the α-TI for these specimens is significantly lower than the distribution observed in Figure 6.3b and what has been previously reported. Oral, *et al*. exhibit surface α-TI = 1.0 for their specimens that were doped with vitamin E for 16 hours at 100°C.[8]

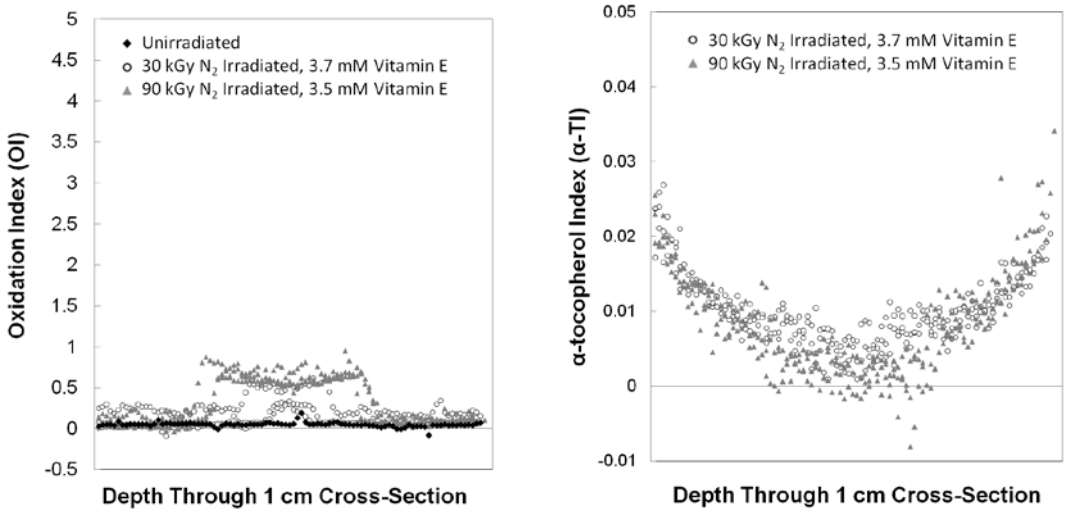

(a) (b)

Figure 6.6: The oxidation index (OI) depth profile (a) and α-tocopherol index distribution (b) in 1 cm^3 vitamin E-doped (3.6 mM ± 0.5 mM) UHMWPE. Due to the lower vitamin E concentration in the center of the 1 cm cross-section, a significant amount of oxidation is observed in the bulk of the irradiated, doped and aged specimens.

6.4.4 Oxidation in the Presence of Trace Nitroxide Concentrations

Most profoundly, the oxidation profile determined from a series of specimens mistakenly infiltrated with trace levels of TEMPO shows very low oxidation. The specimens described in section 6.3 were infiltrated with 66 μM ± 8.5 μM TEMPO from the aging vessel. Specimens irradiated both in air and in N_2 were exposed to the aggressive aging environment of 73 psi O_2 at 70°C. The resulting oxidation profiles are shown in Figure 6.6. The specimens irradiated in air (Figure 6.7a) exhibit a significant level of oxidation in the bulk of the sample, yet a lower level at the surface and sub-surface, similarly to that of the low concentration α-tocopherol specimens in Figure 6.6a. This could occur because there is a degree of oxygen diffused throughout the samples and so this sample set has already began to oxidize during and after irradiation. Secondly, as the low levels of TEMPO diffuse into the sample, they will react with the alkyl and peroxyl radicals at the surface and the first 1 – 2 mm of the specimen depth. As a consequence, these low levels of nitroxide are not sufficient to scavenge all the free radicals produced during an irradiation in air.

On the other hand, the specimens irradiated in N_2 show very low oxidation levels (Figure 6.7b). Since these samples are irradiated in an inert environment, most radiolytically-produced free radicals will bimolecularly crosslink. Therefore, the number of residual free radicals remaining when these samples are exposed to the aggressive accelerated aging environment is lower than in the air-irradiated UHMWPE. Correspondingly, the 66 μM of TEMPO is, in fact, enough to prevent oxidation during the duration of aging for UHMWPE irradiated in N_2 but not in air.

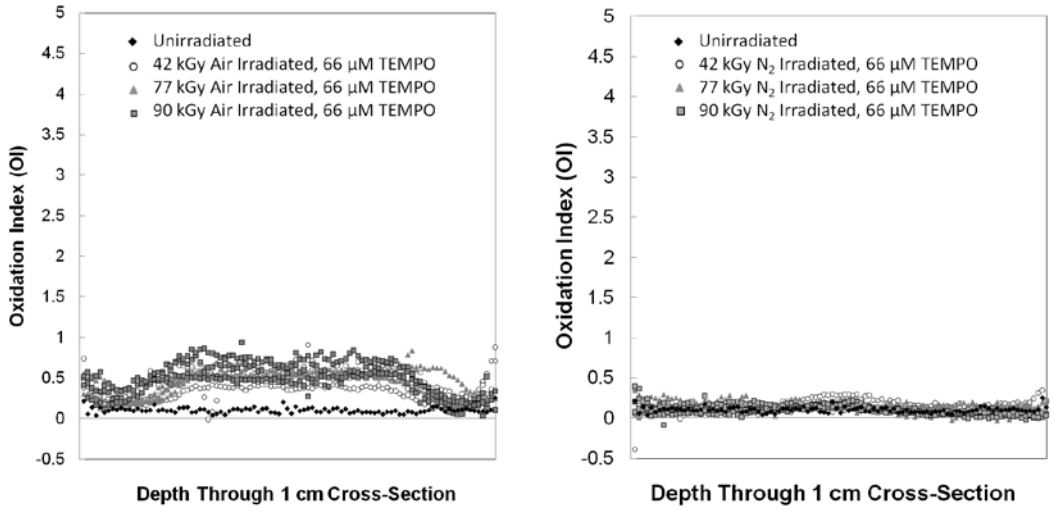

(a) (b)

Figure 6.7: Oxidation index (OI) depth profile of 1 cm^3 UHMWPE specimens irradiated in air (a) and N_2 gas (b) and doped with 66 µM TEMPO during the 14 day accelerated aging in 73 psi O_2 at 70°C. The low oxidation levels in the nitrogen-irradiated specimens indicate that 66 µM of TEMPO is enough to prevent oxidation during the duration of aging.

There are some limitations on these studies. The distribution of nitroxide antioxidants through the specimen depth was not determined, and thus a direct correlation to the vitamin E distribution cannot be made. Similarly, vitamin E was not infiltrated at micro-molar concentrations, as with TEMPO, to confirm that it does not prevent oxidation at these levels. Because the accelerated aging was not performed in one oxygen bomb simultaneously, equal oxidative conditions cannot be confirmed. Even though pressure readings were monitored, slight differences in O_2 pressure could impact the amount of oxidation over the accelerated aging period. Lastly, the irradiation absorbed doses between aging groups 1-4 are not equal and thus difficult to compare. Overall, although three to five specimens were used per sample set, a rigorous study would repeat these experiments for confirmation of these trends.

6.4.5 Reaction Mechanisms

The mechanisms by which antioxidants prevent oxidation of UHMWPE are as follows. Theoretically, in the absence of oxygen, α-tocopherol stabilizes alkyl radicals through the hydrogen transfer mechanism (equation 6.9)[114] where a hydrogen is abstracted from α-tocopherol. The α-tocopheryl radical (α-TO$^{\bullet}$) either dimerizes or is stable on its own:

$$R^{\bullet} + \alpha\text{-TOH} \rightarrow RH + \alpha\text{-TO}^{\bullet} \qquad (6.9)$$

This equation 6.9 competes with the bimolecular crosslinking reaction between two alkyl radicals, if vitamin E is consolidated with UHMWPE resin prior to irradiation. When added after irradiation through diffusion, the crosslinking reaction is predominant. Similarly, in the absence of oxygen, the nitroxide stabilizes the alkyl radical through radical-radical interactions (equation 1.12, repeated here).[38, 40, 41, 53] When added after irradiation, crosslinking is dominant, as shown in section 5.2.4. If nitroxides are added before irradiation, equation 1.12 is dominant, provided the concentration of nitroxides is equal to or greater than the concentration of alkyl radicals. Furthermore, at low dose rates, reaction 1.12 is completely dominant and no crosslinking occurs (section 5.2.4).

$$R\cdot + >NO\cdot \rightarrow >NOR \qquad (1.12)$$

However, it is not possible to remove all dissolved oxygen from the polymer and during aging there is a high concentration of oxygen on the surface which decreases with depth into the bulk. Thus, in the presence of oxygen, the above

reactions are also in direct competition with O_2 for alkyl radicals. Other possible reactions are disproportionation (equation 1.5) to produce *trans*-vinylenes and the reaction of alkyl radicals with vinyl unsaturations to form allyl radicals. While these reactions do occur, in the presence of oxygen, the dominant competing reactions are shown in a schematic in Figure 6.8.

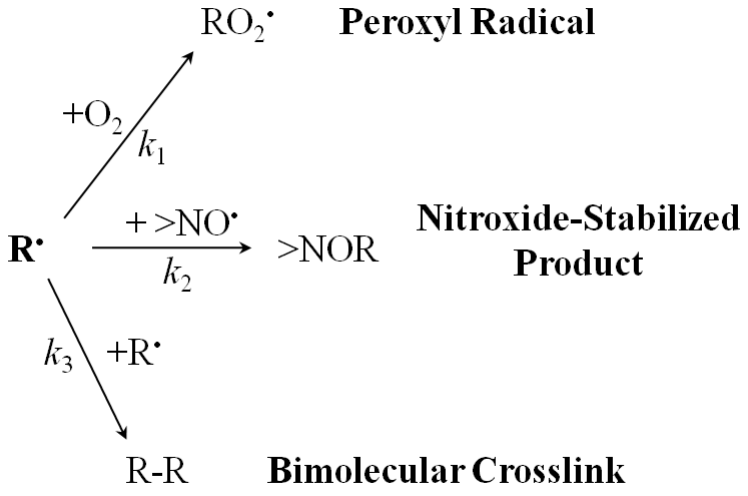

Figure 6.8: Schematic of three likely reactions of the alkyl radical ($R^{\bullet}$) to form the corresponding peroxyl radical ($RO_2^{\bullet}$), a nitroxide-stabilized product (>$NOR^{\bullet}$), and to bimolecularly crosslink with another alkyl radical. Other possible reactions are disproportionation (equation 1.5) to produce *trans*-vinylenes and the reaction of alkyl radicals with vinyl unsaturations to form allyl radicals. These reactions are discussed in chapter 4.

The rate equation for the competing reactions of the formation of the peroxyl radical and stabilization by vitamin E, is shown in equation 6.10, and stabilization by the nitroxide is shown in equation 6.11.

$$-\left[\frac{dR^{\bullet}}{dt}\right] = k_1[R^{\bullet}][O_2] + k_2[R^{\bullet}][\alpha - TOH] + k_3[R^{\bullet}]^2 \qquad (6.10)$$

$$-\left[\frac{dR^{\bullet}}{dt}\right] = k_1[R^{\bullet}][O_2] + k_2[R^{\bullet}][> NO^{\bullet}] + k_3[R^{\bullet}]^2 \qquad (6.11)$$

Overall, $k_1 > k_3 > k_2$, since k_1 is always greatest (diffusion controlled) and $k_3 > k_2$, as reported by Beckwith, *et al*.[52] Therefore, the peroxyl radical reaction is predominant provided there is oxygen dissolved in the specimen. The concentration ratio of reacting species also determines which reaction will dominate. With a *G*-value of 4 for alkyl radical production, 3 mM of alkyl radicals are produced during a 100 kGy irradiation dose. However, the specimens described in this chapter were crosslinked and conditioned at room temperature for 1 - 80 days. Even one day allows ample time for the majority of the alkyl and allyl radicals to recombine in an inert environment (section 5.2.4). While the initial alkyl radical concentration is 3 mM, after irradiation it is likely to be much lower due to crosslinking. From EPR, the observed paramagnetic concentration of TEMPO or Tempol is 66 μM for "Age 1", 1-3 mM for "Age 4" and 14-18 mM for "Age 3." The diffused concentration of oxygen is 51 μM (equation 5.5) in an inert environment. During accelerated aging, there is 73 psi O_2 in the pressurized oxygen bomb. Using the same equation, the dissolved oxygen concentration could be as high as 1.3 mM on the surface of the polymer. So for each aging case, a different scenario can be determined.

In the case of "Age 1" contaminated samples $[O_2] > [>NO^{\bullet}]$ and the production of peroxyl radicals is the dominant reaction during aging. While $[RO_2^{\bullet}] > [>NO^{\bullet}]$, there is still very minimal amount of oxidation. This indicates that $[RO_2^{\bullet}] \leq [R^{\bullet}] \leq [>NO^{\bullet}]$ and 66 μM of TEMPO can scavenge the alkyl and peroxyl radicals. As a result, the specimens irradiated in an inert environment show almost no oxidation. The specimens irradiated in air do show some bulk oxidation, so the $[RO_2^{\bullet}]$ can be

presumed to be slightly higher than [>NO$^{\bullet}$]. Therefore, the antioxidant only scavenges peroxyl radicals at the surface as it diffuses into the polymer.

In the case of "Age 4," peroxyl radicals forms during aging, but it is likely that [>NO$^{\bullet}$] ≥ [$RO_2^{\bullet}$] since the nitroxide is present in millimolar concentrations. Since these specimens are irradiated in an inert environment, almost all alkyl radicals crosslink or form allyl radicals. Consequently, oxidation is low. More so, in the case of "Age 3," peroxyl radical production is still predominant during aging. However, as peroxyl radicals form, [NO$^{\bullet}$] » [$RO_2^{\bullet}$] and all of the peroxyl radicals are scavenged. The result is very low oxidation levels, with OI < 0.2.

Hence, it can be expected that in the presence of oxygen, peroxyl radicals form predominantly where the [O_2] > [R$^{\bullet}$] ≈ [>NO$^{\bullet}$]. Therefore, the reactions expected to prevent oxidation in UHMWPE are the stabilization of the peroxyl radicals by vitamin E and nitroxides, (equations 1.11 and 6.11, respectively).

$$\alpha\text{-TOH} + RO_2^{\bullet} \rightarrow \alpha\text{-TO}^{\bullet} + ROOH \qquad (1.11)$$

$$>NO^{\bullet} + RO_2^{\bullet} \leftrightarrow >NOOOR \rightarrow >N^{+}=O + RO_2^{-} \qquad (6.11)$$

The product formed by the addition of the nitroxide radical to the peroxyl radical, is an unstable amino trioxide. The amino trioxide decomposes to form the corresponding oxoammonium cation of the nitroxide and RO_2^-.[54] This RO_2^- is much more stable than the reactive peroxyl radical and oxidation products are not expected to form.

Ultimately, these data demonstrate that the nitroxide content required to prevent oxidation is substantially lower than vitamin E. Only 66 μM of TEMPO

inhibits any large scale oxidation, while 3.6 mM vitamin E yields considerable oxidation in the bulk since it is inhomogeneously distributed. This implies nitroxides are much more efficient at preventing oxidation in UHMWPE than phenols like vitamin E. Also, the nitroxide concentrations necessary to prevent UHMWPE oxidation are at least two orders of magnitude lower than vitamin E. This means a lower initial concentration can be used that will lower the potential for antioxidant elution, increasing patient safety. However, the nitroxide concentration at which there are substantial effects on patient safety are unknown. Therefore, the concentrations that can be both prevent oxidation and still ensure no harm to the patient in the case of antioxidant elution from the implant must be determined. The fact that two orders of magnitude lower concentration of nitroxide can be used versus vitamin E is important but must be explored further in toxicology and aging studies.

6.5 Conclusions

The resistance of UHMWPE to oxidation is dependent on antioxidant and oxygen concentrations. All three antioxidants, vitamin E, TEMPO and Tempol, protect UHMWPE at high concentrations. Albeit when concentrations are reduced, it is clear that vitamin E cannot prevent oxidation under a certain concentration level. More so, if the distribution is inhomogeneous, unstabilized areas become susceptible to oxidation. On the contrary, the data show that even at concentrations two orders of magnitude lower, the nitroxide TEMPO prevents oxidation, even if in direct competition with oxygen. This means nitroxides are a more efficient antioxidant that can be used in lower concentrations for increased implant efficacy and patient safety.

Chapter 7: Effect of Nitroxides on Mechanical Properties of UHMWPE

7.1 Introduction

Major contributing factors to the performance of UHMWPE in total joint replacements are mechanical properties. Tensile properties provide a measure of the strength of a particular material, or its ability to withstand load. As load-bearing articular surfaces, the tensile properties of UHMWPE in total knee and hip replacements are important to implant longevity. The tensile properties of virgin, crosslinked,[26, 97, 104, 115] remelted[6, 116] and vitamin E-doped[102] UHMWPE have been previously evaluated. Virgin UHMWPE that has not been irradiated or modified exhibits high toughness, tensile strength and ductility. Crosslinking UHMWPE lowers polymer ductility and has shown to slightly increase yield strength and elastic modulus.[97, 104] Additionally, due to the physical restrictions on polymer chains from crosslinks, elongation and tensile stress at break are reduced.[26, 97, 115] Remelting the polymer to reduce free radicals after irradiation also alters the crystal structure and percent crystallinity, which in turn reduces the mechanical and fatigue properties of UHMWPE.[6, 100, 117] Overall, crystallinity and crosslink density are the largest two factors affecting tensile properties of UHMWPE.[97, 100] The addition of vitamin E to reduce residual free radicals, on the other hand, enhances mechanical properties, despite plasticization of the polymer.[8] Tensile strength and elongation are increased for UHMWPE consolidated or doped with vitamin E.[33, 102] Therefore, it is expected that other antioxidants, like nitroxides, will result in a

similar enhancement of mechanical properties due to plasticization by the additive molecule.

The mechanical properties of UHMWPE are evaluated by testing the polymer in uniaxial tension. The tensile specimen is shaped like a "dog bone" and pulled in tension with a constant rate until failure. The progression of the experiment is characterized by a plot of stress versus strain. From the initial linear elastic part of the plot, the Young's modulus (or the modulus of elasticity, *E*) can be calculated from equation 7.1, where engineering stress, σ_{eng}, is the load divided by initial area, and the engineering strain, ε_{eng}, is the change in sample length divided by the initial length:

$$E = \frac{\sigma_{eng}}{\varepsilon_{eng}} = \frac{load/area_i}{\Delta length / length_i} = \frac{P/A_o}{\frac{l_f - l_o}{l_o}} \qquad (7.1)$$

The elastic modulus characterizes the initial, most linear region that is representative of the polymer chains stretching and aligning in the direction of tension. Once the chains have aligned, the stress vs. strain plot deviates from linearity and the engineering stress reaches a maximum at the yield strength (σ_{YS}). The strain continues to increase but the engineering stress remains at an approximate plateau level as the cross-section of the specimen becomes reduced. If the actual cross-sectional area is taken into account, the true stress would continue to rise. However, in this study, the actual cross-section is not measured as the specimen is pulled in tension, and the apparent engineering stress (force / initial area) is reported. As the polymer continues to stretch, it becomes strain hardened and the engineering stress continues to rise. Ultimately, the specimens fracture at the ultimate tensile strength (σ_{UTS}). Toughness of the polymer is defined as the area under the stress vs.

strain curve. These mechanical properties are affected by the material structure and morphology changes that result from polymer modification through crosslinking, thermal treatment or doping with antioxidants.

7.2 Objectives

This chapter explores the effect of high degrees of crosslinking and high concentrations of antioxidants (15-18 mM) on the tensile properties of UHMWPE. Specimens pulled in uniaxial tension containing vitamin E, TEMPO, and Tempol are compared to γ-irradiated and 150°C remelted UHMWPE. This control material is representative of typical industry processing. Engineering stress vs. engineering strain plots are recorded for five specimens per processing condition and irradiation dose. The yield strength, σ_{YS}, ultimate tensile strength, σ_{UTS}, elastic modulus, *E*, and percent elongation are measured for each specimen. Trends of mechanical properties with crosslinking dose and type of antioxidant are evaluated here.

7.3 Experimental Method

Tensile specimens were cut from UHMWPE rod stock donated by Biomet, Inc. The rod is cut into 5 mm thick disks that are machined to a 3 mm thick rectangle at the center of the disk, leaving 5 mm thick ends on either side. This complex shape is used because it requires the least amount of machining. These specimens are then cleaned with acetone and sonicated in deionized H_2O for 10 minutes each. Subsequently, the specimens are dried and packaged in N_2 in the LabMaster 130 glove box (MBraun, Stratham, NH) using aluminized polyethylene foil (MIL-B-

131H, Bell Fibre Products Corp., Columbus, GA). Specimens are irradiated to 62 kGy and 110 kGy using the low dose rate ^{60}Co γ source (2.26 kGy per hour).

After irradiation, specimens are either remelted at 148°C for two hours, infiltrated with α-tocopherol (two hours in the liquid plus 72 hour homogenization at 100°C) or intriltrated with the nitroxides TEMPO or Tempol (72 hours at 100°C). The vitamin E concentration was not determined for these specimens but was estimated to be 15.3 mM (0.7 wt%) from a previous trial with the same conditions. TEMPO doping used 0.336 wt% powder per specimen weight and Tempol doping used 0.37 wt% of the antioxidant powder. Individual group concentrations are summarized in the top section (Age 3) of Table 6.1. On average the specimens contained 17.0 mM ± 1.1 mM TEMPO and 15.3 mM ± 3.5 mM Tempol. After processing, samples are aged according to section 2.10 for 14 days at 70°C, 73 psi O_2.

After aging, dog bone specimens are cut with a custom die with the dimensions indicated in Figure 7.1. This is a custom, non-standard tensile specimen shape, which is scaled to approximately 1/6th of the size of ASTM specimen Type III. In size, this specimen is closest to Type V. While this geometry is non-standard and does not conform exactly to ASTM D638 (Standard Test Method for Tensile Properties of Plastics), the die used is the only die that could cut a complete tensile specimen from the limited sample size of the donated UHMWPE disks. These specimens are uniaxially pulled in tension until failure with an Instron 33R4465 materials testing machine with a 5 mm/min ramp rate and 1 kN load cell.

The bulk material from which tensile specimens are cut is also characterized by DSC (section 2.8) and FTIR spectroscopy (section 2.9). Plugs of 3.5 mm diameter

are cut from the material for DSC analysis. Thin films of 100 μm thickness are microtomed for FTIR analysis from the 3 mm cross-sectional area next to the location from which the dog bone samples are cut.

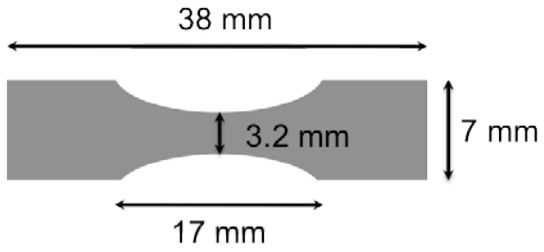

Figure 7.1: Schematic of custom tensile specimen shape (not to scale) used for uniaxial tensile testing of UHMWPE that is irradiated and remelted or doped with vitamin E, TEMPO or Tempol. The specimen is proportionally closest to ASTM Type III and Type V in size. The specimen thickness is 3 mm.

Statistical analysis is performed with StatPlusMac LE software. Basic statistics comparing means between two sample groups, with uneven variances (heteroscedastic) are used to calculate *p*-values of significance. The Student's t-test with a two-tailed distribution is calculated with a reliability level $\alpha = 0.05$. *P*-values that are greater than 0.05 are considered not significant, $0.05 < p < 0.01$ are significant, $0.01 < p < 0.001$ are very significant, and $p < 0.001$ are extremely significant. All calculated two-tailed *p*-values for σ_{UTS}, σ_{YS}, *E* and elongation percentage are summarized in Appendix B, Table B.1-B.4.

7.4 Results and Discussion

7.4.1 Characterization of Tensile Specimens

In addition to testing mechanical properties of the dog bone specimens, the bulk material used was characterized by DSC and FTIR. The percentage crystallinity and melting point of these irradiated, doped and aged materials is thoroughly discussed in section 5.3, while crystallinity trends will be referenced in this chapter. FTIR analysis of the 3 mm thick specimen material cross-section is analyzed for oxidation index (OI), α-tocopherol index (α-TI) and *trans*-vinylene index (TVI), as defined in section 6.1. The 3 mm specimen cross-sectional OI for remelted, vitamin E-doped, TEMPO-doped, and Tempol-doped specimen is plotted as a function of depth in Figure 7.2. Surface OI is very high in both the unirradiated and irradiated, remelted specimens, as shown in Figure 7.2a. Unirradiated specimens exhibiting high carbonyl absorbance, a FTIR measure of ketones, acids, esters and other oxidation products, indicate that this oxidation does not occur as a result of high residual free radical concentration from irradiation, but rather from the remelting process. This high surface oxidation in the 3 mm cross-section appears to be even higher that the slight surface oxidation observed in the same material with a 5 mm cross-section, shown in Figure 6.2b. Surface oxidation can reduce the strength of the remelted polymer, and this is evaluated in section 7.4.2.

It is plausible a 3 mm thickness melts more than a thicker material during the short remelting process. This 150°C remelting is not anticipated to melt the polymer to a degree that is loses its shape, but rather to allow polymer chains more ability to reptate, for residual radicals to recombine. In a thinner material, the surface crystals

may melt to a larger extent than in the bulk, incorporating more oxygen into the material upon recrystallization. This also indicates that the aluminized polyethylene packaging in which the disks were encapsulated for irradiation in N_2 gas also did not withstand the remelting process. Since the package is bonded through melted polyethylene, 150°C temperatures would melt this packaging bond, allowing O_2 from the oven to diffuse through the packaging. In contrast, the vitamin E-doped (Figure 7.2b), TEMPO-doped (Figure 7.2c) and Tempol-doped (Figure 7.2d) specimens all generally show low oxidation, OI < 0.5.

The distribution of α-tocopherol, or the α-TI, throughout the vitamin E-doped specimen is shown in Figure 7.3. Analogous to the profile seen in Figure 6.3b, this distribution is again inhomogeneous. In contrast to the 5 mm cross-section, the difference in bulk and surface concentration is not as dramatic. The 3 mm thickness shows more homogeneous vitamin E distribution than 5 mm, as it takes less time for the molecule to diffuse across the thinner specimens. Overall, this α-TI profile indicates that there is less vitamin E across the 3 mm cross-section than the 5 mm cross-section, if comparing Figures 7.3 and 6.3b. The tensile specimens cut from the 3 mm cross-section therefore may have less than 0.7 wt% vitamin E. This could instigate that the supposed concentration of vitamin E is lower than that of TEMPO or Tempol in the tensile specimens, although each antioxidant has approximately equal total disk concentrations measured gravimetrically. Rather, it can be assumed that the same bulk effects occur with the nitroxides. In other words, the TEMPO and Tempol concentrations and distributions could be lower in the 3 mm cross-sections as well.

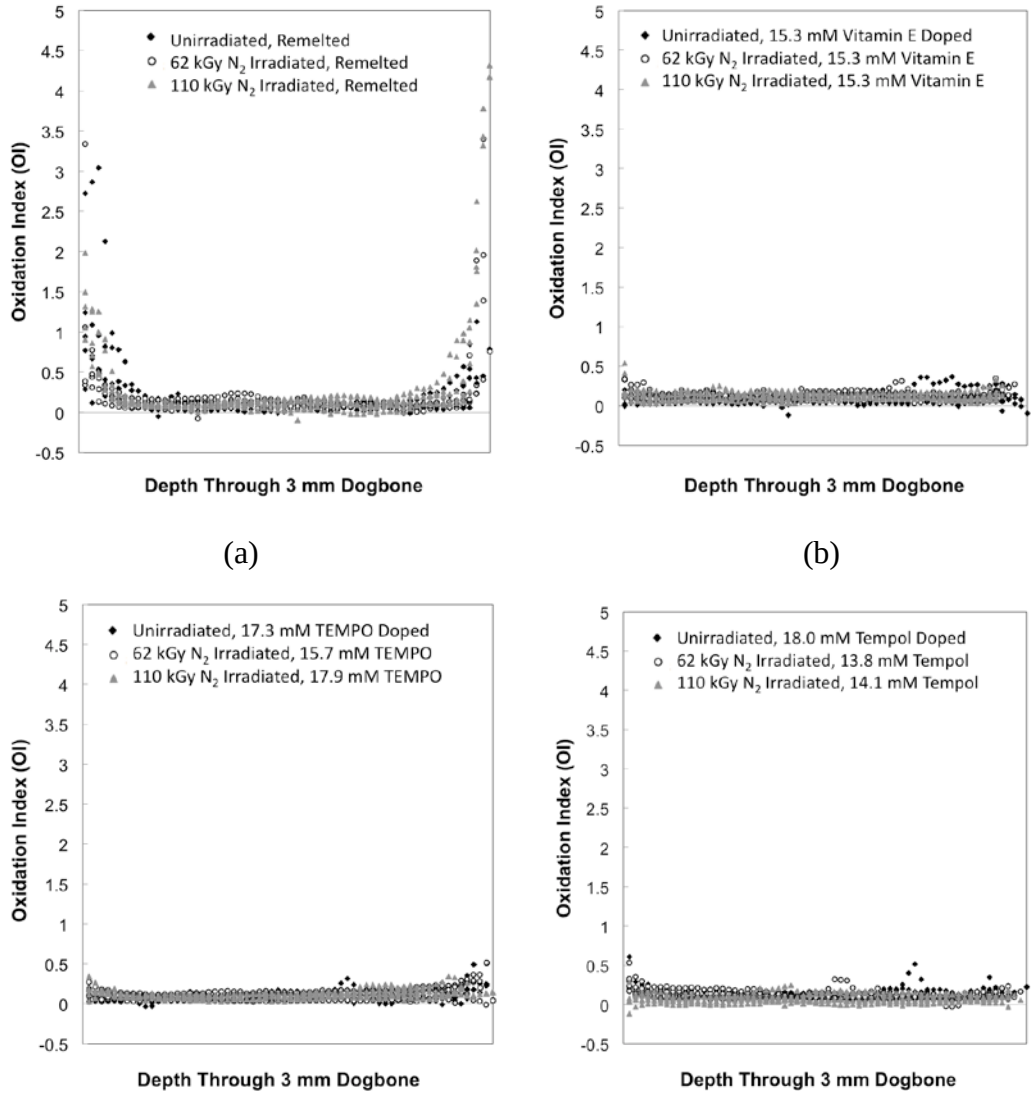

Figure 7.2: Oxidation index (OI) depth profiles of 3 mm cross-sections of bulk material from which tensile specimens were cut for tensile testing. The irradiated and remelted specimens show severe surface oxidation (a). The three antioxidants, vitamin E (b), TEMPO (c) and Tempol (d) all show low oxidation levels through the specimen bulk material.

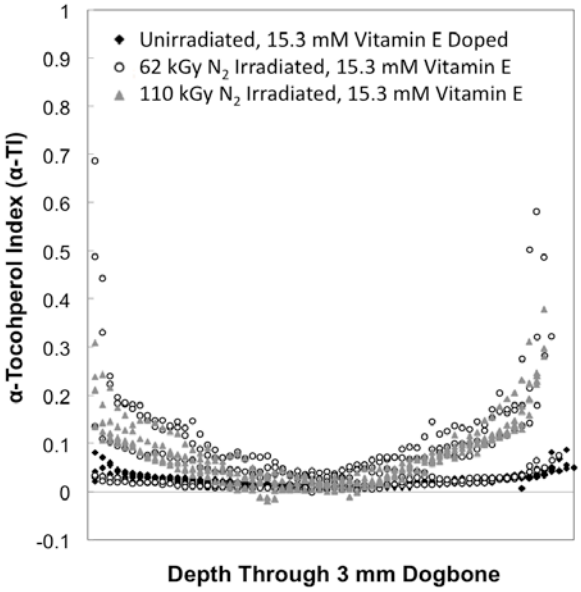

Figure 7.3: The α-tocopherol index (α-TI) through the depth of the 3 mm cross-section of vitamin E-doped bulk material from which tensile dog bones were cut. The distribution of vitamin E through the specimens is not completely homogeneous yet more evenly distributed than in the 5 mm cross-section in Figure 6.3b.

7.4.2 Tensile Properties of Irradiated and Remelted UHMWPE

Typical engineering stress vs. strain plots of unirradiated, 62 kGy irradiated, and 110 kGy irradiated and remelted UHMWPE are shown in Figure 7.4. Each stress vs. strain curve is an individual specimen that is indicative of typical group behavior. A table of tensile properties averaged for the five specimens per condition (four for 62 kGy irradiated and remelted) are shown in Table 7.1. This data confirm two effects of processing on tensile properties. First of all, the process of remelting the UHMWPE reduces tensile strength. The manufacturer specifies the virgin GUR 1050 material provided had a σ_{UTS} = 50.5 MPa, a σ_{YS} = 21.4 MPa and 362% elongation, which is within the typical reported range for polymer of this resin type.[33, 116] The plots indicate that with increasing radiation dose and corresponding crosslink

density, the σ_{UTS}, toughness and elongation of the specimen at failure are reduced. The remelting process allows more crosslinks to form and subsequently reduces crystallinity. The 62 kGy irradiated and remelted specimens have 63.0% ± 2.3% crystallinity, compared to the virgin material, which has 66.6% ± 3.0% crystallinity. Additionally, increasing radiation dose further reduces elongation and tensile strength. As the polymer is crosslinked with increased radiation dose, the σ_{UTS} is reduced from 50.5 MPa for virgin material to 30.0 MPa ± 2.5 MPa for the unirradiated remelted polymer to 24.5 MPa ± 1.3 MPa for the 110 kGy irradiated and remelted polymer (29% reduction that is very significant: $p = 0.005$ based on the Student's t-test with $\alpha = 0.05$).

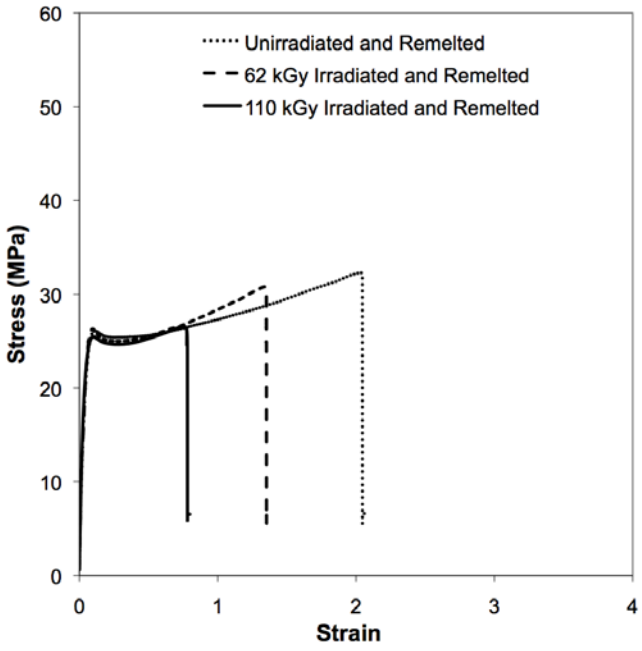

Figure 7.4: An engineering stress vs. strain plot of unirradiated, 62 kGy irradiated and 110 kGy irradiated UHMWPE remelted at 150°C for 2 hours. These specimens exhibit behavior typical of crosslinked and remelted UHMWPE, with lower tensile strength than virgin UHMWPE and reduced strength with increasing crosslink density. The curves shown indicate individual specimen stress vs. strain curves that are typical of the sample group.

The reduction in σ_{UTS} is expected since ductility is reduced, as the polymer chains are physically crosslinked and the chains cannot slip past one another as much as the virgin polymer. As a consequence, there is 45% less elongation between unirradiated UHMWPE (266% ± 42%) and the 110 kGy crosslinked and remelted specimens (146% ± 17%) (very significant, $p = 0.002$ according to the Student's t-test with $\alpha = 0.05$) and the stresses at which a high σ_{UTS} would be observed are not reached.

Crosslinking also enhances the stiffness of the polymer,[97] resulting in an increase in the modulus and yield strength (σ_{YS}). Although the σ_{YS} increases, it does not change significantly ($p > 0.34$ between all remelted specimens) with crosslinking of the remelted specimens (around 26.0 MPa). However, the σ_{YS} is approximately 20% higher for irradiated and remelted specimens, as the virgin material according to the manufacturer's specification. Similarly, the elastic modulus increases slightly from a value of 0.957 GPa for the unirradiated, remelted polymer to 1.036 GPa for the 110 kGy irradiated and remelted UHMWPE although the change is not statistically significant ($p > 0.145$ between all remelted specimens).

Table 7.1: Tensile Properties of UHMWPE Irradiated and Remelted

	Ultimate Tensile Strength (MPa)		Yield Strength (MPa)		Elongation (%)		Elastic Modulus (GPa)	
Unirradiated and Remelted	30.02	± 2.54	25.76	± 0.25	266	± 42	0.957	± 0.019
62 kGy Irradiated and Remelted	28.15	± 2.79	26.03	± 0.71	206	± 36	1.009	± 0.054
110 kGy Irradiated and Remelted	24.46	± 1.30	26.30	± 1.09	146	± 17	1.036	± 0.103

P-Value Key:	$0.05 < p < 0.01$ Significant	$0.01 < p < 0.001$ Very significant	***p* < 0.001 Extremely significant**

It was noted earlier that the irradiated as well as the unirradiated and remelted specimens were highly oxidized on the surface. This could embrittle the polymer, reducing σ_{UTS} and the degree of elongation. The values for σ_{UTS} for irradiated and remelted UHMWPE are comparable to previous studies, although the calculated values are lower than what is typically reported. For example, Bistolfi, *et al*., report a σ_{UTS} = 37.1 MPa ± 3.9 MPa, a σ_{YS} = 18.9 MPa ± 0.3 MPa, an elongation percentage of 240 % ± 29 % and an elongation modulus, *E*, of 0.625 GPa ± 0.048 GPa for UHMWPE irradiated to 50 kGy in air by gamma irradiation and remelted at 170°C for four hours.[116] In comparison, in this study UHMWPE crosslinked in N_2 and remelted at 150°C for 2 hours exhibits a 24% lower σ_{UTS}. Additionally, the σ_{YS} reported by Bistolfi *et al*., is 37% higher than the values of the specimens tested here (Table 7.1). Also, the elastic modulus, *E*, is significantly higher in the irradiated and remelted specimens reported by Bistolfi. The discrepancy in σ_{UTS} could be in the processing differences (extruded versus compression molded). Furthermore, Sobieraj *et al*. demonstrate that highly crosslinked and 150°C remelted UHMWPE has a σ_{UTS} = 40.85 MPa ± 6.32 MPa, a σ_{YS} = 21.82 MPa ± 0.35 MPa, and an elongation percentage of 246% ± 20%.[26] The σ_{YS} and elongation are comparable but the σ_{UTS} is again lower in this present study. This could indicate that the high surface oxidation has embrittled the polymer during remelting, resulting in lower toughness and σ_{UTS}.

However, Oral *et al*. show σ_{UTS} = 33 MPa ± 2 MPa for irradiated and remelted UHMWPE[102] and Puertolas *et al*. demonstrate σ_{UTS} = 33.1 MPa ± 4.2 MPa for 50 kGy irradiated and 32.9 MPa ± 4.0 MPa for 100 kGy irradiated UHMWPE, both remelted at 150°C for two hours.[6] As a consequence, the discrepancy in calculated

σ_{UTS} between studies may be due to resin consolidation method, resulting crystallinity and crosslinking dose rate. In fact, Bistolfi *et al*. uses an air irradiation, which will produces less crosslinking, since some radicals react with O_2. As a result, it can be concluded that the tensile properties of the control (irradiated and remelted) UHMWPE presented here are rather comparable and typical of what is expected for such processing.

7.4.2 Tensile Properties of UHMWPE Doped with α-Tocopherol

The engineering stress vs. apparent strain plots for unirradiated, 62 kGy irradiated and 110 kGy irradiated and α-tocopherol doped UHMWPE are shown in Figure 7.5. Each stress vs. strain curve is an individual specimen that is indicative of typical group behavior. The calculated mechanical properties of vitamin E doped UHMWPE are shown in Table 7.2. These plots exhibit the same trend of decreasing elongation and toughness with increasing irradiation dose. However, a statistically significant difference with Figure 7.4 (remelted) and Fig 7.5 (vitamin E) is greater toughness, tensile strength and elongation for the crosslinked and vitamin E doped polymer versus irradiated and remelted. This confirms previous studies that indicate that vitamin E increases mechanical properties of crosslinked UHMWPE.[8] The crystallinity increases from 66.6% ± 3.6% in the virgin UHMWPE to 69.0% ± 2.3%, 70.7% ± 1.3%, and 77.1% ± 2.3% in the unirradiated, 62 kGy irradiated, and 110 kGy irradiated vitamin E-doped specimens. Crystallinity increases with radiation dose, as reported previously,[97, 101] perhaps due to plasticization by vitamin E, allowing more chain movement to form crystals. The σ_{UTS} and elongation percent decrease

with increasing radiation dose as with remelted UHMWPE because of the increased crosslink density. According to Chapter 5, the crosslink density of UHMWPE doped after crosslinking should be comparable to the crosslink density of irradiated and annealed UHMWPE. However, the irradiated and remelted UHMWPE may have an even higher crosslink density since the 150°C thermal processing allows increased chain motion to allow residual radicals to recombine to form crosslinks. Thus, the crosslink densities of remelted specimens are possibly higher than of antioxidant-doped UHMWPE.

The σ_{UTS} increases from remelted to vitamin E doped UHMWPE at every radiation dose: 42% between unirradiated groups ($p = 0.0001$, extremely significant), 48% between 62 kGy irradiated groups ($p = 0.0002$, extremely significant) and 66% between 110 kGy irradiated groups ($p = 0.0003$, extremely significant). However, within the vitamin E-containing groups, σ_{UTS} does not change significantly ($p > 0.53$), although there is an 11.6% reduction from 42.6 MPa ± 1.5 MPa for unirradiated, doped specimens to 37.6 MPa ± 7.4 MPa for 110 kGy irradiated and vitamin E doped UHMWPE. The σ_{UTS} is expected to decrease as ductility is reduced with increasing radiation dose, because the polymer chains cannot slip past one another. Also crosslink density is increased so the higher σ_{UTS} cannot be reached prior to fracture as suggested previously for the remelted samples in Figure 7.4. However, the σ_{UTS} does not significantly change between vitamin E specimen groups in Figure 7.5. This may be a result of the vitamin E plasticizing effect which reduces the attainable stress due to increased molecular slippage during elongation,[37] thus reducing the σ_{UTS} values that are coincidently the same.

The elongation percentage decreases approximately 38% from 391% ± 35% in unirradiated to 244% ± 23% in 110 kGy irradiated and doped specimens (p = 0.0003, extremely significant) due to the restricted chain movement due to crosslinking. The σ_{YS} does increase slightly from unirradiated to 62 kGy irradiated vitamin E doped UHMWPE (p = 0.0078, significant) and to 110 kGy irradiated vitamin E doped UHMWPE (p = 0.0037, significant). Additionally, the elastic modulus, E, increases slightly with radiation dose, and this change is statistically significant (p = 0.0116 for unirradiated to 62 kGy irradiated, significant; p = 0.0271 from 62 kGy to 110 kGy irradiated, significant).

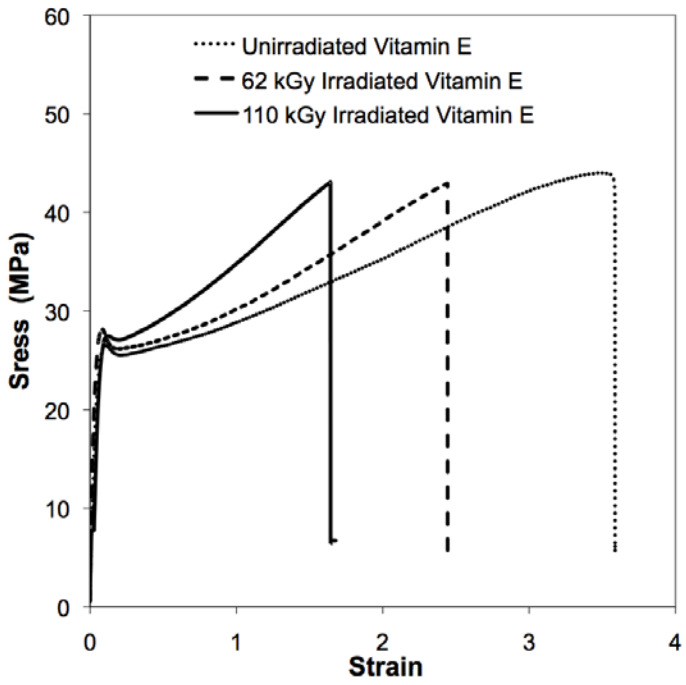

Figure 7.5: Engineering stress vs. strain plot of unirradiated and irradiated UHMWPE doped with α-tocopherol at 100°C for 2 hours and homogenized for 72 hours at 100°C. These specimens exhibit behavior similar to previous studies characterizing vitamin E-doped UHMWPE. The curves shown indicate individual specimen stress vs. strain plots that are typical of the sample group.

Table 7.2: Tensile Properties of UHMWPE Irradiated and Doped with α-tocopherol (Vitamin E)								
	Ultimate Tensile Strength (MPa)		Yield Strength (MPa)		Elongation (%)		Elastic Modulus (GPa)	
Unirradiated and Vitamin E Doped	42.57	± 1.53	26.05	± 0.54	391	± 35	0.942	± 0.025
62 kGy and Vitamin E Doped	41.81	± 2.42	27.61	± 0.77	320	± 26	1.089	± 0.081
110 kGy and Vitamin E Doped	40.71	± 2.55	27.61	± 0.54	**251**	**± 20**	0.968	± 0.042
P-value Key:	0.05 < *p* <0.01 Significant		0.01 < *p* < 0.001 Very significant		***p* < 0.001 Extremely significant**			

Oral *et al*. demonstrated that blending α-tocopherol with UHMWPE increases the σ_{UTS} from 33 MPa ± 3 MPa for 100 kGy irradiated, remelted and aged specimens to 51 MPa ± 2 MPa for 0.3 wt% blended, 100 kGy irradiated and aged specimens.[33] While the blended vitamin E specimens show a higher σ_{UTS}, because the α-tocopherol is added prior to irradiation, the crosslink density is likely to be 40 – 50 % lower. In fact, a later study by the same authors indicate that irradiated vitamin E-doped and aged UHMWPE show a σ_{UTS} = 45 MPa ± 2 MPa, a σ_{YS} = 25 MPa ± 1 MPa and 234% ± 21% elongation at break.[102] The σ_{UTS} values reported here for 110 kGy irradiated and 0.7 wt% doped UHMWPE are approximately 10% lower than what is shown by Oral *et al*. but this is likely to not be statistically significant (as 11.6% σ_{UTS} reduction within the specimens tested here is not significant). The difference in σ_{UTS} can be attributed to different resin batch consolidation modes and the resulting crystallinities, as well as irradiation dose rate. The σ_{YS} and elongation at break reported here are within 10% of the values published by Oral *et al*. Overall, the vitamin E-doped specimens tested here show very typical tensile properties, as compared to previous literature.

7.4.3 Tensile Properties of UHMWPE Doped with Nitroxides

Similarly, the apparent stress vs. strain plots for unirradiated, 62 kGy irradiated and 110 kGy irradiated UHMWPE doped with TEMPO are shown in Figure 7.6a and specimens doped with Tempol are shown in Figure 7.6b. Each stress vs. strain curve is an individual specimen that is indicative of typical group behavior. Calculated tensile properties of the UHMWPE doped with TEMPO and Tempol are shown in Table 7.3 and 7.4, respectively. The nitroxide infiltrated specimens demonstrate the same principles indentified earlier and show very high statistical correlation to the tensile properties of vitamin E doped specimens. The difference in σ_{UTS} between all antioxidant containing groups is not statistically significant ($p >$ 0.11). Increasing radiation dose similarly reduces toughness, σ_{UTS} and elongation percentage within each antioxidant groups. UHMWPE doped with nitroxides exhibit much higher toughness, tensile strength and elongation than the remelted polymer. TEMPO and vitamin E show a similar magnitude in percent elongation and tensile strength indicating a plasticization effect that is not indicative of a specific antioxidant or reaction mechanism. It is possible that the presence of the antioxidant molecule in between polymer chains allows the chains to extend further. This compares to what has been previously reported for plasticizers.[8]

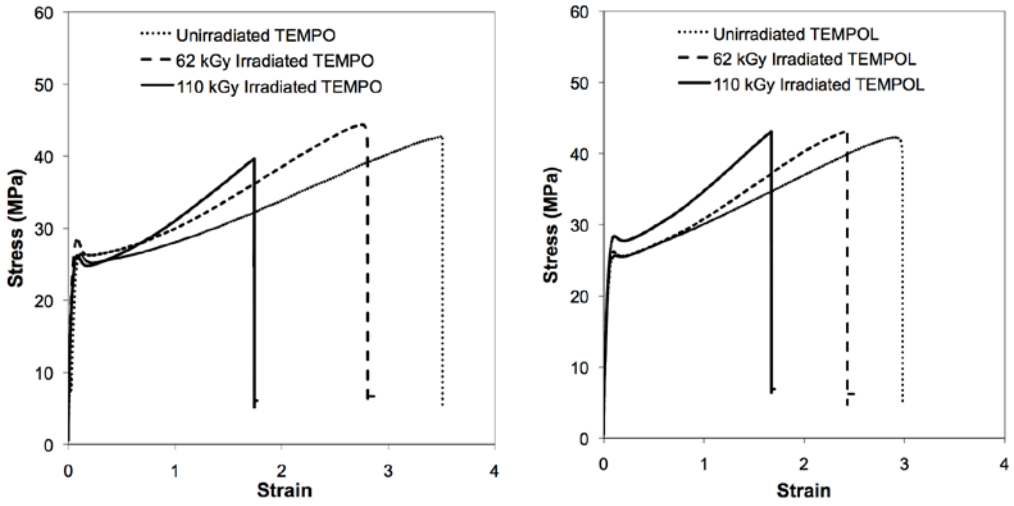

Figure 7.6: Engineering stress vs. strain plot of unirradiated and irradiated UHMWPE doped with TEMPO (a) and Tempol (b) at 100°C for 72 hours. These specimens exhibit tensile properties similar to vitamin E-doped UHMWPE. The curves shown indicate individual specimen stress vs. strain plots that are typical of the sample group.

The TEMPO-doped specimens do not exhibit a significant increase in crystallinity. The percentage crystallinity is 66.3% ± 0.8%, 71.3% ± 2.3% and 70.8% ± 2.1% for unirradiated, 62 kGy irradiated and 110 kGy irradiation UHMWPE. TEMPO-doped UHMWPE σ_{UTS} is reduced 12.6% from 41.4 MPa ± 1.5 MPa for unirradiated specimens to 37.4 MPa ± 5.3 MPa of 110 kGy irradiated specimens, yet these changes are not statistically significant ($p > 0.24$). The elongation percentage subsequently drops 393% ± 37% to 231% ± 33% ($p = 0.0003$, extremely significant). TEMPO-doped specimens exhibit a statistically significant increase in yield strength ($p = 0.048$ for increase between unirradiated and 110 kGy irradiated TEMPO doped UHMWPE) and an extremely significant increase in elastic modulus ($p = 0.0003$). Overall, the tensile properties of TEMPO-doped specimens as a function of radiation dose are very similar to that of vitamin E-containing UHMWPE. The increased

elongation due to plasticization also increases the ultimate tensile strength as increasing elongation also increases the stress endured by the specimen.

Table 7.3: Tensile Properties of UHMWPE Irradiated and Doped with the Nitroxide TEMPO

	Ultimate Tensile Strength (MPa)		Yield Strength (MPa)		Elongation (%)		Elastic Modulus (GPa)	
Unirradiated and TEMPO Doped	41.43	± 1.54	26.11	± 0.31	393	± 37	0.832	± 0.102
62 kGy Irradiated and TEMPO Doped	40.78	± 2.01	27.21	± 0.89	342	± 36	1.087	± 0.090
110 kGy Irradiated and TEMPO Doped	37.44	± 5.31	27.60	± 1.07	**231**	**± 33**	1.102	± 0.077

P-value Key:	$0.05 < p < 0.01$ Significant	$0.01 < p < 0.001$ Very significant	***p* < 0.001 Extremely significant**

The specimens tested in uniaxial tension containing Tempol continue to exhibit the same trends for plasticizers. Similar to TEMPO, the Tempol-containing specimens do not exhibit a significant increase in crystallinity: 65.6% ± 1.5%, 71.1% ± 1.5% and 72.3% ± 1.8% for unirradiated, 62 kGy irradiated and 110 kGy irradiated Tempol-doped UHMWPE. Similar to vitamin E, the difference in σ_{UTS} between unirradiated, 62 kGy irradiated and 110 kGy irradiated and Tempol-doped UHMWPE is not statistically significant ($p > 0.13$). The elongation percentage shows an expected decrease from 364% ± 36% for unirradiated specimens, to 317% ± 27% for the 62 kGy irradiated and doped specimens (although this is not statistically significant using a two tailed t-test, $p = 0.0505$), to 243% ± 35% for the 110 kGy irradiated and Tempol doped specimens ($p = 0.0014$, very significant). The yield strength of Tempol doped specimens shows an increase with increasing dose from 26.38 MPa ± 1.06 MPa for unirradiated Tempol-doped samples to 28.20 MPa ± 0.53 MPa for 110 kGy irradiated and Tempol-doped UHMWPE (significant, $p = 0.0152$).

However, the slight increase in elastic modulus is not statistically significant ($p > 0.37$).

Table 7.4: Tensile Properties of UHMWPE Irradiated and Doped with the Nitroxide Tempol

	Ultimate Tensile Strength (MPa)		Yield Strength (MPa)		Elongation (%)		Elastic Modulus (GPa)	
Unirradiated and Tempol Doped	40.60	± 0.90	26.38	± 1.06	364	± 36	1.014	± 0.085
62kGy Irradiated and Tempol Doped	42.35	± 1.86	27.19	± 0.83	317	± 27	1.055	± 0.043
110 kGy Irradiated and Tempol Doped	37.38	± 4.98	28.20	± 0.53	243	± 35	1.090	± 0.041

P-value Key:	$0.05 < p < 0.01$ Significant	$0.01 < p < 0.001$ Very significant	**$p < 0.001$ Extremely significant**

7.4.4 Comparison of Tensile Properties of Different Processing Conditions

For the most part, each of the processing conditions (remelted or doped with the three antioxidants) show similar trends toward reduced toughness, elongation and ultimate tensile strength with increasing crosslink densities dependent on absorbed radiation dose. More crosslinks reduce polymer chains motion, limiting elongation and increase in the level of stress prior to failure. The processing conditions (four sample sets) are compared at each irradiation dose in Figure 7.7. Most significantly, the difference in toughness, σ_{UTS} and elongation between remelted UHMWPE and polymer infiltrated with antioxidants, is dramatic. As previously discussed, the unirradiated specimens (Figure 7.7a) either remelted or doped with the three antioxidants exhibit much longer elongation than the 62 kGy irradiated specimens (Figure 7.7b) and nearly twice the elongation percentage as 110 kGy irradiated samples (Figure 7.7c). At each radiation dose level, the antioxidant-containing

UHMWPE demonstrates increased ductility and toughness, with higher σ_{UTS} and elongation percentage.

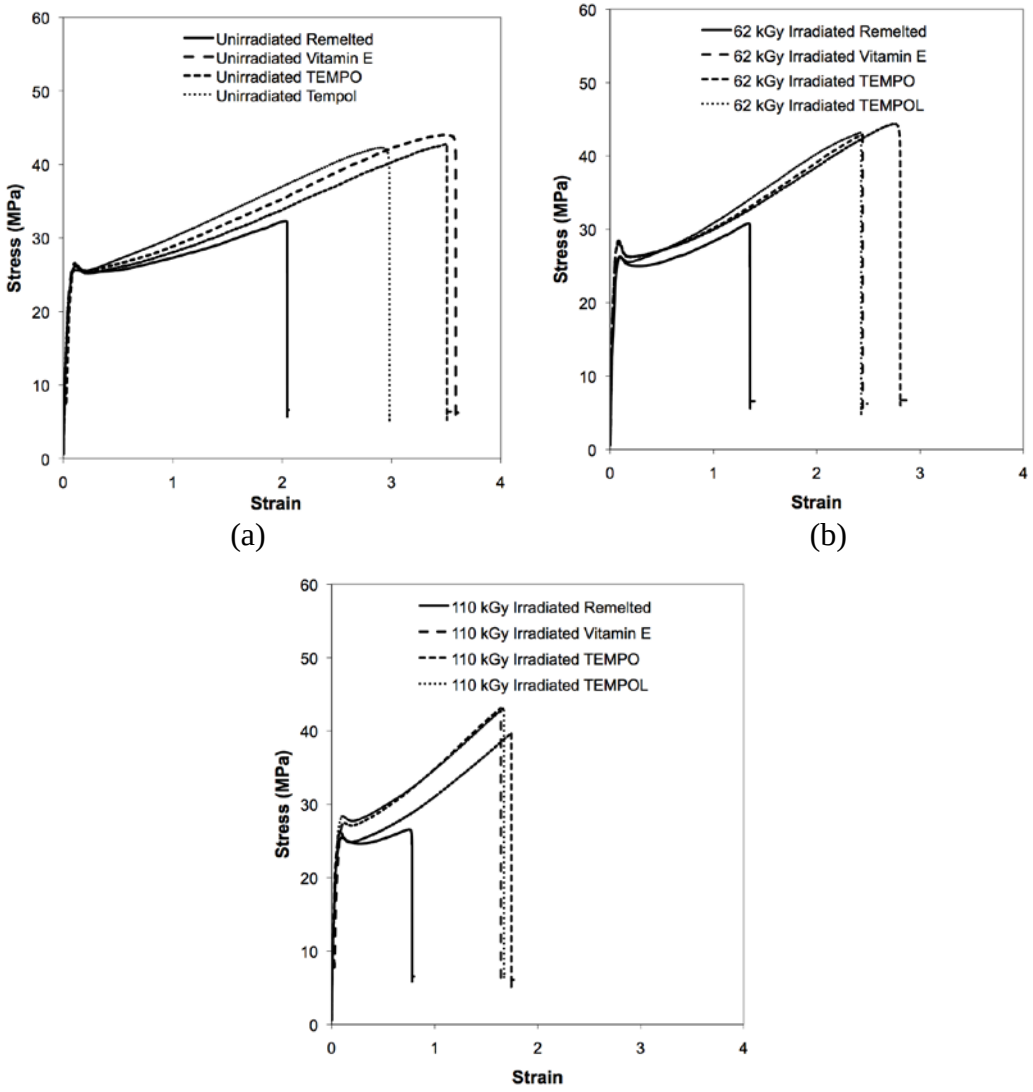

Figure 7.7: Engineering stress vs. strain plots of unirradiated (a), 62 kGy irradiated (b), and 110 kGy irradiated (c) UHMWPE that was afterward remelted at 150°C for 2 hours, doped (2 hours) with vitamin E and homogenized (72 hours) at 100°C, or doped with TEMPO or Tempol at 100°C for 72 hours. The three antioxidants show plasticization of the UHMWPE where the specimens elongate significantly more than the remelted specimens. The antioxidants also demonstrate increased toughness and ultimate tensile strength. The curves shown indicate individual specimen stress vs. strain plots that are typical of the sample group.

Table 7.5 illustrates how close the calculated tensile values are for all three antioxidants at 110 kGy. This table shows that highly crosslinked UHMWPE doped with the three antioxidants vitamin E, TEMPO and Tempol all show very similar σ_{UTS}, σ_{YS}, elongation percentage and elastic modulus, *E*. The σ_{UTS} and percent elongation are significantly higher for the three antioxidants versus the remelted polymer. The σ_{YS} and *E* of the three antioxidants show slightly higher values from the remelted polymer. The elongation percentage is significantly higher for polymer plasticized with antioxidants than for crosslinked and remelted UHMWPE, as expected and discussed previously.

Table 7.5: Tensile Properties of UHMWPE 110 kGy Irradiated and Remelted or Doped with Vitamin E, TEMPO or Tempol

110 kGy Irradiated	Ultimate Tensile Strength (MPa)		Yield Strength (MPa)		Elongation (%)		Elastic Modulus (GPa)	
Remelted	24.46	± 1.30	26.30	± 1.09	146	± 17	1.036	± 0.103
Vitamin E	**37.56**	**± 7.37**	26.42	± 2.70	**244**	**± 23**	0.801	± 0.375
TEMPO	36.23	± 5.34	27.80	± 0.99	231	± 33	1.127	± 0.087
Tempol	35.62	± 5.85	26.76	± 3.24	228	± 45	0.962	± 0.185

P-value Key:	$0.05 < p < 0.01$ Significant	$0.01 < p < 0.001$ Very significant	$p < 0.001$ **Extremely significant**

Furthermore, the trends of tensile properties with ionizing radiation dose for remelted, vitamin E-doped, TEMPO-doped, and Tempol-doped specimens are shown in bar charts in Figure 7.8. This figure demonstrates the differences between the remelted and antioxidant-doped specimens, at each radiation dose rate. For example, the σ_{UTS} exhibits a decrease with increasing ionizing radiation dose (Figure 7.8a). This is mostly due to the impact of crosslinking,[97] as discussed previously. The increase in σ_{UTS} from remelted to antioxidant containing UHMWPE at each dose is

extremely significant, in almost all cases. Elongation percentage decreases dramatically because crosslinking restricts chain movement (Figure 7.8b). Also, elongation very significantly increases from irradiated and remelted UHMWPE to irradiated and antioxidant-containing UHMWPE, at each dose.

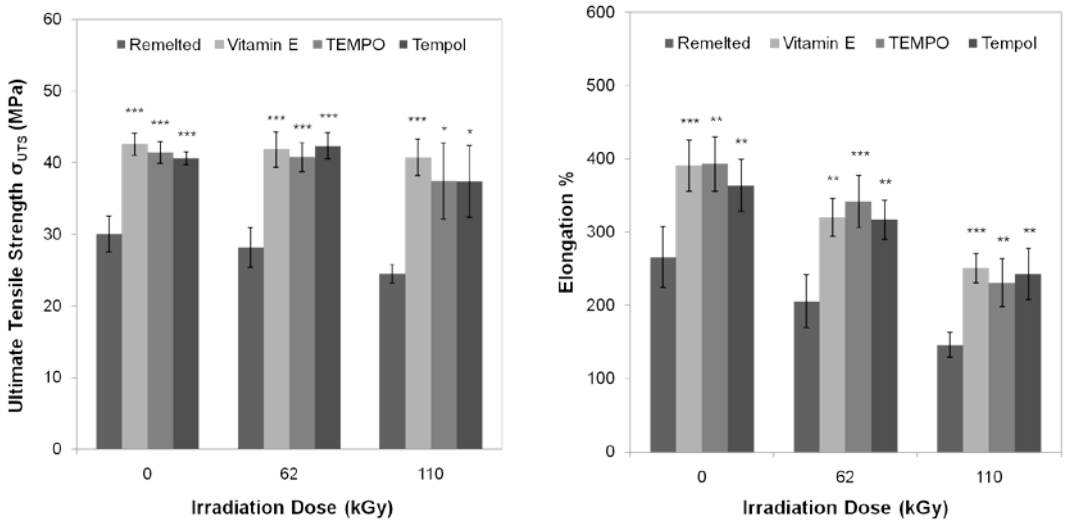

(a) (b)

Figure 7.8: Plots of the ultimate tensile strength, σ_{UTS} (a) and elongation percentage at failure (b) for the irradiated and remelted, vitamin E-doped, TEMPO-doped and Tempol-doped specimens, at each ionizing radiation dose. These values are representative of four to five specimens for each point. * denotes statistically significant ($0.05 < p < 0.01$), ** denotes very statistically significant ($0.01 < p < 0.001$), and *** denotes extremely statistically significant ($p < 0.001$) according to a Student's t-test with $\alpha = 0.05$.

Additionally, the effect of ionizing radiation dose on tensile properties of each processing group is also important, as shown in Figure 7.9. The σ_{YS} exhibits a slight increase with increasing radiation dose, as the material stiffens with crosslinking (Figure 7.9a)[104] in the antioxidant-containing specimens. Vitamin E, TEMPO and Tempol doped specimens show a significant increase in yield strength with crosslinking. While it is subtle, there is a small increase in the elastic modulus, E,

due to increased stiffness due to crosslinking (Figure 7.9b),[104] which is statistically significant in vitamin E and TEMPO-containing specimens.

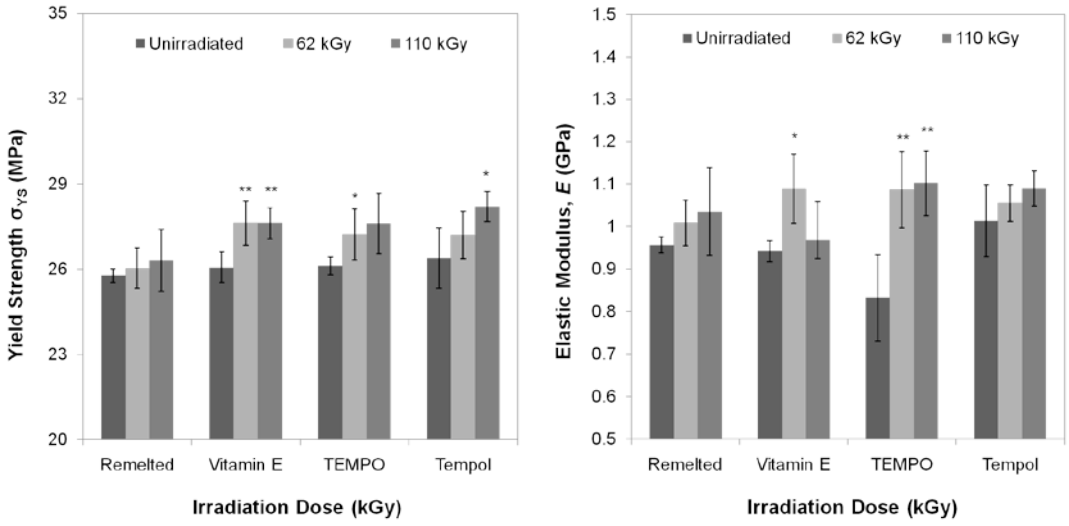

(a) (b)

Figure 7.9: Plots of the yield strength, σ_{YS} (a) and elastic modulus, E (b) of the irradiated and remelted, vitamin E-doped, TEMPO-doped and Tempol-doped specimens irradiated to a range of ionizing radiation doses. These values are representative of four to five specimens for each point. * denotes statistically significant ($0.05 < p < 0.01$), ** denotes very statistically significant ($0.01 < p < 0.001$), and *** denotes extremely statistically significant ($p < 0.001$) according to a Student's t-test with $\alpha = 0.05$.

These antioxidants are infiltrated into UHMWPE at the same concentration and thus should have equal antioxidative capability, as shown by the low oxidation levels in FTIR cross-section analysis. Additionally, the same number of molecules should be present for each antioxidant, imposing the same degree of plasticization. One aspect that does not have a clear effect is molecular size. With a 430.71 g/mol molecular weight (versus 156.25 g/mol and 172.24 g/mol for TEMPO and Tempol, respectively), the vitamin E molecule is larger and could potentially cause a higher degree of plasticization, because it would cause more swelling. Yet the elongation

and mechanical properties of vitamin E, TEMPO and Tempol are comparable. This size difference may not have a significant effect here, while larger molecules with 1000 g/mol or more may demonstrate such an effect more clearly.

7.5 Conclusions

The addition of an antioxidant or additive molecule to UHMWPE seemingly plasticizes the polymer, increasing the toughness, elongation and σ_{UTS} from irradiated and remelted specimens. The remelted specimens demonstrate a loss in σ_{UTS} from the virgin material. However, the yield strength is increased for crosslinked UHMWPE, for all processing conditions. As the specimens tested here are doped with antioxidants after crosslinking, the radiation dose has a significant effect on the reduction in toughness, elongation and σ_{UTS}. In fact, tensile properties depend more on the crosslink density and on the plasticization effect of antioxidants, rather than crystallinity, as some other authors have noted.[7] The reduction in tensile properties due to crosslinking can be counterbalanced by the addition of an antioxidant, such as vitamin E, TEMPO or Tempol. These plasticizer molecules will swell the polymer, allowing easier chain motion. Overall, a high crosslink density to prevent wear, higher toughness and ultimate tensile strength and increased oxidation resistance can be imparted to UHMWPE through careful processing diffusing antioxidants after inert irradiation.

Chapter 8: Conclusions and Future Work

8.1 Conclusions

The novel doping of UHMWPE with the nitroxides, TEMPO and Tempol, is demonstrated to i) increase the polymer's resistance to post-irradiation oxidation, ii) have the same crosslink density as irradiated and annealed UHMWPE, and iii) enhance its tensile strength. Radical-radical interactions between nitroxide radicals and those produced in UHMWPE (alkyl and peroxyl) are shown, through EPR and FTIR measure of the oxidation index, to be the main mechanisms of residual radical scavenging. Also, the fast reaction of alkyl radicals with the nitroxide is shown by pulse radiolysis to be a second order reaction with a reaction rate constant of $k' = 1 \times 10^9$ mol $L^{-1}s^{-1}$. The nitroxide has shown to be a suitable additive for increasing the lifetime of UHMWPE in total joint replacements.

In an inert environment, nitroxide radicals compete for alkyl free radicals and the primary reactions are bimolecular crosslinking and the formation of a nitroxide complex intermediate, through radical-radical interactions. For example, this is the case when UHMWPE is packaged and irradiated in N_2 or argon and where the concentration of dissolved oxygen is lower than that of the nitroxide. The >NOR complex dissociates to form $>NO^-$ and a cation on the polymer chain. The cation is then deprotonated to form a vinyl group (equations 4.2 and 4.3).

$$R\cdot + >NO\cdot \rightarrow >NOR \rightarrow >NO^- + \ \sim CH_2C^+HCH_2CH_2\sim \qquad (4.2)$$

$$\sim CH_2C^+HCH_2CH_2\sim \ \rightarrow \ \sim CH_2CH{=}CHCH_2\sim + H^+ \qquad (4.3)$$

However, in the presence of oxygen, the corresponding peroxyl radicals can form. Still, nitroxides prevent further oxidation products from being produced through an electron transfer reaction (equation 1.11). This occurs where UHMWPE is irradiated in air or during accelerated aging when the concentration of oxygen is much higher than that of the nitroxide.

$$RO_2\cdot + >NO\cdot \leftrightarrow \text{intermediate} \rightarrow >N^+=O + RO_2^- \qquad (1.11)$$

Regardless, even at micromolar concentrations, nitroxides prevent hydroperoxides, ketones and other oxidation products from forming. The nitroxide also acts like a plasticizer, like vitamin E, and increases crystal size, the melting point, toughness, elongation and ultimate tensile strength of UHMWPE. Two drawbacks associated with the use of nitroxides, as opposed to vitamin E, are their potential toxicity and low vapor pressure. Further biocompatibility investigation into the effect of nitroxides on cellular viability and elution out of the polymer are necessary before the additive can be used in joint replacements. The low vapor pressure of TEMPO makes the molecule difficult to use. However, specialized handling such as a dedicated doping chamber would eliminate this issue.

Oxidation indices demonstrate that the nitroxide content required to prevent oxidation is substantially lower than vitamin E. Micromolar concentrations of TEMPO have been shown to prevent oxidation, when in direct competition for residual free radicals with oxygen. In contrast, vitamin E concentration two orders of magnitude higher is difficult to distribute homogeneously in the polymer, possibly leaving the bulk material susceptible to considerable oxidation.

The results show that, doping of UHMWPE with nitroxides like TEMPO or Tempol produce nearly optimal polymer properties and that nitroxides are more efficient at preventing oxidation in UHMWPE than phenols like vitamin E. The addition of TEMPO and Tempol after crosslinking in an inert environment does not compromise the crosslink density that maintains wear-resistance. These two molecules reduce oxidation of UHMWPE more completely than remelted or vitamin E doped UHMWPE. The infiltration of UHMWPE with nitroxides also increases polymer toughness, ultimate tensile strength and percent elongation.

8.2 Future Work

The development of the novel use of nitroxide antioxidants in UHMWPE leads to further research directions. There remain several unanswered questions involving the chemistry of free radical reactions between nitroxides and the polymer, the resulting mechanical properties, and the stability of these molecules in the polymer for a long period of time. Any of these research directions serve as a natural progression for further study.

First of all, the final product of carbon-centered free radicals and nitroxides is only theorized. One option for future work is the use of X-ray Photoelectron Spectroscopy (XPS) to confirm the dissociation of >NOR or other potential bonds that form between the molecule and polymer. This has been used by Kang *et al*. to differentiate the types of oxidation bonds that form, C-O, C=O and C-O-O based on the different bond energies dependent on the C – O structure.[99] This technique could be used to explore the types of oxidation products that form in the presence of

nitroxides, and to determine if the nitroxide reacts, bonds or then dissociates from the polymer chain, in the presence and absence of oxygen. Additionally, further pulse radiolysis studies investigating the reaction of alkyl and nitroxide radicals in the presence of oxygen could confirm which reaction is predominant. Careful identification of *trans*-vinylene concentrations would allow comparison between the reaction rate constants as well.

Furthermore, the evaluation of the wear-resistance and fatigue-crack resistance properties of nitroxide-infiltrated UHMWPE is necessary to validate the use of the molecule. Pin on disk (POD) or hip/knee simulator wear testing of UHMWPE, comparing processing conditions is a necessary application-based measure of nitroxide performance in total joint replacements. For industry acceptance of a new additive molecule, wear rates per sliding distance and million wear cycles should be compared between different antioxidants. The wear rates, failure mode, particle size distribution and shape analysis should generate substantial evidence of failure mechanisms of UHMWPE.

Lastly, the elution of antioxidants out of the polymer is an issue yet to be resolved. While some authors state that vitamin E does not migrate out of the UHMWPE,[73] there is evidence to the contrary in low density polyethylene.[118] This is an important issue for patient safety, as any molecules that migrate out will enter the blood stream and potentially pass through the blood-brain barrier (BBB). Not only does this pose a risk of toxicity but also the molecules and their potential degradation products should be evaluated for carcinogenicity. Nitroxides have been shown to pass through the BBB,[57] thus their elution and that of their degradation

products out of the polymer must be reduced to an FDA-acceptable level. Additionally, the concentration of nitroxides in UHMWPE must be significantly lower than the toxicity levels of the molecule. Aside from toxicity, the elution of the nitroxides, vitamin E and any of their degradation products should be quantified. Studies toward this end are required. This area of research is not yet clearly defined and there are no standards or guidance written on the topic. It is likely that liquid chromatography – mass spectrometery (LC/MS) techniques can be used to analyze the eluents from UHMWPE. A refluxing hexane bath can be used to extract the elution products that can then be evaluated by LC/MS or other MS techniques.

As a consequence, the UHMWPE industry and the approaches to reduce oxidation, wear and osteolysis continue to expand. The mechanisms by which these techniques reduce oxidation and debris production should be determined. Not only would this future research be of scientific value and add to our wealth of knowledge, but it is also a matter of patient safety, affecting millions of patients per year.

Appendix A: Kinetics Calculations for Pulse Radiolysis [119]

Case I: Pseudo-first order species decay

$R + B \rightarrow M$ where $[B]_o >> [R]_o$

In the case of alkyl radical, allyl radical or nitroxide intermediate decay, only the reactant, *R*, absorbs:

$$-\frac{d[R]}{dt} = k'[R]$$

where in the case i) $k' = k$

ii) $k' = k[B]_o$

iii) $k' = k_1 + k_2 + \ldots + k_m[B]_o + k_m + [B]_o + \ldots$

$$\int_{[A]_o}^{[A]_t} d\ln[R] = -\int_o^t k'\,dt$$

$$\ln[R]_t - \ln[R]_o = -k't$$

Assuming Beer's law, where ε^{λ} is the molar absorptivity, *c* is the concentration and *l* is the path length:

$$D = optical \cdot density = \ln\left(\frac{I_o}{I_t}\right) = \varepsilon^{\lambda} \cdot c \cdot l$$

$\ln D_t = -k't + \ln D_o$

$2.303 \ln D_t = -k't + 2.303 \ln D_o$

The slope of a plot of ln(D) versus time produces a straight line with slope:

$$Slope = -\frac{k'}{2.303}$$

For example, the decay of alkyl radicals at 240 nm in neat octane is represented by data shown in on a 20 microsecond time scale in Figure A.1 below. A plot of the ln(D) versus time produces a plot with a slope of 1.0×10^4, shown in Figure A.2. Since $Slope = -\frac{k'}{2.303}$, the $k_{obs} = 2.3 \times 10^4\ s^{-1}$. The same type of fit is performed for cases II and III described below.

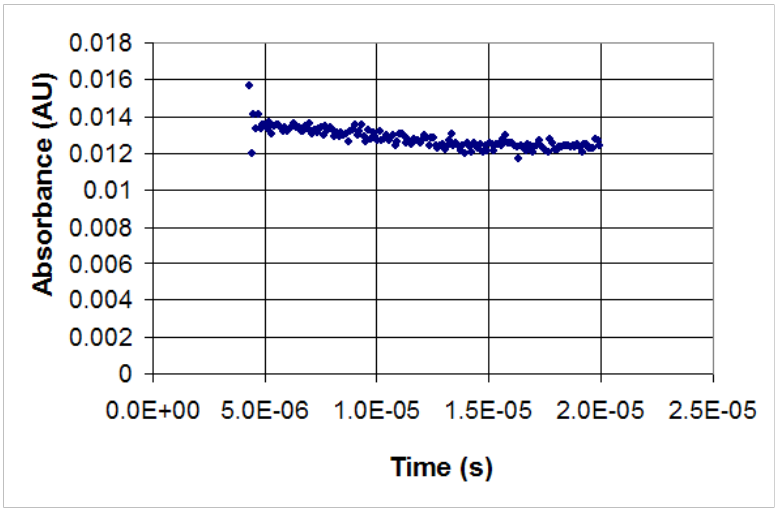

Figure A.1: Decay of alkyl radical in neat octane, measured by 240 nm absorbance within 20 μs of the average of four to five 30 ns pulses with 10 Gy/pulse.

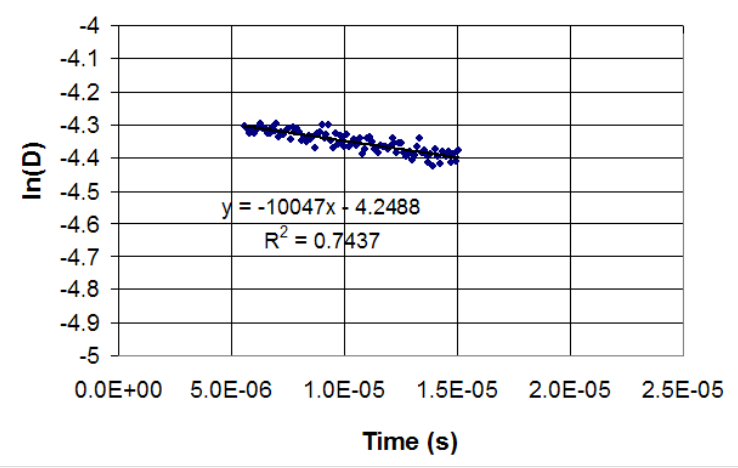

Figure A.2: First order fit of the decay of alkyl radicals in neat octane at 240 nm, where the slope of ln(D) versus time is multiplied by 2.303 to obtain the k_{obs}.

Case II: Pseudo-first order species build-up

$R + B \rightarrow M$ where $[B]_o >> [R]_o$

If only the product building up absorbs:

$$\frac{d[M]}{dt} = k'[R]$$

where in the case i) $k' = k$

ii) $k' = k[B]_o$

$x = [M]$ and $[R]_o - x = [R]$

$$\int_o^{[M]_t} \frac{dx}{[R]_o - x} = \int_o^t k' dt$$

$$-\ln ([R]_o - [M]_t) + \ln ([R]_o) = k't$$

If the reaction goes to completion:

$$[A]_o \cong [M]_\infty$$

$$\ln ([M]_\infty - [M]_t) - \ln ([M]_\infty) = - k't$$

Assume Beer's Law:

$$\ln (D_\infty - D_t) = - k't + \ln(D_\infty)$$

A plot of $\ln(D_\infty - D_t)$ versus time will give a straight line with slope:

Slope = $- k't$

Case III: Second order species decay

$R + R \rightarrow M$

If only R absorbs:

$$\frac{-d[R]}{dt} = k^1[R]^2$$

where in the case 1) $k^1 = 2\,k$

2) $k^1 = k$

$$-\int_{[A]_o}^{[A]_t} \frac{d[R]}{[A]^2} = +\int_0^t k^1 dt$$

$$\frac{1}{[A]_t} = \frac{1}{[A]_o} = k^1 t$$

Assuming Beer's Law:

$$\frac{1}{D_t} = \frac{k^1 t}{\varepsilon^{\lambda} 2} + \frac{1}{D_o}$$

A plot of $1/D_t$ vs. t gives a straight line with:

$$\text{Slope} = \frac{k^1}{\varepsilon^{\lambda} 2}$$

Appendix B: *P*-Values Evaluating Significance Between Tensile Tested UHMWPE Processing

Figure B.1: P-values of Yield Strength, σ_{UTS}, During Tensile Testing Between Different Processing Groups, Determined from a Student's T-Test Heteroscedastic Mean Comparison with α=0.05 and Two Tailed Distribution

	Unirradiated Remelted	62 kGy Remelted	110 kGy Remelted	Unirradiated Vitamin E	62 kGy Vitamin E	110 kGy Vitamin E	Unirradiated TEMPO	62 kGy TEMPO	110 kGy TEMPO	Unirradiated Tempol	62 kGy Tempol	110 kGy Tempol
Unirradiated Remelted	-	0.3384	0.0048	**0.0001**	**0.0001**	**0.0004**	**0.0006**	**0.0001**	0.0174	**0.0003**	**0.0003**	0.0547
62 kGy Remelted	0.3384	-	0.0709	**0.0010**	**0.0002**	**0.0006**	0.0010	**0.0006**	0.0269	0.0011	**0.0006**	0.0231
110 kGy Remelted	0.0048	0.0709	-	**0.0000**	**0.0000**	**0.0003**	**0.0000**	**0.0000**	0.0174	**0.0000**	**0.0000**	0.0150
Unirradiated Vitamin E	**0.0001**	0.0010	**0.0000**	-	0.8592	0.5780	0.8879	0.5082	0.2293	0.2733	0.4921	0.2037
62 kGy Vitamin E	**0.0001**	**0.0002**	**0.0000**	0.8592	-	0.5363	0.7771	0.4873	0.2026	0.3489	0.7042	0.1788
110 kGy Vitamin E	**0.0004**	0.0006	**0.0003**	0.5780	0.5363	-	0.6409	0.9650	0.3292	0.9365	0.3331	0.3003
Unirradiated TEMPO	**0.0006**	0.0010	**0.0000**	0.8879	0.7771	0.6409	-	0.5859	0.2421	0.3450	0.4202	0.2156
62 kGy TEMPO	**0.0001**	**0.0006**	**0.0000**	0.5082	0.4873	0.9650	0.5859	-	0.2994	0.8594	0.2371	0.2689
110 kGy TEMPO	0.0174	0.0269	0.0174	0.2293	0.2026	0.3292	0.2421	0.2994	-	0.3261	0.1527	0.9880
Unirradiated Tempol	**0.0003**	0.0011	**0.0000**	0.2733	0.3489	0.9365	0.3450	0.8594	0.3261	-	0.1131	0.2940
62 kGy Tempol	**0.0003**	**0.0006**	**0.0000**	0.4921	0.7042	0.3331	0.4202	0.2371	0.1527	0.1131	-	0.1318
110 kGy Tempol	0.0547	0.0231	0.0150	0.2037	0.1788	0.3003	0.2156	0.2689	0.9880	0.2940	0.1318	-

P-value:

>0.05: Not significant	0.01 to 0.05: Significant	0.001 to 0.01: Very significant	**<0.001: Extremely significant**

Figure B.2: P-values of Yield's Strength, σ_{YS}, During Tensile Testing Between Different Processing Groups, Determined from a Student's T-Test Heteroscedastic Mean Comparison with α=0.05 and Two Tailed Distribution

	Unirradiated Remelted	62 kGy Remelted	110 kGy Remelted	Unirradiated Vitamin E	62 kGy Vitamin E	110 kGy Vitamin E	Unirradiated TEMPO	62 kGy TEMPO	110 kGy TEMPO	Unirradiated Tempol	62 kGy Tempol	110 kGy Tempol
Unirradiated Remelted	-	0.5177	0.3423	0.3138	0.0038	0.0033	0.0846	0.0169	0.0412	0.2701	0.0140	**0.0010**
62 kGy Remelted	0.5177	-	0.6633	0.9486	0.1525	0.0124	0.8273	0.0614	0.0536	0.5664	0.0614	0.0027
110 kGy Remelted	0.3423	0.6633	-	0.6680	0.0651	0.0581	0.7300	0.1583	0.1066	0.8993	0.1644	0.0141
Unirradiated Vitamin E	0.3138	0.9486	0.6680	-	0.0078	0.0037	0.8369	0.0416	0.0540	0.5605	0.0370	**0.0006**
62 kGy Vitamin E	0.0038	0.1525	0.0651	0.0078	-	0.9974	0.0102	0.4755	0.9572	0.0744	0.4375	0.2127
110 kGy Vitamin E	0.0033	0.0124	0.0581	0.0037	0.9974	-	0.0046	0.4392	0.9571	0.0656	0.3972	0.1688
Unirradiated TEMPO	0.0846	0.8273	0.7300	0.8369	0.0102	0.0046	-	0.0478	0.0701	0.6115	0.0418	**0.0009**
62 kGy TEMPO	0.0169	0.0614	0.1583	0.0416	0.4755	0.4392	0.0478	-	0.5434	0.2149	0.9716	0.0771
110 kGy TEMPO	0.0412	0.0536	0.1066	0.0540	0.9572	0.9571	0.0701	0.5434	-	0.1209	0.5161	0.4027
Unirradiated Tempol	0.2701	0.5664	0.8993	0.5605	0.0744	0.0656	0.6115	0.2149	0.1209	-	0.2137	0.0152
62 kGy Tempol	0.0140	0.0614	0.1644	0.0370	0.4375	0.3972	0.0418	0.9716	0.5161	0.2137	-	0.0624
110 kGy Tempol	0.0010	0.0027	0.0141	**0.0006**	0.2127	0.1688	**0.0009**	0.0771	0.4027	0.0152	0.0624	-

P-value:

>0.05: Not significant	0.01 to 0.05: Significant	0.001 to 0.01: Very significant	**<0.001: Extremely significant**

Figure B.3: P-values of Elastic Modulus, *E*, During Tensile Testing Between Different Processing Groups, Determined from a Student's T-Test Heteroscedastic Mean Comparison with α=0.05 and Two Tailed Distribution

	Unirradiated Remelted	62 kGy Remelted	110 kGy Remelted	Unirradiated Vitamin E	62 kGy Vitamin E	110 kGy Vitamin E	Unirradiated TEMPO	62 kGy TEMPO	110 kGy TEMPO	Unirradiated Tempol	62 kGy Tempol	110 kGy Tempol
Unirradiated Remelted	-	0.1453	0.1714	0.2953	0.0242	0.6529	0.0540	0.0352	0.0347	0.2168	0.0035	0.3491
62 kGy Remelted	0.1453	-	0.6311	0.0835	0.1176	0.2821	0.0158	0.1513	0.1022	0.9035	0.2108	0.7887
110 kGy Remelted	0.1714	0.6311	-	0.1190	0.3879	0.2414	0.0139	0.4279	0.3035	0.7320	0.7162	0.9292
Unirradiated Vitamin E	0.2953	0.0835	0.1190	-	0.0116	0.3081	0.0799	0.0180	0.0220	0.1248	0.0022	0.2711
62 kGy Vitamin E	0.0242	0.1176	0.3879	0.0116	-	0.0277	0.0023	0.9664	0.8119	0.1918	0.4336	0.4428
110 kGy Vitamin E	0.6529	0.2821	0.2414	0.3081	0.0277	-	0.0346	0.0403	0.0278	0.3276	0.0181	0.4198
Unirradiated TEMPO	0.0540	0.0158	0.0139	0.0799	0.0023	0.0346	-	0.0031	0.0027	0.0152	0.0064	0.0458
62 kGy TEMPO	0.0352	0.1513	0.4279	0.0180	0.9664	0.0403	0.0031	-	0.7902	0.2276	0.5007	0.4719
110 kGy TEMPO	0.0347	0.1022	0.3035	0.0220	0.8119	0.0278	0.0027	0.7902	-	0.1474	0.3304	0.3645
Unirradiated Tempol	0.2168	0.9035	0.7320	0.1248	0.1918	0.3276	0.0152	0.2276	0.1474	-	0.3777	0.8581
62 kGy Tempol	0.0035	0.2108	0.7162	0.0022	0.4336	0.0181	0.0064	0.5007	0.3304	0.3777	-	0.7097
110 kGy Tempol	0.3491	0.7887	0.9292	0.2711	0.4428	0.4198	0.0458	0.4719	0.3645	0.8581	0.7097	-

P-value:

>0.05: Not significant	0.01 to 0.05: Significant	0.001 to 0.01: Very significant	**<0.001: Extremely significant**

Figure B.4: P-values of Percent Elongation During Tensile Testing Between Different Processing Groups, Determined from a Student's T-Test Heteroscedastic Mean Comparison with α=0.05 and Two Tailed Distribution

	Unirradiated Remelted	62 kGy Remelted	110 kGy Remelted	Unirradiated Vitamin E	62 kGy Vitamin E	110 kGy Vitamin E	Unirradiated TEMPO	62 kGy TEMPO	110 kGy TEMPO	Unirradiated Tempol	62 kGy Tempol	110 kGy Tempol
Unirradiated Remelted	-	0.0554	0.0020	**0.0009**	0.0436	0.5154	0.0010	0.0160	0.3023	0.0042	0.0576	0.3912
62 kGy Remelted	0.0554	-	0.0350	**0.0002**	0.0030	0.0788	**0.0001**	**0.0008**	0.2437	**0.0003**	0.0022	0.2013
110 kGy Remelted	0.0020	0.0350	-	**0.0000**	**0.0000**	**0.0002**	**0.0000**	**0.0000**	0.0073	**0.0000**	**0.0000**	0.0073
Unirradiated Vitamin E	**0.0009**	**0.0002**	**0.0000**	-	0.0079	**0.0003**	0.9342	0.0578	**0.0003**	0.2655	0.0055	**0.0004**
62 kGy Vitamin E	0.0436	0.0030	**0.0000**	0.0079	-	0.0026	0.0087	0.3180	0.0066	0.0607	0.8441	0.0066
110 kGy Vitamin E	0.5154	0.0788	**0.0002**	**0.0003**	0.0026	-	**0.0003**	0.0031	0.5220	0.0010	0.0040	0.6783
Unirradiated TEMPO	0.0010	**0.0001**	**0.0000**	0.9342	0.0087	**0.0003**	-	0.0572	**0.0003**	0.2504	0.0077	**0.0004**
62 kGy TEMPO	0.0160	**0.0008**	**0.0000**	0.0578	0.3180	0.0031	0.0572	-	0.0029	0.3462	0.2612	0.0043
110 kGy TEMPO	0.3023	0.2437	0.0073	**0.0003**	0.0066	0.5220	**0.0003**	0.0029	-	0.0010	0.0086	0.8610
Unirradiated Tempol	0.0042	**0.0003**	**0.0000**	0.2655	0.0607	0.0010	0.2504	0.3462	0.0010	-	0.0505	0.0014
62 kGy Tempol	0.0576	0.0022	**0.0000**	0.0055	0.8441	0.0040	0.0077	0.2612	0.0086	0.0505	-	0.0131
110 kGy Tempol	0.3912	0.2013	0.0073	**0.0004**	0.0066	0.6783	**0.0004**	0.0043	0.8610	0.0014	0.0131	-

P-value:

>0.05: Not significant	0.01 to 0.05: Significant	0.001 to 0.01: Very significant	**<0.001: Extremely significant**

Glossary

^{60}Co: Cobalt-60

α-TI: α-tocopherol index

ASTM: American Society for Testing and Materials

DSC: Differential scanning calorimetry

EB: Electron beam

EPR: Electron paramagnetic resonance

FTIR: Fourier transform infrared

G: Gauss

OI: oxidation index

MA: Modulation amplitude

mM: millimolar

nm: nanometer

TEMPO: 2,2,6,6-Tetramethyl-piperidine-1-oxyl

Tempol: 4-Hydroxy-2,2,6,6-tetramethylpiperidine-1-oxyl

TMA: Thermomechanical analysis

TVI: *Trans*-vinylene index

UHMWPE: Ultra-high molecular weight polyethylene

μm: micrometer

μM: micromolar

UTS: Ultimate tensile strength

UV-vis: Ultraviolet-visible

YS: Yield strength

Bibliography

1. Kurtz SM. *The UHMWPE Handbook: Ultra-High Molecular Weight Polyethylene in Total Joint Replacement*. 1st ed: Academic Press, 2004.

2. Naidu SH, Bixler BL, Moulton MJR. Radiation-induced physical changes in UHMWPE implant components. *Orthopedics* **20** (2) 137-142 (1997).

3. Older J. Charnley low-friction arthroplasty. *The Journal of Arthroplasty* **17** (6) 675-680 (2002).

4. McKellop H, et al. Development of an extremely wear-resistant ultra high molecular weight polyethylene for total hip replacements. *Journal of Orthopaedic Research* **17** (2) 157-167 (1999).

5. Costa L, et al. Oxidation in orthopaedic UHMWPE sterilized by gamma-radiation and ethylene oxide. *Biomaterials* **19** (7-9) 659-668 (1998).

6. Puertolas JA, *et al*. Influence of the remelting process on the fatigue behavior of electron beam irradiated UHMWPE. *Journal of Biomedical Materials Research Part B* **76B** (2) 346-353 (2006).

7. Oral E, Malhi AS, Muratoglu OK. Mechanisms of decrease in fatigue crack propagation resistance in irradiated and melted UHMWPE. *Biomaterials* **27** (6) 917-925 (2006).

8. Oral E, et al. alpha-tocopherol-doped irradiated UHMWPE for high fatigue resistance and low wear. *Biomaterials* **25** (24) 5515-5522 (2004).

9. Dumbleton JH, et al. The basis for a second-generation highly cross-linked UHMWPE. *Clinical Orthopaedics and Related Research* **453** 265-271 (2006).

10. Sutula LC, et al. Impact of gamma-sterilization on clinical-performance of polyethylene in the hip. *Clinical Orthopaedics and Related Research* **319** 28-40 (1995).

11. Bell CJ, et al. Effect of oxidation on delamination of ultrahigh-molecular-weight polyethylene tibial components. *The Journal of Arthroplasty* **13** (3) 280-290 (1998).

12. Singh D, Merrill RP. Molecular weight distribution of polyethylene produced by Ziegler-Natta catalysts. *Macromolecules* **4** (5) 599-604 (1971).

13. Kurtz SM, et al. Advances in the processing, sterilization, and crosslinking of ultra-high molecular weight polyethylene for total joint arthroplasty. *Biomaterials* **20** (18) 1659-1688 (1999).

14. Bellare A, Schnablegger H, Cohen RE. A small-angle x-ray scattering study of high-density polyethylene and ultrahigh molecular-weight polyethylene. *Macromolecules* **28** (23) 7585-7588 (1995).

15. Singh A. Irradiation of polyethylene: Some aspects of crosslinking and oxidative degradation. *Radiation Physics and Chemistry* **56** (4) 375-380 (1999).

16. Adler G. Cross-linking of polymers by radiation. *Science* **141** 321-329 (1963).

17. Weiss J. Chemical effects in the irradiation of polymers in the solid state. *Journal of Polymer Science* **29** (120) 425-432 (1958).

18. Chappas WJ, Silverman J. The radiation chemistry of crystalline alkanes. *Radiation Physics and Chemistry* **16** (6) 437-443 (1980).

19. Johnson DR, Wen WY, Dole M. Radiation chemistry of polyethylene. XII. Alkyl radical decay and amorphous content. *The Journal of Physical Chemistry* **77** (18) 2174-2179 (1973).

20. Dole M, Milner DC, Williams TF. Irradiation of polyethylene. 2. Kinetics of unsaturation effects. *Journal of the American Chemical Society* **80** (7) 1580-1588 (1958).

21. Wen WY, Johnson DR, Dole M. Second-order diffusion-controlled reaction. Decay of allyl free radicals in irradiated polyethylene. *The Journal of Physical Chemistry* **78** (18) 1798-1804 (1974).

22. Waterman DC, Dole M. Ultraviolet and infrared studies of free radicals in irradiated polyethylene. *The Journal of Physical Chemistry* **74** (9) 1906-1912 (1970).

23. McGinniss VD. In: Mark HF, Bikales NM, Overberger CG, Menges G, Eds. *Encyclopedia of Polymer Science and Engineering*. New York: Wiley & Sons, p. 432 (1986).

24. Kurtz SM, et al. 2006 Otto Aufranc Award paper - Significance of in vivo degradation for polyethylene in total hip arthroplasty. *Clinical Orthopaedics and Related Research* **453** 47-57 (2006).

25. Daly BM, Yin J. Subsurface oxidation of polyethylene. *Journal of Biomedical Material Research* **42** (4) 523-529 (1998).

26. Sobieraj MC, Kurtz SM, Rimnac CM. Notch strengthening and hardening behavior of conventional and highly crosslinked UHMWPE under applied tensile loading. *Biomaterials* **26** (17) 3411-3426 (2005).

27. Kurtz SM, et al. Thermomechanical behavior of virgin and highly crosslinked ultra-high molecular weight polyethylene used in total joint replacements. *Biomaterials* **23** (17) 3681-3697 (2002).

28. Wolf C, et al. Examination of the suitability of α-tocopherol as a stabilizer for ultra-high molecular weight polyethylene used for articulating surfaces in joint endoprostheses. *Journal of Materials Science: Materials in Medicine* **13** 185-189 (2002).

29. Tomita N, et al. Prevention of Fatigue Cracks in Ultrahigh Molecular Weight Polyethylene Joint Components by the Addition of Vitamin E. *Journal of Biomedical Materials Research* **48** (4) 474-478 (1999).

30. Biomet and Massachusetts General Hospital Form Strategic Research Alliance for Regenerex And E-Poly Technologies. *Business Wire*. May 21, 2007.

31. Gijsman P, Smelt H, Schumann D. Hindered Amine Light Stabilizers: A (Better) Alternative For Radiation Cross-linked UHMWPE Implants. 4th UHMWPE International Meeting; Torino, Italy; September 16 - 17, 2009.

32. Chumakov M, Silverman J, Al-Sheikhly M. On the Novel Use of Nitroxides and α-Tocopherol as Radiolytically-Produced Free Radical Scavengers in UHMWPE. 3rd UHMWPE International Meeting; Madrid, Spain; September 14, 2007.

33. Oral E, et al. Characterization of irradiated blends of α-tocopherol and UHMWPE. *Biomaterials* **26** 6657-6663 (2005).

34. Mallegol J, Carlsson DJ, Deschenes L. Post-gamma-irradiation reactions in vitamin E stabilised and unstabilised HDPE. *Nuclear Instruments and Methods in Physics Research Section B* **185** 283-293 (2001).

35. Oral E, et al. The effects of high dose irradiation on the cross-linking of vitamin E-blended ultrahigh molecular weight polyethylene. *Biomaterials* **29** (26) 3557-3560 (2008).

36. Teramura S, et al. Reduction of wear volume from ultrahigh molecular weight polyethylene knee components by the addition of vitamin E. *Journal of Orthopaedic Research* **26** (4) 460-464 (2008).

37. Ward AL, et al. The mechanism of slow crack-growth in polyethylene by an environmental-stress cracking agent. *Polymer* **32** (12) 2172-2178 (1991).

38. Soule BP, et al. The chemistry and biology of nitroxide compounds. *Free Radical Biology and Medicine* **42** (11) 1632-1650 (2007).

39. Haseloff RF, et al. Cytotoxicity of spin trapping compounds. *FEBS Letters* **418** (1-2) 73-75 (1997).

40. Krishna MC, et al. Studies of Structure-Activity Relationship of Nitroxide Free Radicals and Their Precursors as Modifier Against Oxidative Damage. *Journal of Medicinal Chemistry* **41** 3477-3492 (1998).

41. Kocherginsky N, Swartz HM. *Nitroxide Spin Labels*. New York: CRC Press, (1995).

42. Cimino P, Pavone M, Barone V. Structural, thermodynamic, and magnetic properties of adducts between TEMPO radical and alcohols in solution: New insights from DFT and discrete-continuum solvent models. *Chemical Physics Letters* **419** 106-110 (2006).

43. Samuni A. Kinetics and Mechanism of Hydroxyl Radical and OH-Adduct Radical Reactions with Nitroxides and with Their Hydroxylamines. *Journal of the American Chemical Society* **124** 8719-8724 (2002).

44. Griffith OH, Waggoner AS. Nitroxide Free Radicals - Spin Labels for Probing Biomolecular Structure. *Accounts of Chemical Research* **2** 17-24 (1969).

45. Ingham JD. Free Radical Spin Labels for Macromolecules. *Journal of Macromolecular Science-Reviews in Macromolecular Chemistry and Physics* **C2** 279 (1968).

46. Paton RM, Kaiser ET. Dectection of a Michaelis Complex by Spin Labeling in a Model Enzyme System. *Journal of the American Chemical Society* **92** 4723 (1970).

47. Buchaklian AH, Klug CS. Characterization of the walker a motif of MsbA using site-directed spin-labeling electron paramagnetic resonance spectroscopy. *Biochemistry* **44** 5503 (2005).

48. Fischer H. The persistent radical effect: A principle for selective radical reactions and living radical polymerizations. *Chemical Reviews* **101** 3581 (2001).

49. Hawker CJ, Bozman AW, Harth E. New polymer synthesis by nitroxide mediated living radical polymerizations. *Chemical Reviews* **101** 3661 (2001).

50. Tang W, He J, Yang Y. A Facile Synthesis of Cleavable Block Copolymers via Tandem Polymerization of NMRP and ATRP. *Journal of Macromolecular Science A: Pure and Applied Chemistry* **43** 1553-1567 (2006).

51. Tuinman E, et al. Controlled Free-Radical Copolymerization Kinetics of Styrene and Divinylbenzene by Bimolecular NMRP using TEMPO and Dibenzoyl Peroxide. *Journal of Macromolecular Science A: Pure and Applied Chemistry* **43** 995-1011 (2006).

52. Beckwith ALJ, Bowry VW, Ingold KU. Kinetics of nitroxide radical trapping. 1. Solvent effect. *Journal of the American Chemical Society* **114** 4983-4992 (1992).

53. Kieber DJ, Blough NV. Flourescence detection of carbon-centered radicals in aqueous solutions. *Free Radical Research Communication* **10** 108-117 (1990).

54. Goldstein S, Samuni A. Kinetics and Mechanism of Peroxyl Radical Reactions with Nitroxides. *Journal of Physical Chemistry A* **111** 1066-1072 (2007).

55. Swartz HM. Principles of the metabolism of nitroxides and their implications for spin trapping. *Free Radical Research Communications* **9** 399-405 (1990).

56. Suy S, et al. Nitroxides tempol and tempo induce divergent signal transduction pathways in MDA-MB 231 breast cancer cells. *The Journal of Biological Chemistry* **273** (28) 17871-17878 (1998).

57. Zhelev Z, et al. Nitroxyl radicals as low toxic spin-labels for non-invasive magnetic resonance imaging of blood-brain barrier permeability for conventional therapeutics. *Chemical Communications* **1** 53-55 (2009).

58. Suy S, et al. Nitroxide tempo, a small molecule, induces apoptosis in prostate carcinoma cells and suppresses tumor growth in athymic mice. *Cancer* **103** (6) 1302-1313 (2005).

59. Hahn SM, et al. Tempol, a Stable Free Radical, Is a Novel Murine Radiation Protector. *Cancer Research* **52** 1750-1753 (1992).

60. Gomez-Barrena E, et al. Update on UHMWPE research From the bench to the bedside. *Acta Orthopaedica* **79** (6) 832-840 (2008).

61. Moro T, et al. Surface grafting of artificial joints with a biocompatible polymer for preventing periprosthetic osteolysis. *Nature Materials* **3** (11) 829-836 (2004).

62. Kyomoto M, et al. Superlubricious surface mimicking articular cartilage by grafting poly(2-methacryloyloxyethyl phosphorylcholine) on orthopaedic metal bearings. *Journal of Biomedical Materials Research A* **91** (3) 730-741 (2009).

63. Polizu S, et al. Applications of carbon nanotubes-based biomaterials in biomedical nanotechnology. *Journal of Nanoscience and Nanotechnology* **6** (7) 1883-1904 (2006).

64. Lam CW, et al. A review of carbon nanotube toxicity and assessment of potential occupational and environmental health risks. *Critical Reviews in Toxicology* **36** (3) 189-217 (2006).

65. Wang A, et al. Wear, oxidation and mechanical properties of a sequentially irradiated and annealed UHMWPE in total joint replacement. *Journal of Physics D-Applied Physics* **39** (15) 3213-3219 (2006).

66. Oral E, et al. Highly cross-linked ultrahigh molecular weight polyethylene with improved fatigue resistance for total joint arthroplasty - Recipient of the 2006 Hap Paul Award. *Journal of Arthroplasty* **23** (7) 1037-1044 (2008).

67. Baxendale JH, Busi F, Eds. *The Study of Fast Processes and Transient Species by Electron Pulse Radiolysis*. Dordrecht, Holland: D. Reidel Publishing Co., (1981).

68. Silverstein R, Bassler G. *Spectrometric Identification of Organic Compounds*. New York: John Wiley & Sons, (1966).

69. Kaneko F, et al. Molecular-Complex Formation of Syndiotactic Polystyrene with Stable Radical Molecules. *Macromolecular Rapid Communications* **27** 1643-1647 (2006).

70. Albert CF, Busfield WK. Identifying crosslinks in polyethylene following gamma-irradiation in acetylene: A model compound study. *Journal of Polymer Science A: Polymer Chemistry* **35** (8) 1549-1562 (1997).

71. Mikulski CM, Skryantz JS, Karayannis NM. Bond-order of NO group in 2,2,6,6-tetramethylpiperidine nitroxide radical complexes with metal perchlorates. *Inorganic & Nuclear Chemistry Letters* **11** (4) 259-263 (1975).

72. Morat C, Rassat A. Nitroxides. 46. Determination of N-O stretching vibration in free piperidine nitroxide radicals. *Tetrahedron* **28** (3) 735 (1972).

73. Oral E, et al. Migration stability of alpha-tocopherol in irradiated UHMWPE. *Biomaterials* **27** (11) 2434-2439 (2006).

74. Parth M, Aust N, Lederer K. Studies on the effect of electron beam radiation on the molecular structure of ultra-high molecular weight polyethylene under the influence of alpha-tocopherol with respect to its application in medical implants. *Journal of Materials Science – Materials in Medicine* **13** (10) 917-921 (2002).

75. Oral E, et al. Diffusion of vitamin E in ultra-high molecular weight polyethylene. *Biomaterials* **28** (35) 5225-5237 (2007).

76. Kumada T, et al. Dynamic nuclear polarization of high- and low-crystallinity polyethylenes. *Nuclear Instruments and Methods in Physics Research A* **606** (3) 669-674 (2009).

77. Johnson GRA, Willson A. Pulse-radiolysis of polyethylene films - Formation of ions and excited-states of aromatic solutes. *Radiation Physics and Chemistry* **10** (2) 89-97 (1977).

78. Brede O, et al. Time-resolved characterization of radiation-generated species in molten polyethylene. *Radiation Physics and Chemistry* **34** (3) 403-413 (1989).

79. Brede O, Naumann W. Time-resolved experiments on the exciton transfer phenomenon in molten polyethylene. *Radiation Physics and Chemistry* **32** (3) 475-478 (1988).

80. Jonah CD. Decay of geminate ions in hexanes. *Radiation Physics and Chemistry* **21** (1-2) 53-56 (1983).

81. Tagawa S, et al. Picosecond pulse-radiolysis studies of geminate ion recombination in saturated-hydrocarbon. *Radiation Physics and Chemistry* **21** (1-2) 45-52 (1983).

82. Tagawa S, et al. Pulse-radiolysis studies on liquid alkane and related polymers. *Radiation Physics and Chemistry* **34** (4) 503-511 (1989).

83. Koritskii AT, et al. *Academic Nayk U.S.S.R. Vysokomolekulyarnye soedineniya: (High Molecular Compounds)* **1** 1182 (1959).

84. Charlesby A, Ormerod MG, Libby D. Radiation damage in polyethylene as studied by electron spin resonance. *Proceedings of the Royal Society of London Series A-Mathematical and Physical Sciences* **262** (130) 207-218 (1961).

85. Dole M, Cracco F. Radiation chemistry of polyethylene. 5. Hydrogen isotoped exchange studies. *The Journal of Physical Chemistry* **66** (2) 193-201(1962).

86. Allen NS, et al. Ageing and spectroscopic properties of polyethylenes: comparison with metallocene polymer. *Polymer Degradation and Stability* **67** (1) 57-67 (2000).

87. Waterman DC, Dole M. Radiation chemistry of polyethylene. 10. Kinetics of conversion of alkyl and allyl free radicals. *The Journal of Physical Chemistry* **74** (9) 1913-1922 (1970).

88. Wen WY, Johnson DR, Dole M. Radiation Chemistry of Polyethylene. XIII. Alkyl Radical Decay Kinetics in Single Crystalline and Extended-Chain Samples of Linear Polyethylene. *Macromolecules* **7** (2) 199-204 (1974).

89. Patel VM, et al. Radiation Chemistry of Polyethylene. XIV. Allyl Radical Decay Kinetics in Different Types of Polyethylene. *Journal of Polymer Science* **16** 467-484 (1978).

90. Hampton RR. Infrared analysis of low temperature polymers. *Analytical Chemistry* **21** (8) 923-926 (1949).

91. Woods RJ, Pikaev AK. *Applied Radiation Chemistry: Radiation Processing*. New York: John Wiley & Sons, (1994).

92. Chateauneuf J, Lusztyk J, Ingold KU. Absolute rate constants for the reactions of some carbon-centered radicals with 2,2,6,6-tetramethylpiperidine-n-oxyl. *Journal of Organic Chemistry* **53** (8) 1629-1632 (1988).

93. Brede O. Pulse radiolysis studies of the action of antioxidants in polyethylene and model systems: 4-methyl-2,6-di-t-butyl-phenol. *Nuclear Instruments and Methods in Physics Research Section B* **106** (1-4) 106-109 (1995).

94. Jahan MS, et al. Combined chemical and mechanical effects on free-radicals in UHMWPE joints during implantation. *Journal of Biomedical Materials Research* **25** (8) 1005-1017 (1991).

95. Wolf C, et al. Stabilisation of crosslinked ultra-high molecular weight polyethylene (UHMW-PE)-acetabular components with alpha-tocopherol. *Journal of Materials Science – Materials in Medicine* **17** (12) 1323-1331 (2006).

96. Chiesa R, et al. Enhanced wear performance of highly crosslinked UHMWPE for artificial joints. *Journal of Biomedical Materials Research* **50** (3) 381-387 (2000).

97. Lee SM, et al. Modification of microstructures and physical properties of ultra high molecular weight polyethylene by electron beam irradiation. *Journal of Polymer Science B – Polymer Physics* **43** (21) 3019-3029 (2005).

98. Gent AN, Vickroy VV. Elastic behavior birefringence and swelling of amorphous polyethylene networks. *Journal of Polymer Science Part A2* **5** 47-61 (1967).

99. Kang PH, Nho YC. The effect of gamma-irradiation on ultra-high molecular weight polyethylene recrystallized under different cooling conditions. *Radiation Physics and Chemistry* **60** (1-2) 79-87 (2001).

100. Turell MB, Bellare A. A study of the nanostructure and tensile properties of ultra-high molecular weight polyethylene. *Biomaterials* **25** (17) 3389-3398 (2004).

101. Bhateja SK, Yarbrough SM, Andrews EH. Radiation-induced crystallinity changes in linear polyethylene - Long-term aging effects in pressure-crystallized ultra-high molecular weight polymer. *Journal of Macromolecular Science B - Physics* **B29** (1) 1-10 (1990).

102. Oral E, et al. Wear resistance and mechanical properties of highly cross-linked, ultrahigh-molecular weight polyethylene doped with vitamin E. *Journal of Arthroplasty* **21** (4) 580-591 (2006).

103. Painter PC, Coleman MM. *Fundamentals of Polymer Science: An Introductory Text*. New York: CRC Press, (1997).

104. Bhateja SK, Andrews EH. Effect of high-energy radiation on the uniaxial tensile creep-behavior of ultrahigh molecular-weight polyethylene. *Polymer* **24** (2) 160-166 (1983).

105. Mazzucco DC, Dumbleton J, Kurtz SM. Can accelerated aqueous aging simulate in vivo oxidation of gamma-sterilized UHMWPE? *Journal of Biomedical Materials Research Part B* **79B** (1) 79-85 (2006).

106. Jacob RJ, et al. Time- and depth-dependent changes in crosslinking and oxidation of shelf-aged polyethylene acetabular liners. *Journal of Biomedical Materials Research* **56** (2) 168-176 (2001).

107. Taddei P, et al. Oxidation in ultrahigh molecular weight polyethylene and cross-linked polyethylene acetabular cups tested against roughened femoral heads in a hip joint simulator. *Biomacromolecules* **7** (6) 1912-1920 (2006).

108. Costa L, et al. Oxidation and oxidation potential in contemporary packaging for polyethylene total joint replacement components. *Journal of Biomedical Materials Research Part B* **78B** (1) 20-26 (2006).

109. Bracco P, et al. Oxidation behaviour in prosthetic UHMWPE components sterilised with high energy radiation in a low-oxygen environment. *Polymer Degradation and Stability* **91** (9) 2030-2038 (2006).

110. Setnescu R, et al. Chemiluminescence study on the oxidation of several polyolefins: II. Chemiluminescence from gamma-irradiated polymers. *Polymer Degradation and Stability* **61** (1) 109-117 (1998).

111. Gulmine JV, et al. Degradation profile of polyethylene after artificial accelerated weathering. *Polymer Degradation and Stability* **79** (3) 385-397 (2003).

112. Harrick NJ. Transmission spectra without interference-fringes. *Applied Spectroscopy* **31** (6) 548-549 (1977).

113. Blanchet TA, Burroughs BR. Numerical oxidation model for gamma radiation-sterilized UHMWPE: Consideration of dose-depth profile. *Journal of Biomedical Materials Research* **58** (6) 684-693 (2001).

114. Burton GW, Ingold KU. Autoxidation of biological molecules. 1. The antioxidant activity of vitamin-E and related chain-breaking phenolic antioxidants *invitro*. *Journal of the American Chemical Society* **103** (21) 6472-6477 (1981).

115. Narkis M, et al. Structure and tensile behavior of irradiation-cross-linked and peroxide-cross-linked polyethylenes. *Journal of Macromolecular Science B - Physics* **B26** (1) 37-58 (1987).

116. Bistolfi A, et al. Tensile and Tribological Properties of High-Crystallinity Radiation Crosslinked UHMWPE. *Journal of Biomedical Materials Research Part B* **90B** (1) 137-144 (2009).

117. Muratoglu OK, et al. Effect of radiation, heat, and aging on in vitro wear resistance of polyethylene. *Clinical Orthopaedics Related Research* **417** 253-262 (2003).

118. Siro I, et al. Release of alpha-tocopherol from antioxidative low-density polyethylene film into fatty food simulant: Influence of complexation in beta-cyclodextrin. *Food Additives and Contaminants* **23** (8) 845-853 (2006).

119. Tang FW. *The Effects of Small Amounts of Methanol on the Ionizing Radiation Induced Polymerization and Photopolymerization of Styrene.* Ph.D. Thesis. University of Maryland, College Park, (1990).